Application of the 190Pt-186Os isotope decay system to dating platinum-group minerals

JUDITH ANN COGGON

Application of the ^{190}Pt-^{186}Os isotope decay system to dating platinum-group minerals

Judith Ann Coggon

A thesis submitted in partial fulfilment of the requirements for the degree of Doctor of Philosophy at Durham University

Department of Earth Sciences, Durham University

June 2010

“zap zap zap…”

ABSTRACT

Constraining the formation age of platinum-group minerals (PGM) in placer deposits has traditionally been very challenging. The ^{190}Pt-^{186}Os decay system, measured by laser ablation multi-collector ICPMS (LA-MC-ICPMS), has been demonstrated as a useful geochronometric tool for detrital PGM grains. However, it is difficult to appraise the method accuracy using detrital PGM. In this thesis two examples are presented that verify the accuracy and precision of the technique in geologically well constrained situations.

The age of the Bushveld Complex has been measured using various radioisotope chronometers which yield ages ranging from 1921 – 2165 Ma, although an age of 2054 Ma is widely accepted. We present an accurate isochron age of 2012 ± 47 Ma (2σ, n = 50, MSWD = 1.19) for *in situ* Bushveld PGM, demonstrating the validity of multi-grain Pt-Os ages. Precision on the Bushveld LA-MC-ICPMS Pt-Os age is comparable to the Re-Os and Rb-Sr ages but data acquisition is easier and less time consuming. Scatter on the isochron may result from analytical artefacts or from post-crystallisation disturbance of the Pt-Os system within Pt-rich PGM grains via exsolution or deformation followed by incomplete sampling of the resulting within-grain heterogeneities.

Placer PGM derived from the Meratus ophiolite, southeast Borneo yield a precise Pt-Os isochron age of 197.8 ± 8.1 Ma (2σ, n = 260, MSWD = 0.90). This is consistent with published age constraints and provides the first direct date for the igneous rocks of the Meratus ophiolite, highlighting the utility of the Pt-Os geochronometer as a tool for dating ophiolites, layered intrusions and placer platinum mineralisation despite potential derivation of PGM from various isolated chromitites.

Analysis of large PGM populations has allowed improvement on published constraints for Pt/Os inter-element fractionation occurring during ablation analysis of PGE sulphides and alloys. This is estimated to amount to between 2 – 2.5 %.

Declaration

I declare that this thesis, which I submit for the degree of Doctor of Philosophy at Durham University, is my own work and not substantially the same as any which has previously been submitted at this or any other university.

Judith Coggon

Durham University

June 2010

Acknowledgements

The initial idea for this project was conceived by my excellent team of supervisors: Graham Pearson, Geoff Nowell and Steve Parman. They have provided first class advice and guidance ever since, while allowing me the independence to develop this research to compliment my interests. They have shared their expertise in the lab and the field and have taught me to present my research effectively. I thank them for their support and encouragement and for the great opportunities and experiences they have provided over the last three years.

Many others also deserve thanks for their contributions since October 2007; Chris Dale, Akira Ishikawa, Nadine Wittig and Chris Otley are thanked for all their help in the lab. Colin Macpherson and Dave Selby provided constructive discussion of Pt-Os isochron ages and their implications. The Parman/Danielson family were wonderful hosts in Massachusetts. Roz was always available for geological discussion and advice. Staff and postgrads in Durham gave their friendship and got me through it all, particularly Rich and Mallows, Mark, Niamh, Brown, Jaqs, Yuanyuan, Izzy, Ali, McNeill, Alex and the rest of the geochemistry bay. Roon, thank you for invaluable assistance in the field, friendship, tolerance, motivation and everything that you've taught me. Finally, my family, thank you for the unending supply of love, support and nutrition. I am very proud to be part of it all and you have given me a standard to aspire to.

CONTENTS

Electronic Appendices

(NB. All Appendices are provided as electronic copies, Appendices 4 – 6 and 9 are also provided as hard copies.)

List of Figures

1 Introduction

1.1 Rationale and Background

The platinum-group elements (PGE) have a huge and varied range of applications in modern technologies (e.g. automobile catalysts, jewellery, petroleum catalysts, anti cancer drugs, electrical components). The consequence of great demand combined with the scarcity of these metals in the Earth's upper continental crust (0.34 ppb Ru, 0.52 ppb Pd, 0.031 ppb Os, 0.022 ppb Ir, 0.5 ppb Pt; Rudnick and Gao, 2003) is their intrinsically high economic value (Pt = 1515 $/troy oz, Rh = 2600 $/troy oz, 06/06/2010, Johnson Matthey Base Price). Despite the aforementioned low crustal abundances, discrete platinum-group minerals (PGM - PGE-rich minerals such as sulphides, arsenides, tellurides and alloys) are ubiquitous and are concentrated in a modest number of stratiform complexes (e.g. Bushveld Complex, RSA; Noril'sk, Ural Mountains, Russia; Stillwater, Montanna, USA; Sudbury Complex, Ontario, Canada), Alaskan-type intrusions (e.g. Nizhni Tagil, Russia; Goodnews Bay, Alaska; Tulameen, Canada), Alpine-type (ophiolitic) series (e.g. Troodos, Cyprus; Josephine, OR, USA; Trinity, CA, USA) and numerous placer deposits (Fig. 1.1).

Figure 1. 1 Global distribution of PGM placers (orange triangles) and significant PGE-bearing stratiform complexes (purple squares). After Weiser (2002).

Well constrained ages for *in situ* PGE mineralisation are extremely important in the construction of models for ore genesis and in predicting the extent of mineral reserves. Crystallisation ages for PGM extracted from detrital deposits provide valuable information relating to the primary source of the mineralisation and may be used as an exploration tool, in a similar manner to indicator minerals in exploration for undiscovered kimberlites.

Layered mafic/ultramafic intrusions provide the largest economic deposits and are the main source of PGE produced today (Weiser, 2002) although they are limited in number (Fig. 1.1). Precise ages have been provided for many of these layered intrusions by radiometric dating of whole-rock and silicate phases using well established geochronometers such as U-Pb, Sm-Nd, Rb-Sr and Re-Os (e.g. Schoenberg et al., 1999; Buchanan et al., 2004; Reisberg et al., 2006; Scoates & Friedman, 2008). Although these systems can be used to date magmatic events they do not directly date the associated mineralisation, and in ultra-depleted harzburgites and dunites that host platiniferous PGE these techniques often cannot be applied at all. While the Re-Os system has found some application in dating large layered intrusions (e.g. Schoenberg et al., 1999), ages are often imprecise and are compromised by crustal contamination.

Alluvial PGM deposits are relatively abundant and have a longer economic history than stratiform deposits (Weiser 2002), but are generally orders of magnitude smaller. Alluvial PGM deposits are typically very poorly constrained in terms of age and geological context. They may be derived from layered intrusions or ophiolitic chromitites. Stratigraphic constraints can give estimates of minimum depositional ages but opportunities for direct application of radioisotope chronometers are rare. Using traditional geochemical approaches there is no reliable way of directly dating PGM using conventional radioisotope systems; thus constraining the age of alluvial PGM derived from ultramafic bodies, or potentially derived from more than one body, is very problematic.

The ^{187}Re-^{187}Os isotope system has been applied extensively to detrital PGM populations. Re-Os model ages have advanced our understanding of large mantle melting events and Os isotope data derived from PGM have been critical in exploring the evolution and heterogeneity of the mantle (e.g. Allègre and Luck, 1980; Hart and Kinloch, 1989; Hattori and Hart, 1991; Walker et al., 2002; Meibom et al., 2004; Pearson et al., 2007; Shi et al., 2007). However, our knowledge of the crystallisation mechanisms of these phases, particularly PGE alloys, is poor. Debate over the origin of detrital PGE alloys has been vigorous, with three main groups of theories:

1) *PGE alloys are secondary, low temperature phases that form by lateritic-type crystallisation within placers in a tropical environment* (Bowles, 1986; 1988). This theory is based on a model for leaching by meteoric water of PGE from the host anorthosite of the Freetown Layered

Complex, Sierra Leone, followed by transport and subsequent deposition as a result of increased pH and decreased Eh. This model is consistent with the reported distribution of PGM in the Freetown Peninsula, though the author notes that it is unquantified and "speculative".

2) *PGE alloys are magmatic minerals whose crystallisation is intimately related to chromitite formation* (Peck et al., 1992; Brenker et al., 2003). Strong evidence supporting this theory has been presented for PGE alloys from a variety of locations globally. Brenker et al. (2003) found syn- and pre-genetic silicate (including boninitic) and chromite inclusions in detrital Os-rich alloys from California and Oregon, USA. Analyses of these inclusions indicate that the alloys formed during melting of hydrous upper mantle, in an arc environment. The study also provides evidence of the strong association between PGE alloys and chromitites. Peck et al. (1992) found strikingly similar results in detrital PGE alloys from Tasmania and concluded that they must form in the oceanic lithospheric upper mantle during a boninitic melting event. A magmatic origin is further supported by two studies of PGE alloys from Borneo; both Os (Hattori et al., 1992) and S (Hattori et al., 2004) isotopes in primary and alluvial PGM are consistent with magmatic genesis during melting of refractory mantle and S isotopic data rule out genesis in a surface or near surface environment.

3) *PGE alloys crystallised in the outer core or core-mantle transition zone and were transported to the lithosphere as xenoliths in mantle plumes* (Bird and Basset, 1980; Bird et al., 1999). Bird and Basset (1980) reported that detrital PGE alloys from Oregon display magmatic textures and compositions consistent with magmatic genesis at the extremely high temperatures (solidii >> 2500 °C) that are predicted to exist only in the lower mantle or core. Bird et al. (1999) observed an apparent coupling of $^{186}Os/^{188}Os$ and $^{187}Os/^{188}Os$ enrichment relative to chondritic mantle in detrital PGE alloys from Oregon, USA. The authors interpreted this enrichment of both isotope systems as evidence of PGE alloy genesis in a region where a high Pt/Os and Re/Os composition had facilitated radiogenic in-growth of $^{186}Os/^{188}Os$ and $^{187}Os/^{188}Os$ over a substantial period of time prior to crystallisation of the alloys. They suggested that such an enriched region is likely to exist in the Earth's outer core or at the core-mantle transition zone. Mantle plumes and/or convection were proposed as potential mechanisms for the subsequent transport of these alloys to the lithosphere, and lead isotope data were provided as evidence conclusively excluding a crustal origin for the alloys. Repeat analyses by Walker et al. (2005) failed to reproduce the same Os isotope coupling and enrichment. Similar coupled Os isotope systematics observed by Luguet et al. (2008) were explained as a product of time-integrated in-growth following PGE alloy crystallisation. Hence the varied $^{186}Os/^{188}Os$ and $^{187}Os/^{188}Os$ ratios have a non-unique origin.

A magmatic origin (2) is now generally accepted by most who work on PGM, primarily due to the strong association of silicate and chromite inclusions within PGE alloy grains from California (Brenker et al., 2003) and Tasmania (Peck et al., 1992), as described above (further discussion of these theories can be found in Chapter 4, section 5.1). However, while $^{187}Os/^{188}Os$ measurements have yielded model ages that reflect the time-integrated signature of their source, constraints on the timing of PGM crystallisation are sparse. In the majority of published Re-Os studies on detrital PGM, the age of the samples is assumed to be the same as the nearest ophiolite or layered intrusion. Such assumptions can be problematic, especially in areas such as California, where PGM are collected from deposits in coastal and fluvial systems that may drain numerous ophiolites of a range of ages. Such loose age constraints are a weak link in genetic models and cause significant uncertainty when using PGM isotope compositions to evaluate the evolution of the Earth's mantle.

1.2 The Pt-Os chronometer

Though the α-decay of ^{190}Pt to ^{186}Os has been known for three decades the system was neglected for many years, predominantly due to the exceptionally small natural variation in the system, which results from the very low atomic abundance and very long half-life of the parent isotope ^{190}Pt (Table 1.1). The potential of the ^{190}Pt-^{186}Os system as a geochronometer was recognised by Walker et al. (1997) who analysed samples using isotope dilution, ICPMS and N-TIMS. They presented the first Pt-Os isochrons for whole-rock meteoritic samples and PGE-rich sulphides from terrestrial samples of well constrained age. As a result they were able to refine the ^{190}Pt decay constant (1.1×10^{-12} a^{-1}, Al-Bataina and Janëcke, 1987), constraining the value to 1.542×10^{-12} a^{-1} ± 1 %. Begemann et al. (2001) exploited improvements in instrument sensitivity and used MC-ICPMS to more accurately define the atomic percentage of ^{190}Pt (see Table 1.1) allowing them to further refine the decay constant to 1.477×10^{-12} a^{-1} ± 1 %. Despite these advances, no further application of the system as a geochronometer was subsequently employed; instead authors favoured using this system as a magma source tracer (e.g. Brandon et al., 1998; 2006, Luguet et al., 2008).

Table 1.1 Comparison of the Pt-Os and Re-Os decay systems. Data from Begemann et al. (2001) and Smoliar et al. (1996).

Isotope system	Atomic % parent	Atomic % daughter	Decay constant	Half life (Ga)
^{190}Pt-^{186}Os	0.0136	1.586	1.477×10^{-12}	469
^{187}Re-^{187}Os	62.6	1.964	1.66×10^{-11}	41.6

Table 1.2 Some common PGM and their occurrence (Cabri, 2002; Weiser, 2002).

PGM	Ideal formula	Dominant in placers derived from...			Present in placers derived from...			Analysed in this study
		Alaskan-type intrusions	Ophiolite massifs	Stratiform intrusions	Alaskan-type intrusions	Ophiolite massifs	Stratiform intrusions	
Braggite	(Pt,Pd)S				x	x	x	**X**
Erlichmanite	OsS_2				x	x	x	**X**
Iridium	Ir				x	x		
Isoferroplatinum	Pt_3Fe	X	X	X	x	x	x	**X**
Laurite	RuS_2				x	x	x	**X**
Osmium	Os		X	X	x	x	x	
Palladium	Pd							
Platinum	Pt	X			x			
Rhodium	Rh							
Rutheniridosmine	(Ir,Os,Ru)		X		x	x	x	**X**
Ruthenium	Ru		X			x		
Sperrylite	$PtAs_2$			X	x	x	x	**X**
Tetraferroplatinum	PtFe	X	X	X	x	x	x	**?**

The tendency of PGM to be enriched either in P-PGE (platinum-PGE: Pt, Pd, Rh) or I-PGE (iridium-PGE: Ir, Os, Ru) is a result of extremes in mineralogy (Table 1.2) and this generates diverse parent/daughter isotope fractionation. The resulting vast range of Pt and Os concentrations combined with the refractory nature of many PGM, in terms of their insolubility, mean that solution-based analytical techniques are laborious. Hirata et al. (1998) showed that the Pt-Os system can be measured very rapidly by laser ablation multi-collector ICPMS (LA-MC-ICPMS). Nowell et al. (2008) developed the method and applied it to produce precise isochron ages for individual, detrital Os-rich PGE alloy grains. They highlighted the potential of the technique for measurement of the Pt-Os system in large populations of PGM and demonstrated the quality of data produced and the reliability of mass bias and interfering element corrections applied. However, it is difficult to appraise the accuracy of the technique using detrital grains due to uncertainties with regards to their genetic and temporal relationships. This thesis aims to place the Pt-Os chronometer on a firmer base, to underpin its application to the dating and tracing of a wide range of PGM in a variety of environments.

1.3 Thesis aims

1) The principal aim of this project is to further develop the laser ablation MC-ICPMS Pt-Os geochronometry technique and demonstrate its application to a broad range of PGM in addition to the Os-rich minerals that have previously been analysed. By applying the technique to a primary PGM deposit of well constrained age, to generate the first multi-grain laser ablation Pt-Os isochrons, it will be possible to evaluate the validity of the method, including the corrections and processing applied to the raw data. This should also reveal, and allow quantification of, any Pt/Os inter-element fractionation that may occur during ablation and facilitate the refinement of the method to generate a more robust chronometer.

2) A further objective is to apply the Pt-Os geochronometer, measured by LA-MC-ICPMS, to a large population of detrital PGM that can be confidently assumed to be derived from a single ophiolite. The purpose of this is to demonstrate that the method can provide precise and accurate ages for detrital PGM, despite the likelihood that PGM genesis most likely occurred in distinct melt lenses that were isolated during formation within the ophiolite crust.

3) Accurate dating of a population of detrital PGM, including alloys, will provide an opportunity for the evaluation of the assertion of Bowles (1988), that alluvial PGE alloys are secondary minerals precipitated at low temperatures within placers and will allow further constraints of genetic models for PGE alloys.

1.4 Thesis outline

1.4.1 Chapter 2

This chapter provides a detailed description of the method for measurement of the Pt-Os system by LA-MC-ICPMS. The analytical set-up and offline corrections for mass bias and non-molecular interferences are described and the reliability and constraints of these corrections are comprehensively evaluated and discussed. Solution and ablation standard data and ablation sample data are reported. These analyses are reviewed and used to thoroughly evaluate within run, within session and long term reproducibility. Improvements and refinements to the method of Nowell et al. (2008) are described and attempts are made to define the limits of the technique.

1.4.2 Chapter 3

Chapter 3 documents the first ever application of the laser ablation Pt-Os chronometer to temporally well-defined PGE mineralisation. The chronometer is successfully applied to three different PGE mineralised horizons in the largest known PGE repository on Earth, the Bushveld Complex. The accurate Pt-Os isochron age of 2012 ± 47 Ma for the combined dataset demonstrates the validity of the Pt-Os chronometer measured by LA-MC-ICPMS and shows that corrections for mass bias and isobaric interferences are reliable, even at extreme parent/daughter ratios. Precision on the Pt-Os age is 2.3 %, which is shown to be comparable to the Re-Os and Rb-Sr systems for Bushveld samples. Simple modelling shows that up to 2.2 % Pt/Os inter-element fractionation can be accommodated within this uncertainty – a significant refinement of the previous, very loose estimate of 5 % (Nowell et al., 2008). The study highlights the importance of complete sampling of potentially heterogeneous PGM for precise and accurate Os isotope measurement. The technique generates a precise age overall for the Bushveld Complex and for Merensky PGE mineralisation, however insufficient samples were analysed from the Onverwacht and Tweefontein Hill localities to resolve any difference in age between these three individual episodes of mineralisation. In addition it is shown that single grain model ages can be estimated for Pt-rich grains assuming $^{186}Os/^{188}Os_i$ derived from convecting mantle values. These model ages are very close to the multi-grain isochron ages and demonstrate the possibility of single grain Pt-Os dating, similar to molybdenite dating, though with less impressive precision.

Modelling of isotopic mixing between primary mafic magmas and crustal rocks highlights the sensitivity of the Re-Os system, even to low degrees of crustal contamination, relative to the

more robust Pt-Os isotope system. Hence the Pt-Os system may be the more reliable chronometer.

1.4.3 Chapter 4

Chapter 4 presents the results of application of the LA-MC-ICPMS Os method to a population of detrital PGM derived from a single, well-constrained source of poorly constrained age – the Meratus ophiolite, south-eastern Borneo. A wide variety of Pt/Os ratios are exhibited in the PGM suite, while Re/Os ratios are restricted to a narrow range of relatively low values. No correlation exists on a Re-Os isochron diagram; this is attributed to inherent heterogeneity in Os isotope composition of the primary melts from which the PGM crystallised as well as the very restricted range of Re/Os ratios. In contrast, the Pt-Os system defines a precise isochron age of 197.8 Ma ± 8.1 Ma. This is consistent with published age constraints for the Meratus ophiolite and is interpreted as the age of PGM genesis in the lower oceanic lithosphere. The range of Pt/Os fractionation in ophiolitic PGM makes such detrital populations appropriate candidates for successful application of the LA-MC-ICPMS method.

1.4.4 Chapter 5

The final chapter provides a summary of the major conclusions reached in each section and addresses the main thesis aims stated in section 1.2. The advantages and disadvantages of the LA-MC-ICPMS Os method are evaluated. The interpretation and implications of the data presented in each chapter are drawn together and suggestions are made for further work and improvements to be made to the method.

1.5 Author Contributions

1.5.1 Chapter 2

This chapter will be submitted as a paper to *Chemical Geology* or *Journal of Analytical Atomic Spectrometry.*

Judith Coggon: I carried out all analytical work, data filtering and processing. I wrote the chapter in its entirety. I received helpful feedback from my supervisors, whose input improved the clarity and flow of the chapter, but did not change the interpretations or conclusions drawn.

Geoff Nowell and Graham Pearson: As my primary supervisors GP and GN conceived the project and provided support and guidance throughout. Geoff taught me how to use the laser and Neptune, gave invaluable assistance in understanding and applying the data processing method and shared his expertise in interpreting and filtering data.

1.5.2 Chapter 3

This chapter will be submitted as a paper to *Chemical Geology*.

Judith Coggon: I carried out all analytical work, data filtering and processing. I wrote the manuscript in its entirety then passed it on for feedback from the other authors, whose comments improved the structure and clarity of the paper, but did not change the interpretations or conclusions drawn.

Geoff Nowell: GN gave guidance during analytical work along with valuable discussion of data quality and processing. He provided useful feedback on details of the method and significance of data.

Graham Pearson: GP provided support and guidance throughout. He gave critical feedback and helped to clarify the discussion and direction of the manuscript.

Thomas Oberthür: TO provided the Rustenburg mixed PGM samples BVD_8801 and BVD_8801-R2, and compositional data for these samples. He provided useful feedback and discussion relating to the data and origin of historic samples.

Jean-Pierre Lorand: J-PL provided the Onverwacht Pt-Fe nugget (BVD_174-164) and the Rustenburg sperrylite (BVD_ 170-223). He provided helpful feedback and discussion of the data.

Steve Parman: SP provided support throughout. He offered useful suggestions concerning conveying the arguments to a wider audience.

1.5.3 Chapter 4

This chapter has been submitted as a scientific communication to *Economic Geology* and is currently in review

Judith Coggon: I carried out all analytical work, including LA-MC-ICPMS, electron microprobe analyses, SEM imaging and data filtering and processing. I wrote the manuscript in its entirety

then passed it on for feedback from co-authors, whose comments improved the flow of the paper, but did not alter the interpretations or conclusions drawn.

Geoff Nowell: GN provided invaluable assistance with LA-MC-ICPMS analyses and data quality monitoring. He gave vital feedback on issues of the discussion of the data.

Graham Pearson: GP gave useful feedback and support during the conception and later revision of the manuscript.

Steve Parman: SP taught me how to use the SEM and gave advice relating to electron microprobe analyses. His suggestions concerning clarifying and conveying arguments to a wider audience were fundamental to the final manuscript.

1.6 References

Al-Bataina, B., and Janëcke, J., 1987, Half-lives of long-lived alpha emitters: Radiochimica Acta, 42, 159.

Allègre, C.J., and Luck, J.-M., 1980, Osmium isotopes as petrogenetic and geological tracers: Earth and Planetary Science Letters, 48, 148-154.

Begemann, F., Ludwig, K.R., Lugmair, G.W., Min, K., Nyquist, L.E., Patchett, P.J., Renne, P.R., Shih, C.Y., Villa, I.M., and Walker, R.J., 2001, Call for an improved set of decay constants for geochronological use: Geochimica et Cosmochimica Acta, 65, 111-121.

Bird, J.M., and Bassett, W.A., 1980, Evidence of a Deep Mantle History in Terrestrial Osmium-Iridium-Ruthenium Alloys: Journal of Geophysical Research, 85, 5461-5470.

Bird, J.M., Meibom, A., Frei, R., and Nägler, T.F., 1999, Osmium and lead isotopes of rare OsIrRu minerals: derivation from the core-mantle boundary region?: Earth and Planetary Science Letters, 170, 83-92.

Bowles, J.F.W., 1986, The development of platinum-group minerals in laterites: Economic Geology, 81, 1278-1285.

Bowles, 1988, Further Studies of the Development of Platinum-Group Minerals in the Laterites of the Freetown Layered Complex, Sierra Leone, *in* Prichard, H.M., Potts, P.J., Bowles, J.F.W., and Cribb, S.J., eds., Geo-Platinum 87: New York, Elsevier Applied Science, 422.

Brandon, A.D., Walker, R.J., Morgan, J.W., Norman, M.D., and Prichard, H.M., 1998, Coupled ^{186}Os and ^{187}Os evidence for core-mantle interaction: Science, 280, 1570-1573.

Brandon, A.D., Walker, R.J., and Puchtel, I.S., 2006, Platinum-osmium isotope evolution of the Earth's mantle: Constraints from chondrites and Os-rich alloys: Geochimica et Cosmochimica Acta, 70, 2093-2103.

Brenker, F.E., Meibom, A., and Frei, R., 2003, On the formation of peridotite-derived Os-rich PGE alloys.: American Mineralogist, 88, 1731-1740.

Buchanan, P.C., Reimold, W.U., Koeberl, C., and Kruger, F.J., 2004, Rb-Sr and Sm-Nd isotopic compositions of the Rooiberg Group, South Africa: early Bushveld-related volcanism: Lithos, 75, 373-388.

Cabri, L.J., 2002, The Platinum-Group Minerals, *in* Cabri, L.J., ed., The Geology, Geochemistry, Mineralogy and Mineral Beneficiation of Platinum-Group Elements, Volume Special Volume 54, Canadian Institute of Mining, Metallurgy and Petroleum, 13-130.

Hart, S.R., and Kinloch, E.D., 1989, Osmium Isotope Systematics in Witwatersrand and Bushveld Ore-Deposits: Economic Geology, 84, 1651-1655.

Hattori, K., Burgath, K.P., and Hart, S.R., 1992, Os-Isotope Study of Platinum-Group Minerals in Chromitites in Alpine-Type Ultramafic Intrusions and the Associated Placers in Borneo: Mineralogical Magazine, 56, 157-164.

Hattori, K., and Hart, S.R., 1991, Osmium-isotope ratios of platinum-group minerals associated with ultramafic intrusions; Os-isotopic evolution of the oceanic mantle: Earth and Planetary Science Letters, 107, 499-514.

Hattori, K.H., Cabri, L.J., Johanson, B., and Zientek, M.L., 2004, Origin of placer laurite from Borneo: Se and As contents, and S isotopic compositions: Mineralogical Magazine, 68, 353-368.

Hirata, T., Hattori, M., and Tanaka, T., 1998, In situ osmium isotope ratio analyses of iridosmines by laser ablation-multiple collector-inductively coupled plasma mass spectrometry: Chemical Geology, 144, 269-280.

Luguet, A., Pearson, D.G., Nowell, G.M., Dreher, S.T., Coggon, J.A., Spetsius, Z.V., and Parman, S.W., 2008, Enriched Pt-Re-Os isotope systematics in plume lavas explained by metasomatic sulfides: Science, 319, 453-456.

Meibom, A., Frei, R., and Sleep, N.H., 2004, Osmium isotopic compositions of Os-rich platinum group element alloys from the Klamath and Siskiyou Mountains.: Journal of Geophysical Research, 109, B02203.

Nowell, G.M., Pearson, D.G., Parman, S.W., Luguet, A., and Hanski, E., 2008, Precise and accurate $^{186}Os/^{188}Os$ and $^{187}Os/^{188}Os$ measurements by Multi-collector Plasma Ionisation Mass Spectrometry, part II: Laser ablation and its application to single-grain Pt-Os and Re-Os geochronology: Chemical Geology, 248, 394-426.

Pearson, D.G., Parman, S.W., and Nowell, G.M., 2007, A link between large mantle melting events and continent growth seen in osmium isotopes: Nature, 449, 202-205.

Peck, D.C., Keays, R., R., and Ford, R.J., 1992, Direct crystallization of refractory platinum-group element alloys from boninitic magmas: Evidence from western Tasmania: Australian Journal of Earth Sciences, 39, 373-387.

Reisberg, L.C., Tredoux, M., and Harris, C., 2006, Re-Os systematics of the Platreef (Sandsloot mine) of the northern limb of the Bushveld Complex: Geochimica et Cosmochimica Acta, 70, A526-A526.

Rudnick, R.L., and Gao, S., 2003, Composition of the continental crust, *in* Rudnick, R.L., ed., Treatise on Geochemistry, Volume 3, Elsevier, 1-56.

Schoenberg, R., Kruger, F.J., Nagler, T.F., Meisel, T., and Kramers, J.D., 1999, PGE enrichment in chromitite layers and the Merensky Reef of the western Bushveld Complex; a Re-Os and Rb-Sr isotope study: Earth and Planetary Science Letters, 172, 49-64.

Scoates, J.S., and Friedman, R.M., 2008, Precise age of the platiniferous Merensky reef, Bushveld Complex, South Africa, by the U-Pb zircon chemical abrasion ID-TIMS technique: Economic Geology, 103, 465-471.

Shi, R., Alard, O., Zhi, X., O'Reilly, S.Y., Pearson, N.J., Griffin, W.L., Zhang, M., and Chen, X., 2007, Multiple events in the Neo-Tethyan oceanic upper mantle: Evidence from Ru-Os-Ir alloys in the Luobusa and Dongqiao ophiolitic podiform chromitites, Tibet: Earth and Planetary Science Letters, 261, 33-48.

Smoliar, M.I., Walker, R.J., and Morgan, J.W., 1996, Re-Os ages of Group IIA, IIIA, IVA and IVB iron meteorites: Science, 271, 1099-1102.

Walker, R.J., Brandon, A.D., Bird, J.M., Piccoli, P.M., McDonough, W.F., and Ash, R.D., 2005, ^{187}Os-^{186}Os systematics of Os-Ir-ru alloy grains from southwestern Oregon: Earth and Planetary Science Letters, 230, 211-226.

Walker, R.J., Morgan, J.W., Beary, E.S., Smoliar, M.I., Gzamanske, G.K., and Horan, M.F., 1997, Applications of the ^{190}Pt-^{186}Os isotope sytem to geochemistry and cosmochemistry: Geochimica et Cosmochimica Acta, 61, 4799-807.

Walker, R.J., Prichard, H.M., Ishiwatari, A., and Pimentel, M., 2002, The osmium isotopic composition of convecting upper mantle deduced from ophiolite chromites: Geochimica et Cosmochimica Acta, 66, 329-345.

Weiser, T.W., 2002, Platinum-Group Minerals (PGM) in Placer Deposits, *in* Cabri, L.J., ed., The Geology, Geochemistry, Mineralogy and Mineral Beneficiation of Platinum-Group Elements, Special Volume 54, Canadian Institute of Mining, Metallurgy and Petroleum, 721-756.

Johnson Matthey Base Price, accessed 06/06/2010 - http://www.platinum.matthey.com/

2 Mass Spectrometry

2.1 Introduction

The mass spectrum of Os comprises seven isotopes, two of which are radiogenic; ^{187}Os is the daughter isotope produced by the β-decay of ^{187}Re at a half life of 4.16×10^{10} a ± 1% (Smoliar et al., 1996) and ^{186}Os is the product of the α-decay of ^{190}Pt ($t_{1/2} = 4.69 \times 10^{11}$ a ± 1%; Begemann et al., 2001). The Re-Os system has been applied to a vast range of geological problems over the last three decades while the Pt-Os system has remained under-exploited. The preferred method for measurement of $^{187}Os/^{188}Os$ in most geological samples is negative thermal ionisation mass spectrometry (N-TIMS), particularly for samples in which the amount of analyte is low. Measurement of the Pt-Os system by isotope dilution N-TIMS (Walker et al., 1997), by solution MC-ICPMS (Begemann et al., 2001) and by innovative ion probe techniques (e.g. Hart and Kinloch, 1989; Hattori and Hart, 1991; Meibom and Frei, 2002) has provided valuable datasets, although data acquisition by these methods is slow. In samples such as platinum-group element (PGE) sulphides, PGE arsenides and PGE alloys the PGEs are present in high concentrations (e.g. typically ~ 90 wt% Pt in isoferroplatinum and ~ 30 wt% Os in laurite-erlichmanite), making them appropriate candidates for very rapid analysis by laser ablation – multi-collector – ICPMS (LA-MC-ICPMS). The LA-MC-ICPMS technique allows rapid, *in situ*, high precision analysis of Os isotopes in platinum-group minerals (PGM) allowing acquisition of very large datasets such as those required for statistical analysis in isotopic tracing studies (e.g. Pearson et al., 2007). However, the main advantage of this method is that it allows simultaneous measurement of both the $^{187}Os/^{188}Os$ and $^{186}Os/^{188}Os$ ratios, facilitating the exploitation of the Pt-Os chronometer coupled with the Re-Os isotopic tracer.

The wide variety of platinum-group minerals (PGM) that may occur within a single primary deposit provides potential for a very wide range of $^{190}Pt/^{188}Os$ ratios within a single sample population. Coupled with the negligible variation in $^{186}Os/^{188}Os_i$ between mineral species and over Earth history, this provides numerous opportunities for Pt-Os geochronology. In addition, previous studies (e.g. Meibom and Frei, 2002; Pearson et al., 2007) have demonstrated the usefulness of $^{187}Os/^{188}Os$ data, combined with age information, as a tracer of mantle heterogeneity and large mantle melting events.

Hirata et al. (1998) presented a method for measurement of Os isotope systematics by LA-MC-ICPMS but did not describe or appear to have applied any corrections for isobaric interferences. This chapter provides a description of the LA-MC-ICPMS Os method initially developed and

reported by Nowell et al. (2008b) along with new developments and improvements in the analytical procedure used for the acquisition of all Os isotope data presented in this thesis.

2.2 Mass spectrometry

Osmium isotope analyses reported in this thesis were performed on the ThermoFisher Neptune MC-ICPMS at the Northern Centre for Isotopic and Elemental Tracing (NCIET), Durham University. PGM samples were analysed by laser ablation using a New Wave UP213 laser. Prior to each analytical session the Neptune was tuned for maximum sensitivity and peak shape quality. Tuning was performed while aspirating a 1 μg ml^{-1} solution of the Durham Romil Osmium Standard (DROsS) reference material (RM), using an Elemental Scientific Incorporated PFA-50 microflow nebuliser and a Glass Expansion Cinnabar micro cyclonic spray-chamber. Solution aspiration provides a more stable Os signal than ablation of a PGM or PGE alloy standard grain and so facilitates more precise tuning. Samples were analysed during 30 sessions between 18/10/2007 and 12/03/2010. The sensitivity for ^{189}Os was between ~2.7 and 7.2 V for a 1 μg ml^{-1} DROsS solution at an uptake rate of ~ 80 μl min^{-1}. After tuning peak centring was performed, followed by instrument baselines and amplifier gain calibrations.

The Neptune is equipped with a nine Faraday collector array, with 10^{11} Ω resistor amplifiers, and a maximum signal of 50 V on each collector. The Faraday cup configuration (Nowell et al., 2008b; Table 2.1) allows the simultaneous measurement of both the Re-Os and Pt-Os systems, including the Re and W monitor isotopes necessary for correcting for non-molecular isobaric interferences on the Os mass spectrum. The cup configuration also accommodates the option to use either the $^{189}Os/^{188}Os$ or $^{192}Os/^{188}Os$ ratio for mass bias corrections (see section 2.5.1 for further details). During the analyses of high-Pt PGM grains a further advantage of utilising the $^{189}Os/^{188}Os$ ratio for mass bias corrections is that ^{192}Os becomes redundant, allowing for removal of the H4 cup from the collector array. Thus high-Pt, low-Os samples may be ablated at higher laser power and/or spot size, producing higher Os beam intensities without saturating the H4 Faraday with the ^{192}Pt signal.

Table 2. 1 Neptune Faraday cup configuration for the static multi-collection of Os

	L4	L3	L2	L1	Ax	H1	H2	H3	H4[a]
Analyte masses	*^{182}W*	^{184}Os	*^{185}Re*	^{186}Os	^{187}Os	^{188}Os	^{189}Os	^{190}Os	^{192}Os
Non-molecular interferences		^{184}W		^{186}W	^{187}Re			^{190}Pt	^{192}Pt

[a] ^{192}Os was not measured in all analytical sessions due to very high Pt contents of some grains. Monitor isotopes for calculating W and Re non-molecular isobaric interferences are shown in italics.

The laser ablation technique is designed to exploit large populations (commonly 100s) of PGM grains which are often very small (of the order of 100 μm in diameter). As a result the data collection time for sample analyses is necessarily short; Os isotope ratios were measured using a static multi-collection routine of one block of 40 cycles with an integration time of 1 s per cycle.

Raw Os intensity data were corrected offline for instrumental mass bias. Corrections for Re and W isobaric interferences on ^{187}Os, ^{186}Os and ^{184}Os and the Os interference on ^{190}Pt were then applied to all calculated ratios (see section 2.5 for full details of corrections). A 2 sigma rejection was applied to all Os isotope and parent/daughter isotope ratios for all analyses except for internally isotopically heterogeneous samples, since applying a rejection would bias the data (see Chapter 3, section 3.4.2.1 for further details).

Within-run errors for individual solution and laser ablation analyses are reported as 2 standard errors of the mean ($2SE = 2SD/n^{0.5}$; where n is the number of integrations and SD is the standard deviation). Uncertainties reported for laser ablation analyses were calculated to also incorporate external reproducibility (see section 2.6).

2.3 Standard solutions

At the start of each analytical session a DROsS RM standard solution was analysed to assess instrument accuracy and reproducibility. A solution with a concentration of 1 μg ml^{-1} was measured 10 times in each analytical session from 18/10/2007 until 18/02/2008. During this period the Re and W interfering element ratios (IERs), used for interfering element corrections (IECs) (see section 2.5.2), remained constant. However, in subsequent analytical sessions the stability of these ratios deteriorated. As a result it became necessary to modify the method to include regular calibration of these ratios by analysis of a DROsS solution doped with Re and W. Thus in analytical sessions from 11/11/2008 onwards the routine was amended and both pure and doped DROsS solutions were analysed prior to ablation of samples. Initially, five analyses each of 1 μg ml^{-1} pure DROsS and 1 μg ml^{-1} + 0.05 ppm W + 0.01 ppm Re solutions were carried out in each session. Later this was increased, with the final revised method including an additional five analyses of 1 μg ml^{-1} DROsS + 0.1 ppm W + 0.05 ppm Re (see Appendix 1).

The original standard solution measurement routine mimicked that for laser ablation, with a measurement block of 40 cycles, each with a cycle integration time of 1 s (total measurement time of 40 s). From 13/11/2008 onwards the integration time was increased to 4 s (total measurement time of 160 s) in order to achieve a more accurate measurement of the $^{190}Os/^{188}Os$ ratio, which is used to correct for Os interference on ^{190}Pt (see section 2.5.2).

Table 2. 2 Mean Os isotope compositions and reproducibility obtained on DROsS reference material solutions during 30 analytical sessions

Date	n =	$^{190}Os/^{188}Os_{mbc}$	2SE	$^{187}Os/^{188}Os_{mbc}$	2SE	$^{186}Os/^{188}Os_{mbc}$	2SE	$^{184}Os/^{188}Os_{mbc}$	2SE
18/10/2007	10	1.983942	0.000022	0.160920	0.000005	0.119919	0.000004	0.001298	0.000002
19/10/2007	10	1.983946	0.000025	0.160920	0.000004	0.119916	0.000004	0.001304	0.000002
22/10/2007	10	1.983984	0.000042	0.160921	0.000007	0.119919	0.000004	0.001306	0.000002
23/10/2007	10	1.984006	0.000045	0.160916	0.000005	0.119917	0.000004	0.001301	0.000002
24/10/2007	10	1.983924	0.000038	0.160913	0.000007	0.119917	0.000004	0.001306	0.000002
25/10/2007	10	1.983953	0.000037	0.160918	0.000006	0.119916	0.000004	0.001305	0.000002
17/12/2007	10	1.984009	0.000066	0.160916	0.000005	0.119915	0.000005	0.001303	0.000001
18/12/2007	10	1.984026	0.000030	0.160911	0.000005	0.119914	0.000005	0.001307	0.000002
15/01/2008	10	1.983989	0.000045	0.160915	0.000006	0.119923	0.000005	0.001312	0.000004
16/01/2008	10	1.984087	0.000035	0.160922	0.000003	0.119919	0.000004	0.001305	0.000001
31/01/2008	10	1.984076	0.000056	0.160915	0.000008	0.119915	0.000004	0.001306	0.000002
04/02/2008	10	1.984077	0.000039	0.160927	0.000004	0.119920	0.000003	0.001310	0.000002
18/02/2008	10	1.984030	0.000044	0.160926	0.000003	0.119918	0.000005	0.001301	0.000002
11/11/2008	10	1.983974	0.000027	0.160925	0.000004	0.119913	0.000006	0.001302	0.000004
12/11/2008	10	1.983967	0.000035	0.160933	0.000005	0.119922	0.000006	0.001300	0.000005
13/11/2008	10	1.983952	0.000035	0.160916	0.000003	0.119923	0.000003	0.001304	0.000002
14/11/2008	10	1.983952	0.000030	0.160919	0.000004	0.119924	0.000005	0.001310	0.000004
19/11/2008	10	1.983959	0.000019	0.160916	0.000003	0.119909	0.000004	0.001298	0.000002
20/11/2008	10	1.983966	0.000018	0.160925	0.000006	0.119922	0.000003	0.001308	0.000003
08/07/2009	10	1.983927	0.000021	0.160920	0.000002	0.119918	0.000002	0.001305	0.000001
13/07/2009*	10	1.978623	0.000093	0.160925	0.000003	0.119917	0.000003	0.001302	0.000001
14/07/2009*	10	1.978634	0.000026	0.160930	0.000001	0.119915	0.000003	0.001299	0.000001
08/12/2009	12	1.983964	0.000012	0.160922	0.000003	0.119920	0.000002	0.001304	0.000002
20/01/2010	15	1.983987	0.000008	0.160916	0.000003	0.119920	0.000003	0.001303	0.000002
25/01/2010	15	1.984008	0.000019	0.160914	0.000002	0.119917	0.000002	0.001300	0.000003
08/03/2010	15	1.983964	0.000013	0.160921	0.000004	0.119918	0.000003	0.001302	0.000003
09/03/2010	15	1.983960	0.000013	0.160906	0.000002	0.119917	0.000003	0.001305	0.000002
10/03/2010	15	1.983976	0.000014	0.160905	0.000004	0.119921	0.000003	0.001303	0.000002
11/03/2010	15	1.983941	0.000017	0.160915	0.000003	0.119914	0.000002	0.001299	0.000002
12/03/2010	15	1.983979	0.000019	0.160923	0.000004	0.119919	0.000004	0.001304	0.000003
All	**337**	**1.983982[a]**	**0.000007[a]**	**0.160919**	**0.000001**	**0.119918**	**0.000001**	**0.001304**	**0.000001**
Reproducibility (= 2SD/mean) (ppm)		**63[a]**		**117**		**109**		**8024**	
Nowell et al. (2008a)	21	1.983979	0.000030	0.160916	0.000004	0.119909	0.000004	0.001298	0.000002
Nowell et al. (2008b)	5	1.983943	0.000089	0.160921	0.000018	0.119917	0.000020	0.001303	0.000007
Durham N-TIMS (Luguet et al., 2008)	8	1.983803	0.000016	0.160924	0.000004	0.119932	0.000006	0.001306	0.000006

** Sessions with irregular Neptune amplifier behaviour. [a] Calculated excluding data from 13/07/09 and 14/07/09. $_{mbc}$ = mass bias corrected. Disparity between $^{190}Os/^{188}Os$ value of this study and N-TIMS value results from mass bias correction of N-TIMS data using the $^{192}Os/^{188}Os$ ratio.*

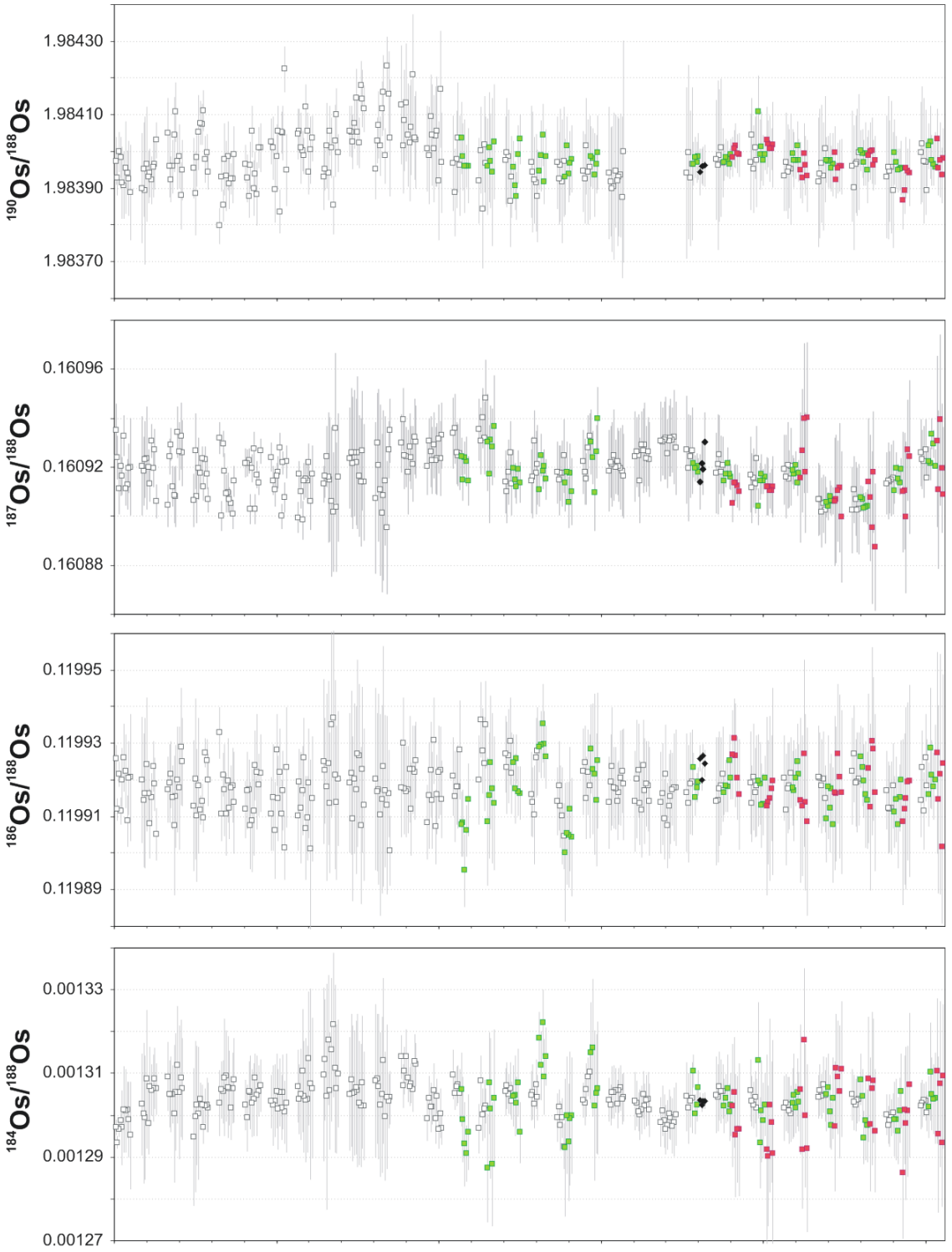

Figure 2. 1 Long term and within-run reproducibility of DROsS solution Os isotope measurements. Pure 1 ppm DROsS, white; 1 ppm DROsS + 0.05 ppm W +0.01 ppm Re, green; 1 ppm DROsS + 0.1 ppm W + 0.01 ppm Re, pink; 1.5 ppm DROsS + 0.1 ppm W + 0.1 ppm Re, black diamonds. $^{190}Os/^{188}Os$ data collected on 13/07/2009 and 14/07/2009 are not shown, see text for explanation (section 2.5.1). 2σ errors.

Mean mass bias corrected isotopic compositions of the DROsS RM solution analysed during 30 laser ablation analytical sessions from 18/10/2007 to 12/03/2010 are presented in Table 2.2. Mean DROsS values from studies by Nowell et al. (2008a, b; measured by MC-ICPMS using the Durham Neptune) and Luguet et al. (2008; measured by N-TIMS) are shown for comparison. Values for $^{187}Os/^{188}Os$, $^{186}Os/^{188}Os$ and $^{184}Os/^{188}Os$ compare favourably with the published data, and long term reproducibility on each ratio is excellent given that data were collected over a period of approximately two and a half years (Fig. 2.1). Reproducibility within individual analytical sessions is also very good for these ratios, ranging from 26 to 160 ppm (2SD) for $^{187}Os/^{188}Os$, 50 to 154 ppm for $^{186}Os/^{188}Os$ and 2.2 to 11.0 ‰ for $^{184}Os/^{188}Os$ (Appendix 1).

Long term reproducibility on the $^{190}Os/^{188}Os$ ratio is poor relative to the other Os ratios at 1279 ppm, and the mean $^{190}Os/^{188}Os$ value of 1.983664 is 150 ppm lower than the average of the published MC-ICPMS data (Table 2.2; Nowell et al., 2008a, b). However, within-session reproducibility on this ratio over the 2.5 year period varied between 16 and 148 ppm. During the 13/07/2009 and 14/07/2009 analytical sessions $^{190}Os/^{188}Os$ ratios were low (mean = 1.978623 and 1.978634 respectively), although reproducibility on this ratio remained at typical values in both sessions (148 and 41 ppm respectively). The low values for the $^{190}Os/^{188}Os$ ratio obtained on the 13/07/2009 and 14/07/2009 sessions were a consequence of a problem with the AU-Interface board in the amplifier unit of the Neptune. The $^{190}Os/^{188}Os$ data from these sessions have been excluded from calculations of overall mean, reproducibility and standard error for the standard solutions (Table 2.2) in order to avoid bias; full disclosure of standard solution data can be found in Appendix 1. Despite the aforementioned problem with the Neptune in July 2009, the excellent isochron correlation exhibited by Bushveld PGM (Chapter 3, Fig. 3.3) analysed during six analytical sessions over a period of eight months demonstrates the consistency of data collected not only between sessions, but before and after instrument ‘down time’.

2.4 Laser ablation

After analysis of DROsS RM solutions at the beginning of each session a manual valve was used to switch the output of the nebuliser and spray-chamber for a New Wave UP213 laser for the analysis of PGM grains. Grains were either mounted in polished resin blocks or on adhesive carbon SEM tabs. It does not appear that the method of mounting has any effect on isotopic measurements within the analytical resolution of this method. The laser ablation cell was connected directly to the Neptune torch via a Teflon out line and not via the built-in bypass and purge valve system of the UP213, since significant trapping of particulate matter has been shown to occur within these valves and can be a major source of cross contamination of samples.

Table 2. 3 UP213 Operating conditions for LA Os isotopic analysis of PGM grains

Parameter	Value
Wavelength	213 nm
Ablation cell	Std New Wave cell
Carrier gas	Ar
Carrier gas flow rate	1.5 l min^{-1}
Spot diameter	60 - 140 µm depending on Os content of sample
Crater depths	~40 - 80 µm
Repetition rate	10 - 20 Hz
Laser power	10 - 100 % depending on Os content of sample
Laser power density	~2 - 7 J cm^{-2}

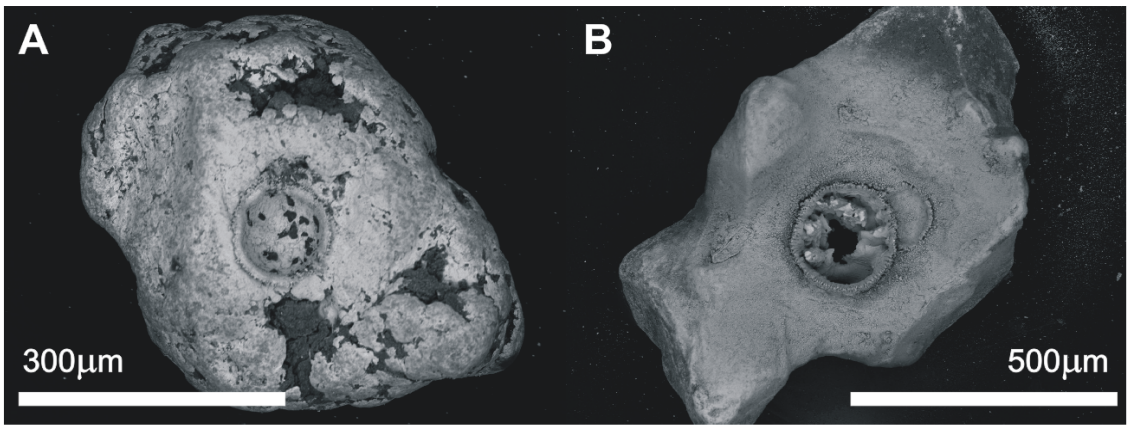

Figure 2. 2 Typical laser ablation pits in A) a PGE sulphide and B) a PGE alloy.

Fixed value and variable laser parameters used in the 30 analytical sessions are presented in Table 2.3. Figure 2.2 shows a characteristic ablation pit in A) a PGE sulphide and B) a PGE alloy after a typical 40 s analysis. The use of He as the carrier gas was unnecessary as there was rarely any problem obtaining a suitable Os signal, instead Ar was used as the carrier gas, although it is recognised that this may increase the levels of inter-element fractionation. The mixed PGM in the populations analysed for this project have, by definition, a variety of Os contents. Hence laser power, repetition rate and to a lesser extent spot size were tailored to produce the optimum signal possible for each grain. Higher Os signals were favoured since larger beam sizes minimize errors on IECs (section 2.5.2). Nowell et al. (2008b) state that ^{188}Os ion beam intensities of 2 – 14 V are preferable; the variety of PGM analysed for this thesis yielded average ^{188}Os ion beam intensities of ~ 0.0015 – 20.7 V. Very low beams result from the low Os concentrations of certain minerals, particularly braggite and sperrylite (i.e. very Pt-rich phases), while high Os signals were generally achieved for laurite and erlichmanite grains. Estimation of total transmission efficiency for Os during laser ablation is not possible due to a

lack of accurate compositional data for the material being ablated, though Nowell et al. (2008b) suggest that it is less than the 0.071 % determined for solutions Nowell et al. (2008a).

2.4.1 Ablation style: spots vs. line rasters

It has been argued that spot ablations allow greater potential for inter-element and even intra-element isotope fractionation relative to line or box rasters since the aspect ratio of a spot ablation is much greater than for a line or box raster. This has certainly been shown to be the case with U-Pb analyses (eg. Horstwood et al., 2003 and references therein). For most PGM samples any type of raster is precluded simply because of sample size. However, on large (> 400 µm) polished PGM there is the opportunity to perform ablations along linear tracks (a flat surface is required to ensure that the laser beam remains focused on the grain for the entirety of the analysis) to investigate possible fractionation processes. Line and spot ablations were measured on 15/12/2009 and 19/01/2010 for two isotopically homogeneous Urals grains, 36720-G4 and -G2, using static multi-collection routines of one block of 40 cycles (as described in section 2.2) with cycle integration times of 0.5, 1 and 4 s (total measurement times of 20, 40 and 160 s respectively). These grains have very low Re/Os and Pt/Os ratios which preclude an investigation of inter-element fractionation but the data do show evidence for intra-element isotope fractionation. It appears that during linear ablations the measured isotope ratios are dependant on the rate of raster - rapid ablations along a line of fixed length yield isotope ratios that are clearly biased in favour of the light isotope (Appendix 2, Fig. 2.3). It is likely that the laser beam moves too rapidly across the surface of the sample during these short acquisition analyses, preventing the critical ablation threshold being reached. In this case it is probable that instead of ablating the material the laser is primarily heating the sample. If so the sample may approach its boiling point, thus fractionation may occur, hence measurements of isotopic ratios are inaccurate. Since this would be a distillation-like process the ‘ablated’ material that is transferred to the mass spectrometer would be enriched in light isotopes, which is exactly what is observed (Fig. 2.3). As a result of these experiments it was decided that the spot analysis with a 1 s integration time was the routine best suited to the PGM samples, since it is rapid enough to allow analysis of the smallest samples, which would be entirely consumed by ablation before completion of a longer measurement routine, while producing accurate data with moderately low within-run errors.

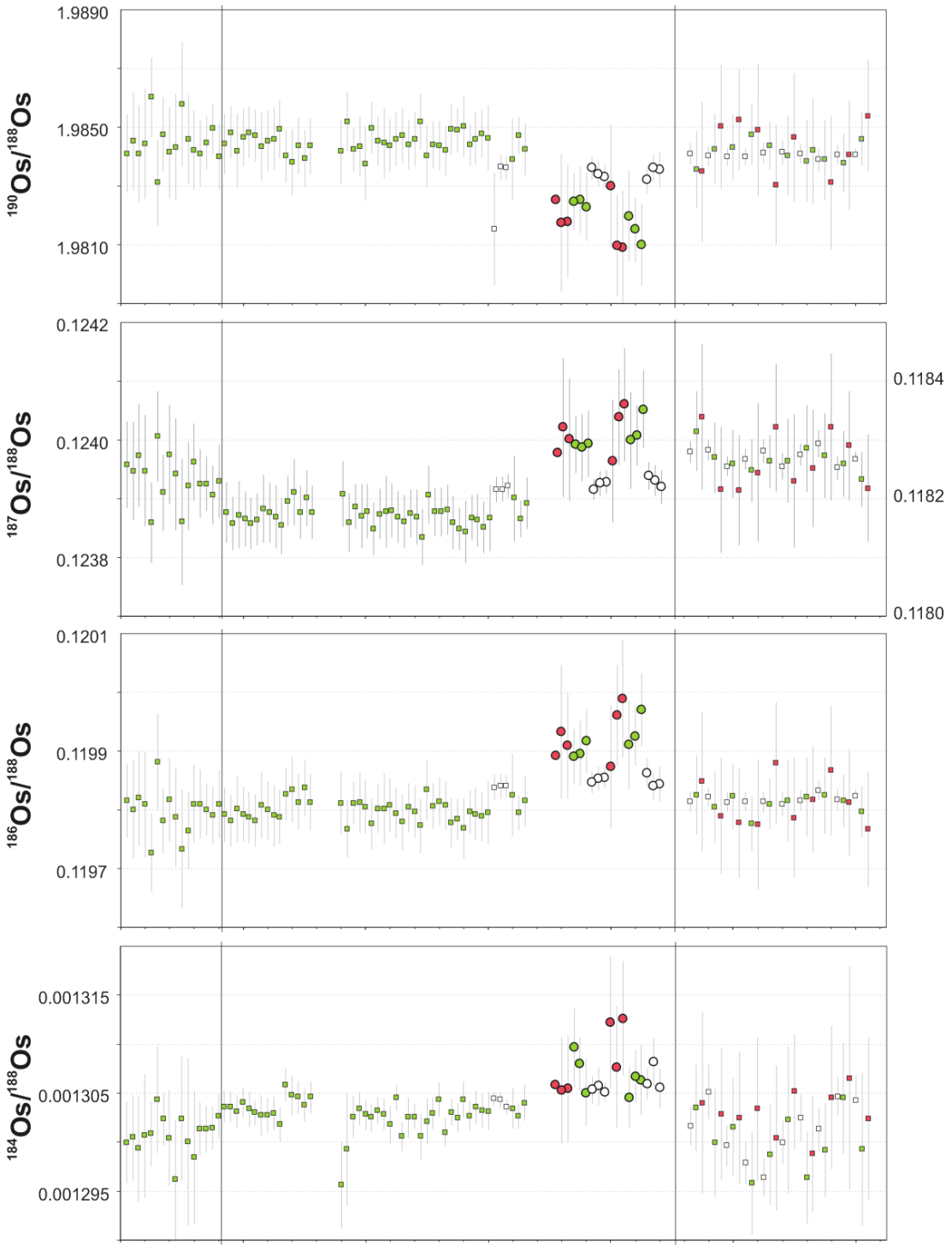

Figure 2. 3 Long term and within-run reproducibility for laser ablation MC-ICPMS Os isotope measurements of Urals 36720 (Os-rich) PGE alloys. For $^{187}Os/^{188}Os$ grain 4 is plotted on the secondary y-axis. Colours signify integration time: 0.5 s, pink; 1 s, green; 4 s, white. Squares indicate spot ablations, circles indicate raster ablations. Error bars are 2σ.

2.5 Mass bias and isobaric interference corrections

2.5.1 Mass bias correction

The Os isotope ratios most commonly used for mass bias corrections during MC-ICPMS analysis, or for mass fractionation during N-TIMS analysis, are the $^{192}Os/^{188}Os$ and $^{189}Os/^{192}Os$ ratios (Hirata et al., 1998; Walker et al., 2005; Shi et al., 2007). In order to exploit the full potential of the present LA-MC-ICPMS technique for Pt-Os chronology it is necessary to analyse grains with a range of parent/daughter isotope ratios for both the Pt-Os and Re-Os isotope systems, i.e. Pt-, Re- and Os-rich grains. In this case the $^{192}Os/^{188}Os$ and $^{189}Os/^{192}Os$ ratios are not ideal for making the mass bias corrections since there is an interference from ^{192}Pt on ^{192}Os. A correction can be applied for this interference by monitoring an interference-free Pt monitor isotope, such as ^{194}Pt, so that these ratios can be used for mass bias corrections. Indeed, this was the approach used by Walker et al. (2005) and Shi et al. (2007). Whilst this approach might be suitable for analysis of low-Pt grains, for Pt-rich grains (particularly those with Pt-rich heterogeneities that may not be resolved by SEM or probe analysis but which are sampled by laser ablation) it is advisable to use the interference free $^{189}Os/^{188}Os$ ratio to correct for instrumental mass bias (Hirata et al., 1998; Nowell et al., 2008b). This prevents errors in the ^{190}Pt interference correction on ^{192}Os being propagated onto other Os isotope ratios via the mass bias correction. A $^{189}Os/^{188}Os$ ratio of 1.21978 was used for the purpose of the mass bias correction (Nowell et al., 2008b).

In order to assess whether Os mass bias behaviour in MC-ICPMS more closely follows the power or exponential laws the natural logarithms of measured Os isotope ratio pairs are plotted in Figure 2.4. Repeat analyses of a standard material should define a linear trend on a ln-ln plot; the slope of this line is a function of the mass difference between the two isotope ratios and can be compared to the ideal slopes calculated using the power and exponential laws. Figure 2.4 shows various plots between $\ln(^{190}Os/^{188}Os)$, $\ln(^{189}Os/^{188}Os)$ and W interference-corrected $\ln(^{186}Os/^{188}Os)$ for the DROsS reference material. As shown in the studies of Nowell et al. (2008a, b), the high stability of instrumental mass bias for the Neptune is demonstrated within individual analytical sessions (two examples highlighted in Fig. 2.4), which exhibit narrow ranges of $\ln(^{189}Os/^{188}Os)$ and $\ln(^{186}Os/^{188}Os)$ values. As a result, little information regarding fit to a particular mass bias law can be garnered from individual sessions so it is necessary to consider data collected during all, or multiple, Os analytical sessions. Collectively, DROsS data collected during 30 analytical sessions define an excellent linear correlation on a plot of $\ln(^{189}Os/^{188}Os)$ versus $\ln(^{186}Os/^{188}Os)$ with a slope of -2.0091 ± 0.011 (Fig. 2.4A). This value is within 4.5 ‰ of the theoretical slope for exponential mass bias behaviour, while the theoretical slope for power

law mass bias is 11.6 ‰ lower than the DROsS slope. The DROsS data collected in this study are consistent with the Department of Terrestrial Magnetism (DTM) Os RM data of Nowell et al. (2008a, b), demonstrating that the Os mass bias during solution analysis on the Neptune MC-ICPMS is very similar to the exponential law. Hence the exponential law is used to correct for mass bias, consistent with standard practice for ICPMS.

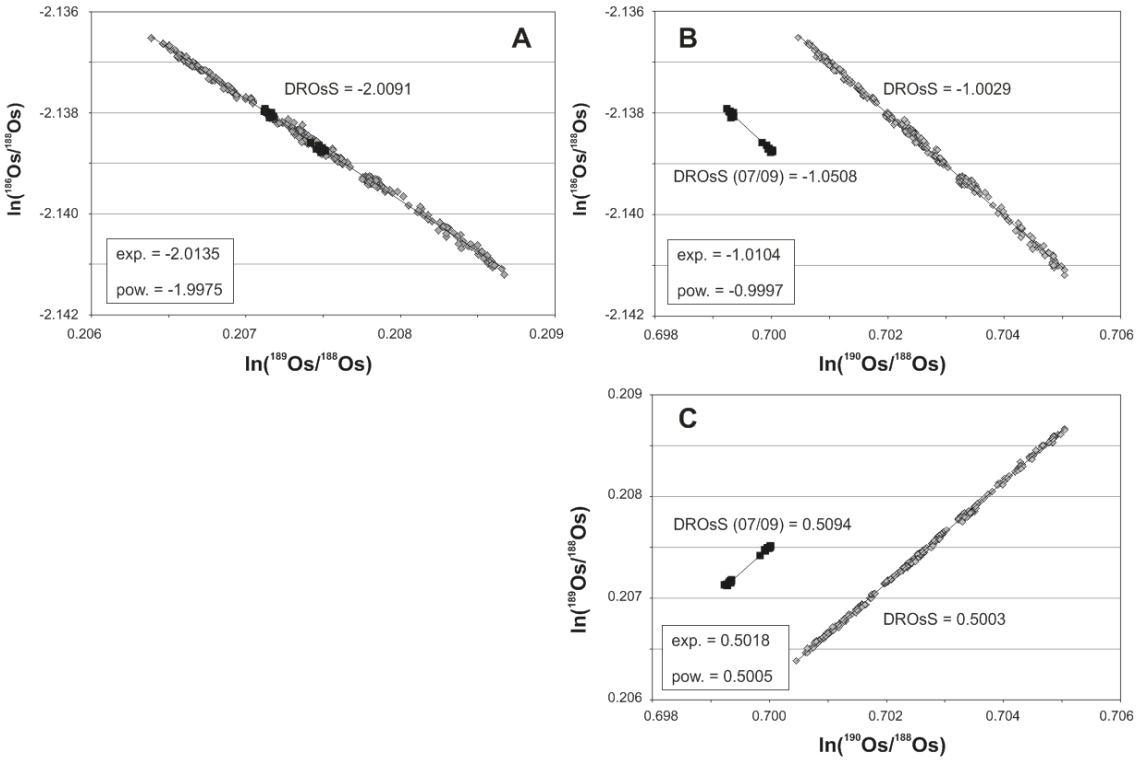

Figure 2. 4 Plots of A) ln(^{189}Os/^{188}Os) versus W interference corrected ln(^{186}Os/^{188}Os), B) ln(^{190}Os/^{188}Os) versus W interference corrected ln(^{186}Os/^{188}Os), and C) ln(^{190}Os/^{188}Os) versus ln(^{189}Os/^{188}Os) for all DROsS solution data. The excellent correlation on all plots demonstrates the stability of Os mass bias behaviour during solution MC-ICPMS analyses, both within and between analytical sessions (data from individual analytical sessions on the 13/07/2009 and 14/07/2009 are highlighted in black). Despite problems with the Neptune amplifiers (see text for details) on the 13/07/2009 and 14/07/2009, which cause an offset in measured ^{190}Os/^{188}Os values, Os mass bias behaviour is consistent with the rest of the data. Theoretical slopes calculated using the exponential and power laws are shown for each plot (text boxes). The data plotted in A) define a slope of -2.0091 ± 0.011, which is within 4.5 ‰ of the theoretical slope for exponential mass bias behaviour and 11.6 ‰ lower than the theoretical slope for power law mass bias behaviour.

Figures 2.4B and C show a disparity between the data collected for DROsS solutions analysed in sessions on 13/07/2009 and 14/07/2009. Data collected in these two sessions are clearly displaced from the trend defined by the other analytical sessions but, nevertheless, still define near identical slopes to the rest of the data on ln(^{190}Os/^{188}Os) versus ln(^{186}Os/^{188}Os) and

ln(^{190}Os/^{188}Os) versus ln(^{189}Os/^{188}Os) plots. This indicates that the mass bias behaviour during these 'anomalous' sessions was consistent with the long term behaviour. The low ln(^{190}Os/^{188}Os) values are an artefact of the malfunction of the AU-Interface board in the amplifier unit of the Neptune, as mentioned in section 2.3. Figure 2.5 demonstrates the undesirable behaviour of the Neptune amplifiers on 13/07/2009 and 14/07/2009. On these dates a very clear 'kick' is seen in the relative gains of the amplifiers assigned to the L1, Ax, H1 and H2 Faraday cups compared to L4, L3, L2 and H3, H4 cups. Despite this amplifier problem, data collected from Bushveld PGM samples before, during and after the malfunction display a very strong correlation when used together to construct a Pt-Os isochron, implying that the data were not significantly affected by this issue.

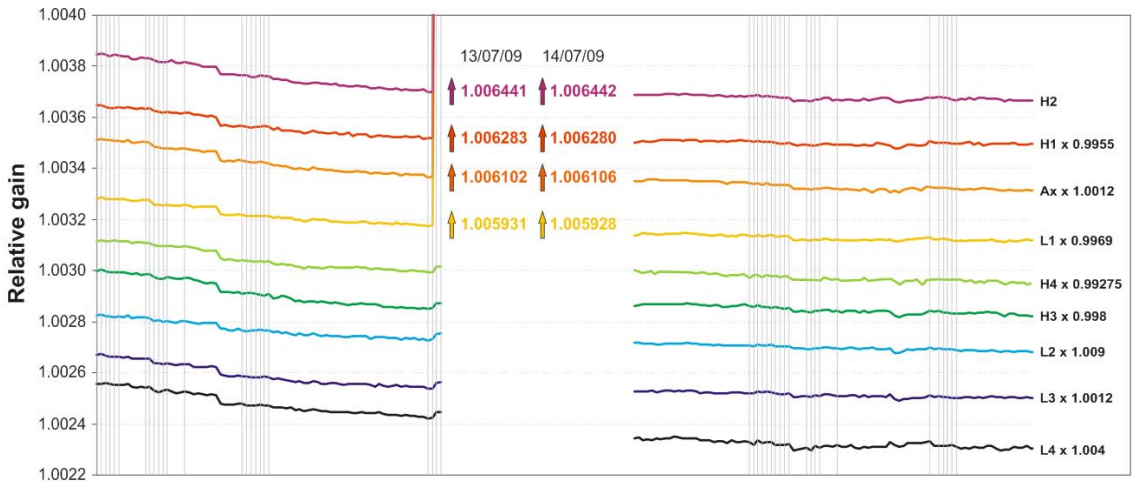

Figure 2. 5 Relative gains for each of the nine Neptune amplifiers over a period of ~2.5 years. Vertical grey lines indicate sessions when Os analyses were carried out. On 13/07/2009 and 14/07/2009 the amplifiers assigned to the L1, Ax, H1 and H2 Faraday cups experienced a very pronounced 'kick' in relative gains due to a malfunction on the AU-Interface board in the Neptune amplifier unit. The strong correlation and accurate age yielded by a Pt-Os isochron for Bushveld PGM constructed using data collected before, during and after this 'kick' suggests that any effect on the data was negligible.

Evaluation of Os mass bias behaviour during laser ablation PGM analysis is complicated by the potential for Pt interferences on ^{190}Os and ^{192}Os and the natural variation in the radiogenic ^{187}Os/^{188}Os and ^{186}Os/^{188}Os compositions of such phases. Figure 2.6 shows that the Os mass bias behaviour of PGM from the Bushveld Complex, Borneo and California is consistent with the DROsS solution data in terms of the natural logarithms of measured ^{190}Os/^{188}Os and ^{189}Os/^{188}Os and W interference corrected ^{186}Os/^{188}Os values. As anticipated, data from each PGM location lie on the same linear array as the DROsS solutions, however numerous grains from each of the localities also exhibit considerable, yet systematic scatter relative to the standard solutions.

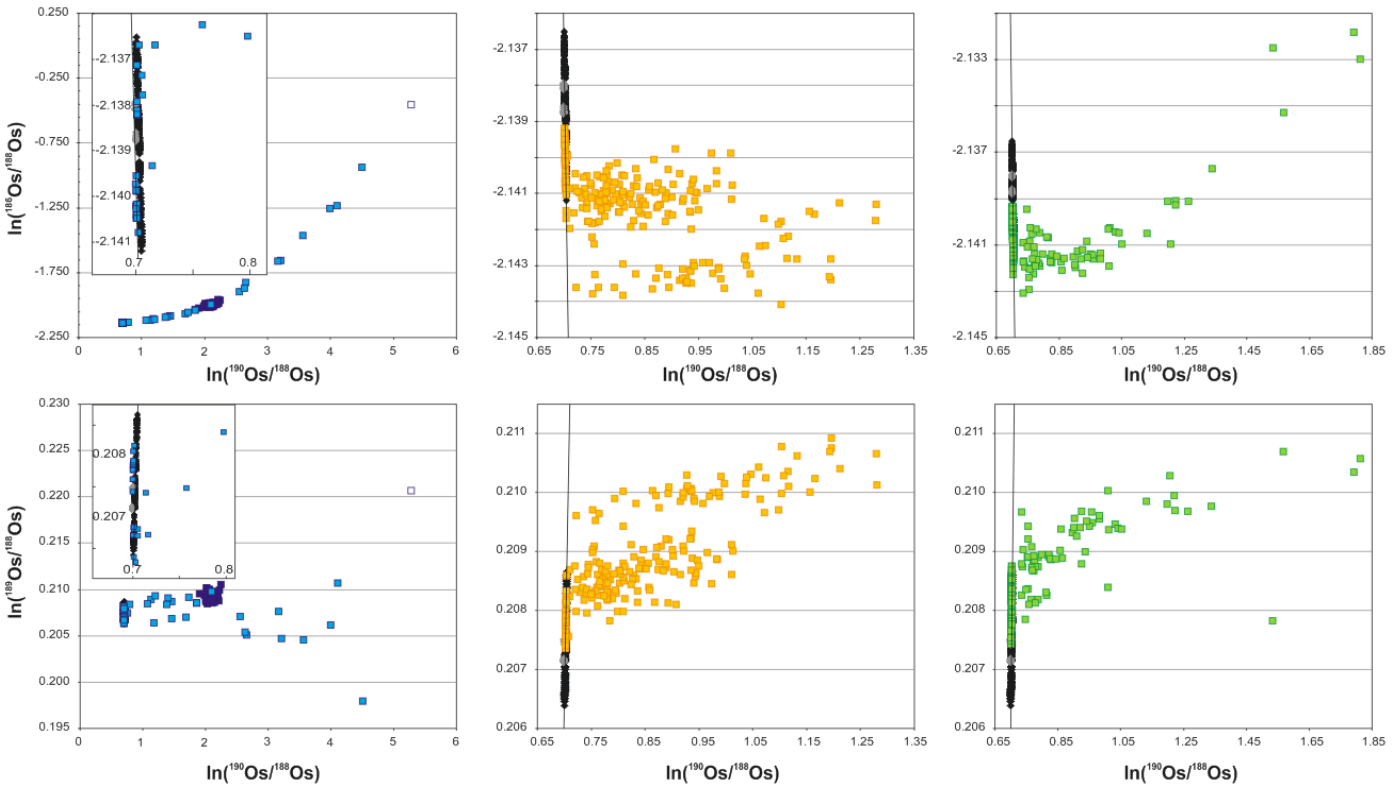

Figure 2. 6 ln(^{190}Os/^{188}Os) versus W interference corrected ln(^{186}Os/^{188}Os) and ln(^{190}Os/^{188}Os) versus ln(^{189}Os/^{188}Os) plots for PGM from the Bushveld Complex (Merensky Reef, pale blue; Onverwacht, dark blue; Tweefontein Hill, white), Borneo (yellow) and California (green). Os mass bias behaviour during laser ablation MC-ICPMS PGM analysis is consistent with DROsS solution data (black, and 13/07/2009 + 14/07/2009 DROsS, grey), with many PGM defining the same slope. PGM rich in time-integrated Pt exhibit scatter relative to the DROsS values.

2.5.2 Non-molecular isobaric interference corrections

An advantage of N-TIMS and solution-mode MC-ICPMS over laser ablation MC-ICPMS for the analysis of Os and for most isotope systems is that, for the former, non-molecular isobaric interferences can be eliminated or minimised via column chemistry and purification of the analyte, whereas with laser ablation the whole sample matrix is introduced in to the mass spectrometer. Thus laser ablation analysis of PGM results in a more complex mass spectrum and a greater potential for non-molecular and molecular isobaric interferences on the analyte element. High mass resolution can be implemented in order to eliminate molecular isobaric interferences from the analyte during ICPMS analysis (Weyer and Schwieters, 2003; Nowell et al., 2008a), however it is also associated with a significant loss in sensitivity. Additionally, in the case of Os (atomic number 76) the potential mixture of hydride, oxide and other more complex but unlikely molecular interferences (depending on matrix composition) can occur at both higher and lower masses than the analyte. In the case where molecular interferences occur on both the high- and low- mass side of the analyte peak at the same time the high "edge" resolution approach used in isotope ratio measurements, where the edge of the collector slit is used to mask the interference, cannot be used. Furthermore, many of the more likely potential molecular interferences require a mass resolution in excess of the maximum MR of 10,000 available with the Neptune, and other MC-ICPMS. Despite not being able to resolve molecular interferences within the analytical resolution of the present LA-MC-ICPMS technique we see no clear evidence (such as sporadic data points) for molecular isobaric interferences, although this does not exclude their presence.

Non-molecular elemental isobaric interferences are more problematic during laser ablation analysis of PGMs and must be corrected for algebraically, which is accomplished via measurement of interference-free monitor isotopes. The main elemental interferences on Os are from Re and W which affect the radiogenic isotopes ^{187}Os and ^{186}Os respectively. In addition, W interferences on the stable ^{184}Os isotope and a minor interference from Pt occurs on the stable ^{190}Os and ^{192}Os isotopes.

In order to correct for Re and W interferences on ^{187}Os, ^{186}Os and ^{184}Os the ^{185}Re and ^{182}W intensities were monitored during each analysis. Initially, values derived by Nowell et al. (2008a) for the ^{185}Re/^{187}Re, ^{182}W/^{186}W and ^{182}W/^{184}W IERs necessary for accurate IECs were used. From February 2008 onwards the analytical routine was modified to assess variability in these ratios between sessions. Subsequently, these ratios were derived at the start of each analytical session via analysis of two 1 μg ml^{-1} DROsS standard solutions doped with different

concentrations of Re and W and a pure 1 μg ml^{-1} DROsS solution. The data collected for these three solutions were then regressed to derive each of the IERs. The IER values derived are specific to this MC-ICPMS instrument. They are the most appropriate values for application of precise and accurate IECs, but are in no way suggested as new determinations of the 'true' stable isotope ratios for W and Re. Long term reproducibility for these ratios is shown in Table 2.4 and DROsS solution data are reported in full in Appendix 1. It should be noted that despite ~ 100 ppm variation on the IERs (~ 8 ‰ on $^{182}W/^{184}W$) over approximately two years, the magnitude of the corrections applied is very small; hence the absolute variation is negligible.

Table 2. 4 Long term variation in interfering element ratios

Analytical session	Interfering element ratios		
	$^{182}W/^{184}W$	$^{182}W/^{186}W$	$^{185}Re/^{187}Re$
18/10/2007	0.863376	0.929231	0.598050
19/10/2007	0.863376	0.929231	0.598050
22/10/2007	0.863376	0.929231	0.598050
23/10/2007	0.863376	0.929231	0.598050
24/10/2007	0.863376	0.929231	0.598050
25/10/2007	0.863376	0.929231	0.598050
17/12/2007	0.863376	0.929231	0.598050
18/12/2007	0.863376	0.929231	0.598050
15/01/2008	0.863376	0.929231	0.598050
16/01/2008	0.863376	0.929231	0.598050
31/01/2008	0.863376	0.929231	0.598050
04/02/2008	0.863376	0.929231	0.598050
18/02/2008	0.863376	0.929231	0.598050
11/11/2008	0.863302	0.929014	0.598098
12/11/2008	0.863376	0.929130	0.598098
13/11/2008	0.863376	0.929130	0.598098
14/11/2008	0.863376	0.929130	0.598098
19/11/2008	0.863302	0.929014	0.598098
20/11/2008	0.863302	0.929014	0.598098
08/07/2009	0.863346	0.929139	0.598159
13/07/2009	0.863346	0.929139	0.598159
14/07/2009	0.863346	0.929139	0.598159
08/12/2009	0.863332	0.929147	0.598036
20/01/2010	0.863332	0.929147	0.598036
25/01/2010	0.863332	0.929147	0.598036
08/03/2010	0.863410	0.929210	0.598160
09/03/2010	0.863390	0.929210	0.598107
10/03/2010	0.863396	0.929255	0.598113
11/03/2010	0.863390	0.929205	0.598145
12/03/2010	0.863410	0.929240	0.598132
Average	*0.863365*	*0.929817*	*0.598083*
2SD	*0.000058*	*0.001574*	*0.000086*
2SDR (ppm)	*67*	*1693*	*143*

The interference-free ^{182}W and ^{183}W isotopes present an opportunity for derivation of W IERs relative to the measured W mass bias, however the analytical set-up allows only one Faraday cup for monitoring W. Since Re only has two isotopes, and only one of these is interference-free, we cannot derive the $^{185}Re/^{187}Re$ ratio relative to Re mass bias. Hence, in all cases IERs were

derived relative to the measured Os mass bias, i.e. Re and W mass bias were assumed to be equal to Os mass bias. The calibrated IERs were used to strip the appropriate amount of interference from each of the analyte isotopes. The correction was performed for each 1 s integration of every analysis and the uncertainty on the corrected Os isotope ratio incorporates the uncertainty of the correction.

The Faraday collector configuration used for this method does not provide an interference-free monitor isotope of Pt. Although is it possible to remove the H4 cup from alignment (as described in section 2.2), in order to analyse larger signal intensities on lower masses, the H4 cup cannot be used to measure mass 194. This limitation is due to the H4 cup being linked by a clamp to the motor driven H3 Faraday cup, which only allows for a maximum ~3 amu mass separation of H3 and H4 when mass 187 is in the axial position. As a consequence of this limitation of the analytical set-up the Pt isobaric interference on ^{190}Os cannot be corrected for in the same way as the Re and W interferences. Instead ^{190}Os is treated as the interfering element on ^{190}Pt. ^{188}Os is used as the monitor isotope and the correction is carried out using the same method as described for Re and W IECs. The ^{190}Os/^{188}Os interfering element ratio was calculated as the mean mass bias-corrected ^{190}Os/^{188}Os value, determined from DROsS analyses performed at the start of each session (Table 2.4). Stripping of the appropriate amount of ^{190}Os yielded the true ^{190}Pt signal, thus the ^{190}Pt/^{188}Os ratio could be derived and mass bias corrected. This method for deriving ^{190}Pt/^{188}Os is robust because ^{190}Os is a stable isotope and ^{189}Os and ^{188}Os are free of non-molecular interferences. As described in section 2.2, in order to analyse low-Os, Pt-rich grains it may be necessary to remove the H4 cup from alignment, as the ^{192}Pt signal may exceed the 50 V saturation limit of the cup. This high signal size would be exaggerated further if the H4 cup was used to monitor the interference-free ^{194}Pt isotope. Hence the method described here of treating Os as the interfering element is not only best suited to the limitations of the Durham Neptune, but also to the variable nature of the samples analysed using this data collection routine.

2.5.3 Accuracy of IECs

2.5.3.1 Rhenium

The majority of previous Re-Os laser ablation studies have neglected to place firm constraints on the accuracy of Re IECs, with attempts made only by Pearson et al. (2002) and Nowell et al. (2008a, b). Corrections for Re interferences during ablation analyses must be based on information from standard solutions by necessity, since no satisfactory PGE ablation standard has yet been defined. As discussed by Nowell et al. (2008a, b), performing such corrections

accurately is difficult due to two factors. Firstly, it is probable that the difference in mass bias behaviour of Os and Re is not constant between solution and laser ablation analyses due to matrix differences and variation in plasma loading. Secondly, any laser-induced fractionation of Re that occurs will alter the Re isotopic composition from the natural composition assumed when applying non-molecular isobaric interference corrections. The degree of consequential inaccuracy is dependent on the magnitude of the total interference correction and will affect any Re-Os isochron age calculated from the data (see below for further details).

Constraints in the literature on the maximum $^{187}Re/^{188}Os$ ratio that can be accurately corrected are varied (1.18, Pearson et al. 2002; 1.6, Shi et al. 2007; 3, Brueckner et al. 2004; 2 – 62, Košler et al. 2003), the most conservative having been suggested by Nowell et al. (2008b) as < 0.5. The maximum $^{187}Re/^{188}Os$ ratio measured for a PGM sample presented in this thesis is 0.32, comfortably shy of the lowest estimate for the maximum value that can be accurately corrected for with reasonable confidence. Nowell et al. (2008b) noted that Re IECs will also break down at low $^{187}Re/^{188}Os$ ratios if the Os beam intensities are low, due to inaccuracies on the measurement of mass 185. Though a deterioration is seen at lower 188 beam intensities, all PGM grains analysed in this study plot within the range of $^{185}Re/^{188}Os$ values measured for pure and doped DROsS standard solutions (Fig. 2.7A). Throughout this study no attempt is made to draw any age information from the Re-Os isotope system since it is advisable to treat laser ablation PGM Re-Os data with caution.

2.5.3.2 Tungsten and osmium

In an early laser ablation Os isotope study of PGM by Hirata et al. (1998) $^{186}Os/^{188}Os$ data were presented but there was no discussion of W corrections or evidence that the authors applied any to sample data. Since W and Os IECs affect the $^{186}Os/^{188}Os$ and $^{190}Pt/^{188}Os$ ratios, which are used to calculate Pt-Os isochron ages it is important to be assured of the accuracy of these corrections. Unlike with Re IECs where assessing the accuracy is difficult without reference material of known $^{187}Os/^{188}Os$ composition, accuracy of W IECs can easily be assessed since $^{184}Os/^{188}Os$ is a stable ratio and in low-Pt PGM the $^{186}Os/^{188}Os$ ratio is virtually invariant. Figure 2.7B demonstrates that the $^{182}W/^{188}Os$ values observed in PGM samples lie within the combined range of ratios measured for DROsS solutions and in-house reference PGM grains, though it is clear that the IECs deteriorate at low Os beam intensities, probably as a result of the high uncertainty on the measurement of ^{182}W at sub 0.1 mV intensities. Figure 2.8 shows that pure and W- and Re-doped DROsS standard solution data are consistent with the accepted $^{184}Os/^{188}Os$ and $^{186}Os/^{188}Os$ ratios for this reference material (Nowell et al., 2008a).

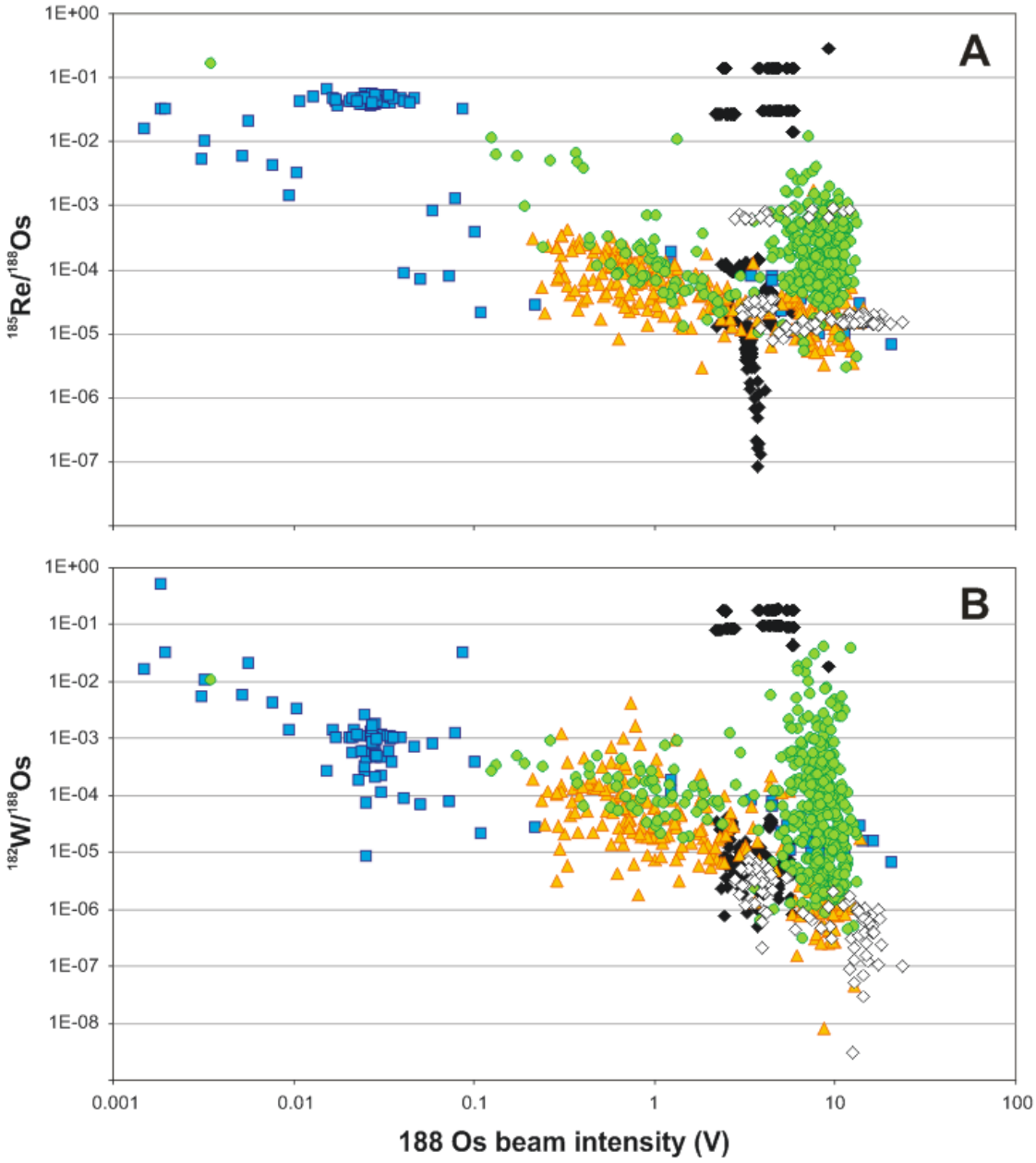

Figure 2. 7 ^{188}Os beam intensity versus $^{185}Re/^{188}Os$ (A) and $^{182}W/^{188}Os$ (B) for DROsS solutions (black diamonds), Urals 36720 PGM standard grains (white diamonds) and PGM from the Bushveld Complex (blue squares), Borneo (yellow triangles) and California (green circles). All PGM samples plot within the range of $^{185}Re/^{188}Os$ values reported for pure and doped DROsS standard solutions and all but one PGM fall within the combined range of $^{182}W/^{188}Os$ values for DROsS solutions and Urals PGM standard grains.

Os-poor PGM samples (those with ^{188}Os beams of between 0.1 and 1 V) show appreciable scatter about the accepted $^{184}Os/^{188}Os$ ratio, but their large uncertainties nevertheless place them within error of the accepted value of 0.001300 (Fig. 2.8A, C). Both the deviation and significant uncertainties result from very low Os beam intensities which are characteristic of Pt-

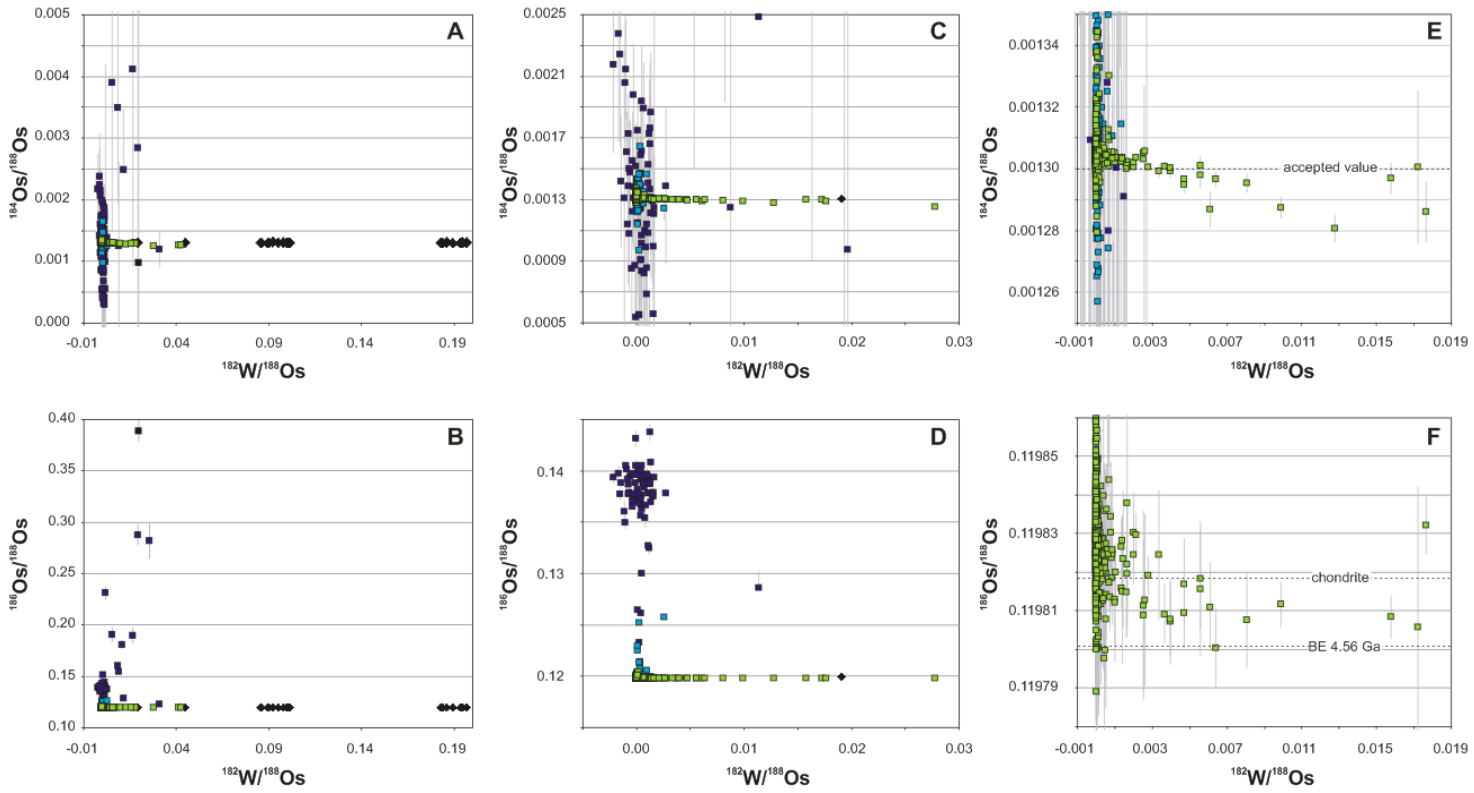

Figure 2. 8 $^{182}W/^{188}Os$ versus $^{184}Os/^{188}Os$ (A, C, E) and $^{186}Os/^{188}Os$ (B, D, F) plots for DROsS solutions (black diamonds) and PGM analyses (squares), divided by ^{188}Os beam intensity (< 0.1 V, dark blue; 0.1 – 1 V, light blue; > 1V, green). Pure and doped DROsS solutions plot within error of the accepted $^{184}Os/^{188}Os$ and $^{186}Os/^{188}Os$ ratios for this reference material. PGM analyses generally plot within error of the accepted $^{184}Os/^{188}Os$ ratio, though greater deviation, both above and below, and larger uncertainties are seen at the lowest Os beam intensities. For discussion of the accuracy of W IECs see text (section 2.5.3.2). Error bars are 1σ.

rich Os-poor grains. The time integrated Pt-rich nature of these grains is confirmed by their elevated $^{186}Os/^{188}Os$ ratios at relatively low $^{182}W/^{188}Os$ values (Fig. 2.8B, D), indicating that the excess signal at mass 186 results from radiogenic in-growth of ^{186}Os from ^{190}Pt rather than interference from ^{186}W. From Figure 2.8E it is apparent that some of the more Os-rich PGM (those with ^{188}Os beams of 1 V and above) also fall above and below the accepted $^{184}Os/^{188}Os$ value of 0.001300 at low $^{182}W/^{188}Os$ ratios, albeit far less so than for PGM with <<1V ^{188}Os (Fig. 2.8C), while at $^{182}W/^{188}Os$ ratios between 0.004 and 0.013 some samples are consistently displaced to low $^{184}Os/^{188}Os$ ratios. The slight scatter on the $^{184}Os/^{188}Os$ ratio at low $^{182}W/^{188}Os$ is due to an unreliable ^{184}W IEC at low Os beam intensities, since even when 1V is achieved for ^{188}Os the ^{184}Os signal remains very small (^{184}Os intensity at 1V ^{188}Os = 1.5mV) at only one order of magnitude above the noise of the amplifiers at 1s integration times. The displacement of those samples below the accepted value at elevated $^{182}W/^{188}Os$ may be due to some slight over-correction for W but this is not a certainty as the two PGM grains with the highest $^{182}W/^{188}Os$ actually have corrected $^{184}Os/^{188}Os$ ratios that are extremely close to the accepted value. Despite the obvious issues with reliability of W IECs at low Os beam intensities and/or elevated $^{182}W/^{188}Os$ this is really only evident on the $^{184}Os/^{188}Os$ ratio. The $^{186}Os/^{188}Os$ ratio remains quite robust since the W IEC is a factor of approximately 87 smaller in magnitude thus there is a huge relative demagnification in error. This is clearly illustrated in Figure 2.8F where PGM with > 1V of ^{188}Os cluster around the accepted $^{186}Os/^{188}Os$ value for chondrite (Walker et al., 2005; the regular ~100 ppm excursion below the present-day chondritic $^{186}Os/^{188}Os$ ratio results from the use of a different mass bias correction ratio in this study; Nowell et al., 2008a, b). Obviously some PGM lie above the chondrite value but these have elevated Pt/Os ratios and so the elevated $^{186}Os/^{188}Os$ is simply due to radiogenic in-growth of ^{186}Os. Importantly, only six grains out of 708 have $^{186}Os/^{188}Os$ ratios lower than the bulk Earth initial ratio and so can be considered unreliable. Furthermore, unlike with the $^{184}Os/^{188}Os$ ratio, those PGM with elevated $^{182}W/^{188}Os$ do not show a consistent displacement to low $^{186}Os/^{188}Os$ ratios (Fig 2.8F). Therefore we infer that for $^{186}Os/^{188}Os$ ratios there is no major issue with the W correction for the PGM analysed in this study.

The accuracy of the interference correction for Os on ^{190}Pt is difficult to assess since the $^{190}Pt/^{188}Os$ ratio may also be subject to inter-element fractionation (see section 2.6.1). However, the precise and accurate Pt-Os isochron presented for Bushveld PGM (Chapter 3, Fig. 3.3) implies that either Pt/Os fractionation is very low and Os IECs are accurate, or a fortuitous combination of coincidences has occurred. In any case the absolute Os IEC on ^{190}Pt is small at high Pt/Os ratios since there is little ^{190}Os present, while at very low Pt/Os ratios the magnitude of the Os IEC correction might be greater but the Pt/Os ratio undergoing correction is low so that the absolute shift of the correction is small. Figure 2.9 shows two isochrons plotted using pre-

and post-W IEC data for PGM from the Merensky Reef of the Bushveld Complex. Both ages are within error of each other, demonstrating that the absolute effect of W IECs on the isochron age is minor.

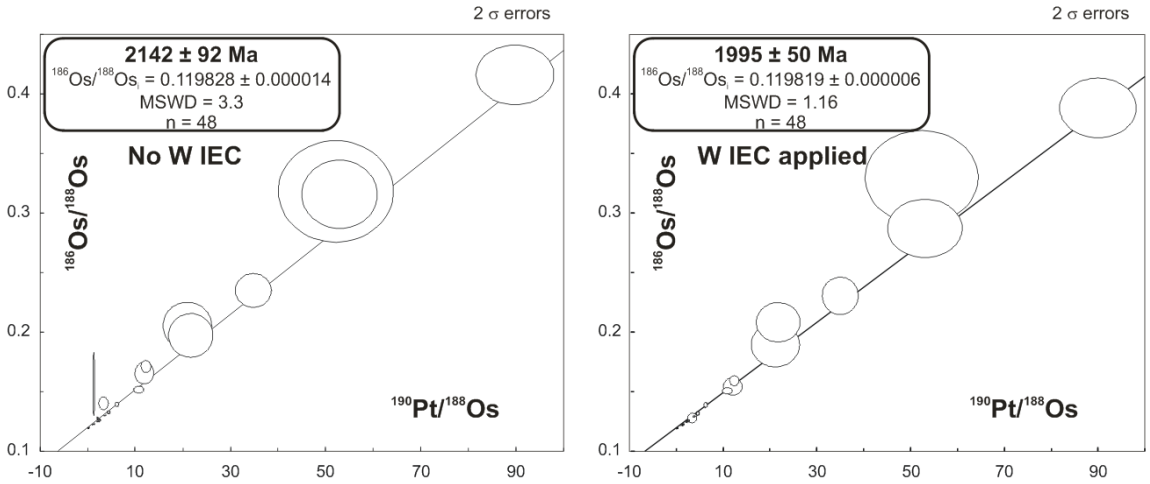

Figure 2. 9 Pt-Os isochrons for Merensky PGM constructed using data before and after application of W IECs. The two isochron ages are within error of each other, showing that the effect of W IECs on the accuracy of Pt-Os isochrons is relatively small. Despite a significant shift in the $^{186}Os/^{188}Os$ values of some of the more Pt-rich grains, there is no systematic change in this ratio with increasing Pt/Os ratio, hence no systematic rotation of the isochron, which would cause a change in the age, occurs.

2.5.3.3 Potential effects of IECs on Pt-Os and Re-Os isochrons

In the case of the β-decay Re-Os chronometer ^{187}Re is isobaric on its daughter isotope ^{187}Os so any inaccuracy with the Re IECs affects both the $^{187}Os/^{188}Os$ and $^{187}Re/^{188}Os$ ratios. The effect of any systematic error with the Re IEC will increase in magnitude as the parent/daughter ratio increases resulting in the rotation of any isochron and a resultant error in the calculated age (Fig. 2.10A). In contrast, the ^{190}Pt parent isotope of the α-decay Pt-Os chronometer is not isobaric on the ^{186}Os daughter and so does not affect both the x- and y- axes of the isochron plot. It is, however, isobaric with the stable ^{190}Os isotope so an interference correction is necessary to derive the x-axis $^{190}Pt/^{188}Os$ parent/daughter ratio. The interference correction necessary to derive the $^{190}Pt/^{188}Os$ ratio has no influence on the $^{186}Os/^{188}Os$ so any inaccuracy causes a horizontal translation of a Pt-Os isochron (Fig. 2.10B). Furthermore, because the present method corrects for interference of ^{190}Os on ^{190}Pt, the magnitude of the IEC actually diminishes with increasing parent/daughter ratio, unlike with Re-Os.

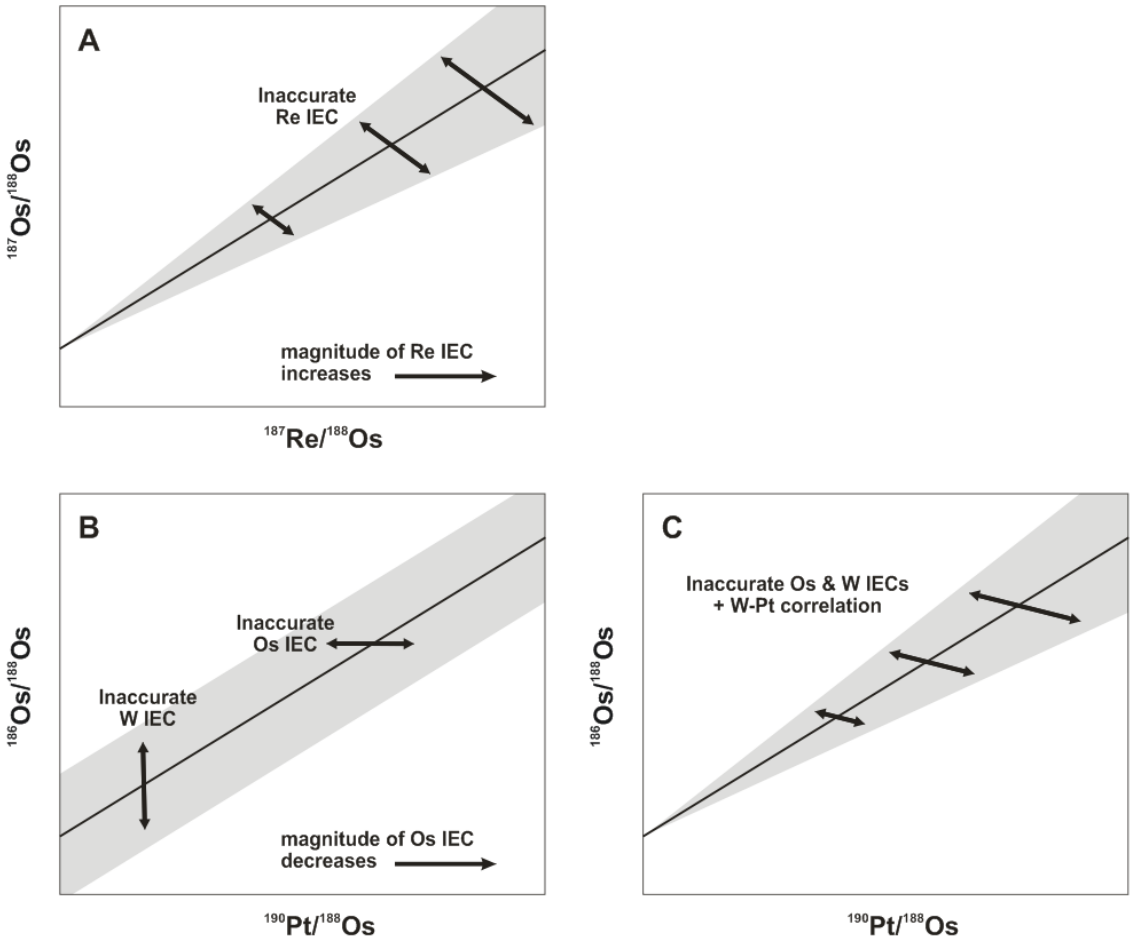

Figure 2. 10 Schematic diagrams illustrating the effects of inaccurate Re IECs on Re-Os (A) and W and/or Os IECs on Pt-Os (B, C) isochrons.

The $^{186}Os/^{188}Os$ ratio suffers an interference from ^{186}W; this only affects the y-axis of the Pt-Os isochron so any inaccuracy of the W IEC will manifest itself in a vertical translation of the Pt-Os isochron (Fig. 2.10B). Hence, in the simplest scenario any inaccuracy in either the Os or W IECs will cause a non-rotational transformation of the isochron so the age remains unaffected. The initial $^{186}Os/^{188}Os$ ratio calculated from the isochron will be affected by inaccuracies in the Os and/or W IECs, however this can be easily recognised in Pt-Os isochrons since the total variation in $^{186}Os/^{188}Os$ in the mantle over Earth history amounts to only 88 ppm. In more complex situations where there is correlation between Pt/Os and W/Os in the samples used to construct a Pt-Os isochron it would be possible to produce rotation of the isochron and hence an erroneous age through inaccuracies in the Os and/or W IECs (Fig. 2.10C). Fortunately there is no clear correlation in the case of the Borneo and California datasets presented in this thesis. There is a general trend in the Bushveld Merensky data with more Pt-rich phases showing some enrichment in W, but there is no linear relationship between the two variables. As a result, any

inaccuracies in the necessary IECs will cause unpredictable translation of grains on an isochron plot (as shown in Fig. 2.9) but no systematic rotation of isochrons constructed using these data.

2.6 Estimating external reproducibility

No mixed-PGE alloy or sulphide solid ablation reference material exists for use in quantifying total transmission efficiency, degree of inter-element fractionation, accuracy of IECs during laser ablation analysis and reproducibility and accuracy of Os isotope ratios. However, natural PGE alloys from the Ural Mountains, Russia, (sample number 36720) have been analysed repeatedly by Nowell et al. (2008b) and during data collection for this thesis and have proven to be isotopically homogeneous within the analytical resolution of the method. Overall reproducibility for $^{186}Os/^{188}Os$ measurements of Urals grain 36720-G1 over a period of ~ one year (176 ppm; n = 16) was used as an estimate of external reproducibility for these ratios for laser ablation of PGM with average ^{188}Os beam intensities of 1 V or more. The value for external reproducibility was incorporated with internal reproducibility (within-run error) for each sample and the error propagation calculation was applied to give an estimate of total errors on the $^{186}Os/^{188}Os$ measurement.

A disadvantage of using the Urals grain 36720-G1 as an ablation reference material is that it is Pt-poor, unlike many of the sample grains analysed. As such, estimates of reproducibility based on 36720-G1 are better suited to PGM samples with similar Os contents and beam intensities. Pt-rich, Os-poor samples have much lower Os beams, therefore PGM which yielded ^{188}Os beam intensities lower than 1 V were allocated an arbitrary value for external reproducibility of 352 ppm (= 2 x 176 ppm). It may be argued that this value ought to be increased further although the effect of doing so on the $^{186}Os/^{188}Os$ ratio would be to reduce the MSWD of any Pt-Os isochrons. The further the value is increased the better the fit of the data would appear despite a lack of any actual improvement in the data themselves.

Unfortunately the $^{190}Pt/^{188}Os$ ratio for grain 36720-G1 is too low (0.000080±0.000411; Nowell et al., 2008b) to be of use in estimating external reproducibility on $^{190}Pt/^{188}Os$ ratios. However, this is not a significant problem since the majority of the error on $^{190}Pt/^{188}Os$ measurements is derived from the within-run error, which dwarfs the long term reproducibility for measurements of this ratio. Total errors on $^{190}Pt/^{188}Os$ measurements incorporate within-run errors plus an estimate of potential inter-element fractionation during ablation between Pt and Os (see below for full details of this estimate) and long term reproducibility.

2.6.1 Constraints on inter-element fractionation of parent/daughter ratios during laser ablation

The accuracy of parent/daughter ratios obtained by LA-MC-ICPMS is affected by the accuracy of any necessary IECs, as discussed in section 2.5.3, but is further complicated by the occurrence of inter-element fractionation (Fryer et al., 1995; Mank and Mason, 1999; Horn et al., 2000; Günther and Hattendorf, 2001; Kroslakova and Günther, 2007). This phenomenon is poorly understood but it is broadly thought of as the combination of fractionation occurring at the ablation site, within the transfer line and in the MC-ICPMS plasma source. The significance of this process can be realised when the potential effect on an isochron diagram is considered; inter-element fractionation would cause rotation of an isochron (thus altering the apparent age) since it would produce a bogus increase or decrease in the range of parent/daughter ratios (Fig. 2.11).

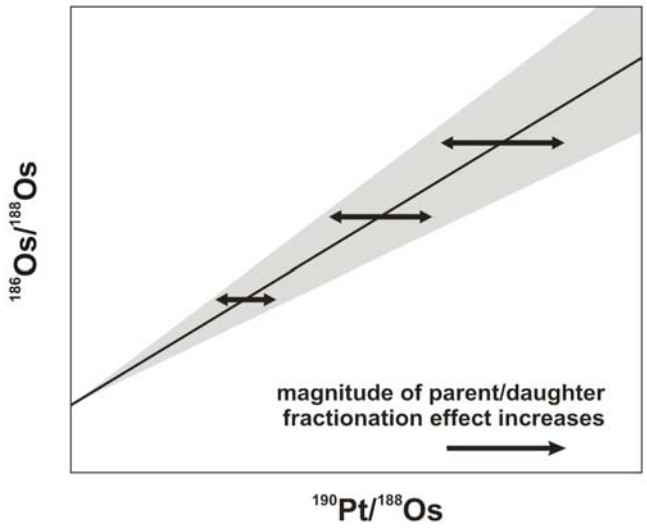

Figure 2. 11 Schematic diagram illustrating the effect of Pt/Os fractionation on a Pt-Os isochron. If fractionation is constant then the absolute magnitude will increase systematically with increasing Pt/Os ratio, causing rotation of the isochron.

The lack of appropriate solid reference materials for laser ablation Os isotope studies has resulted in a deficit of information regarding the degree of inter-element fractionation that occurs during ablation of PGM. As with the study of Nowell et al. (2008b) it is not possible to address Re/Os fractionation here. However, the data presented in this thesis do allow some constraint of the degree of Pt/Os fractionation that occurs during LA-MC-ICPMS. We must assume that fractionation is simple, occurring at a constant amount throughout each analysis and for each mineral phase although we accept that the latter is unrealistic. Nowell et al. (2008b) were able to crudely estimate Pt/Os fractionation during LA-MC-ICPMS to be 5 % or less, based on a single

detrital homogeneous PGE alloy grain, though they were limited by the poor age constraints existing for the ophiolite from which it was derived. The relatively better accuracy and precision of the Bushveld Pt-Os isochron age presented in this study (Chapter 3) provide an opportunity to constrain more confidently Pt/Os fractionation. The 47 Ma uncertainty on the Pt-Os isochron age of 2012 Ma can accommodate up to 2.2 % Pt/Os fractionation during LA-MC-ICPMS (Fig. 3.8; Chapter 3). Only 2 % fractionation is required to shift the absolute Pt-Os age and bring it into exact agreement with the published U-Pb zircon age of 2054 Ma (Scoates and Friedman, 2008).

The accuracy of Re and Os IECs can affect the calculated $^{187}Re/^{188}Os$ and $^{190}Pt/^{188}Os$ parent/daughter ratios, but it is important to note that the IERs themselves are immune to any inter-element fractionation effects.

2.7 Conclusions

1) The LA-MC-ICPMS method provides a mechanism for accurate and precise measurement of Os isotope ratios in a range of PGM species. Repeat analyses of homogenous in-house standard PGE alloy grains demonstrate the very good external reproducibility of Os isotope measurements.

2) Stability of instrumental Os mass bias for the Neptune in solution mode is excellent, both within individual analytical sessions and over a period of two and a half years. A very strong linear correlation is observed on a plot of $\ln(^{189}Os/^{188}Os)$ versus $\ln(^{186}Os/^{188}Os)$ for DROsS data, with a slope that is consistent with the theoretical slope for exponential mass bias behaviour. Os mass bias behaviour during laser ablation PGM analysis of samples from the Bushveld Complex, Borneo and California is consistent with that exhibited by DROsS solutions.

3) Interfering element corrections for W, Re and Os are accurate and correction ratios have remained relatively stable over a two and a half year period. All PGM samples analysed in this study fall within the range of $^{185}Re/^{188}Os$ and $^{182}W/^{188}Os$ values measured for DROsS standard solutions and standard grains. It is clear from $^{184}Os/^{188}Os$ ratios that at very low Os beam intensities the W IECs deteriorate due to the greater uncertainty on the measurement of ^{182}W at sub 0.1mV intensities. However, despite the increased uncertainty for the W IEC on ^{184}Os at low Os beam intensities it is not significant for the W IEC on ^{186}Os since the correction is a factor of ~87 smaller.

4) Comparison of spot and line ablation styles at a range of cycle integration times has provided evidence for intra-element isotope fractionation under certain conditions. During linear ablations along a line of fixed length the rate of raster affects the measured isotope ratios, with

bias in favour of light isotopes during rapid ablations. Spot analyses with a 1 s integration time are preferred, since this measurement routine is rapid enough to allow analysis of small samples without producing intra-element isotope fractionation, while providing accurate and relatively precise data.

5) Further constraints have been defined for the phenomenon of inter-element fractionation, which occurs during laser ablation MC-ICPMS analyses. We estimate that Pt/Os fractionation may amount to between 2 and 2.5% during laser ablation PGM analyses.

2.8 References

Begemann, F., Ludwig, K.R., Lugmair, G.W., Min, K., Nyquist, L.E., Patchett, P.J., Renne, P.R., Shih, C.Y., Villa, I.M., and Walker, R.J., 2001, Call for an improved set of decay constants for geochronological use: Geochimica et Cosmochimica Acta, 65, 111-121.

Brueckner, H.K., Van Roermund, H.L.M., and Pearson, N.J., 2004, An Archean(?) to Paleozoic Evolution for a Garnet Peridotite Lens with Sub-Baltic Shield Affinity within the Seve Nappe Complex of Jamtland, Sweden, Central Scandinavian Caledonides: Journal of Petrology, 45, 415-437.

Fryer, B.J., Jackson, S.E., and Longerich, H.P., 1995, The design, operation and role of the laser-ablation microprobe coupled with an inductively coupled plasma; mass spectrometer (LAM-ICPMS) in the earth sciences: Canadian Mineralogist, 33, 303-312.

Günther, D., and Hattendorf, B., 2001, Elemental Fractionation in LA-ICPMS, *in* Sylvester, P.J., ed., Mineralogical Association of Canada (MAC) Short Course Series, Volume 29, 83-91.

Hart, S.R., and Kinloch, E.D., 1989, Osmium Isotope Systematics in Witwatersrand and Bushveld Ore-Deposits: Economic Geology, 84, 1651-1655.

Hattori, K., and Hart, S.R., 1991, Osmium-isotope ratios of platinum-group minerals associated with ultramafic intrusions; Os-isotopic evolution of the oceanic mantle: Earth and Planetary Science Letters, 107, 499-514.

Hirata, T., Hattori, M., and Tanaka, T., 1998, In-situ osmium isotope ratio analyses of iridosmines by laser ablation-multiple collector-inductively coupled plasma mass spectrometry: Chemical Geology, 144, 269-280.

Horn, I., Rudnick, R.L., and McDonough, W.F., 2000, Precise elemental and isotope ratio determination by simultaneous solution nebulization and laser ablation-ICPMS: application to U-Pb geochronology: Chemical Geology, 164, 281-301.

Košler, J., Simonetti, A., Sylvester, P.J., Cox, R.A., Tubrett, M.N., and Wilton, D.H.C., 2003, Laser-ablation ICPMS measurements of Re/Os in molybdenite and implications for Re-Os geochronology: Canadian Mineralogist, 41, 307-320.

Kroslakova, I., and Günther, D., 2007, Elemental fractionation in laser ablation-inductively coupled plasma-mass spectrometry: evidence for mass load induced matrix effects in the ICP during ablation of a silicate glass: Journal of Analytical Atomic Spectrometry, 22, 51-62.

Ludwig, K., 2003, Isoplot/Ex, version 3: a geochronological toolkit for Microsoft Excel, Geochronology Centre Berkeley.

Mank, A.J.G., and Mason, P.R.D., 1999, A critical assessment of laser ablation ICPMS as an analytical tool for depth analysis in silica-based glass samples: Journal of Analytical Atomic Spectrometry, 14, 1143–1153.

Meibom, A., and Frei, R., 2002, Evidence for an ancient osmium isotopic reservoir in Earth: Science, 296, 516-518.

Nowell, G.M., Luguet, A., Pearson, D.G., and Horstwood, M.S.A., 2008a, Precise and accurate $^{186}Os/^{188}Os$ and $^{187}Os/^{188}Os$ measurements by multi-collector plasma ionisation mass spectrometry (MC-ICPMS) part I: Solution analyses: Chemical Geology, 248, 363-393.

Nowell, G.M., Pearson, D.G., Parman, S.W., Luguet, A., and Hanski, E., 2008b, Precise and accurate $^{186}Os/^{188}Os$ and $^{187}Os/^{188}Os$ measurements by Multi-collector Plasma Ionisation Mass Spectrometry, part II: Laser ablation and its application to single-grain Pt-Os and Re-Os geochronology: Chemical Geology, 248, 394-426.

Pearson, D.G., Parman, S.W., and Nowell, G.M., 2007, A link between large mantle melting events and continent growth seen in osmium isotopes: Nature, 449, 202-205.

Pearson, N.J., Alard, O., Griffin, W.L., Jackson, S.E., and O'Reilly, S.Y., 2002, *In situ* measurement of Re-Os isotopes in mantle sulfides by laser ablation multicollector-inductively coupled plasma mass spectrometry: analytical methods and preliminary results: Geochimica et Cosmochimica Acta, 66, 1037-1050.

Scoates, J.S., and Friedman, R.M., 2008, Precise age of the platiniferous Merensky reef, Bushveld Complex, South Africa, by the U-Pb zircon chemical abrasion ID-TIMS technique: Economic Geology, 103, 465-471.

Shi, R., Alard, O., Zhi, X., O'Reilly, S.Y., Pearson, N.J., Griffin, W.L., Zhang, M., and Chen, X., 2007, Multiple events in the Neo-Tethyan oceanic upper mantle: Evidence from Ru-Os-Ir alloys in the Luobusa and Dongqiao ophiolitic podiform chromitites, Tibet: Earth and Planetary Science Letters, 261, 33-48.

Smoliar, M.I., Walker, R.J., and Morgan, J.W., 1996, Re-Os ages of Group IIA, IIIA, IVA and IVB iron meteorites: Science, 271, 1099-1102.

Walker, R.J., Brandon, A.D., Bird, J.M., Piccoli, P.M., McDonough, W.F., and Ash, R.D., 2005, ^{187}Os-^{186}Os systematics of Os-Ir-ru alloy grains from southwestern Oregon: Earth and Planetary Science Letters, 230, 211-226.

Walker, R.J., Morgan, J.W., Beary, E.S., Smoliar, M.I., Gzamanske, G.K., and Horan, M.F., 1997, Applications of the ^{190}Pt-^{186}Os isotope sytem to geochemistry and cosmochemistry: Geochimica et Cosmochimica Acta, 61, 4799-807.

Weyer, S., and Schwieters, J.B., 2003, High precision Fe isotope measurements with high mass resolution MC-ICPMS: International Journal of Mass Spectrometry, 226, 355-368.

3 Application of the ^{190}Pt-^{186}Os decay system to dating platinum-group element mineralisation in the Merensky Reef and other mineralised horizons of the Bushveld Complex

Abstract

Constraining the formation age of platinum-group element (PGE) mineralisation via direct dating of platinum-group minerals (PGM) has traditionally been challenging. Re-Os geochronology has been employed in various studies of Bushveld lithologies, however no precise Re-Os isochron ages have been achieved on either of the two major PGE mineralised units, the Merensky Reef and the UG2 chromitite. Previous studies have shown that Re-Os systematics in Bushveld rocks and minerals are complex and scattered. This is unsurprising given the sensitivity of the system to processes such as crustal contamination of primary melts and R-Factor fractionation, which can cause variation in $^{187}Os/^{188}Os_i$ ratios. In contrast, the Pt-Os system is very robust during such processes as a result of the very low magnitude of variation in initial $^{186}Os/^{188}Os$ ratios throughout Earth history. We chose to use the Pt-Os system to attempt to date PGM from PGE-rich horizons of the Bushveld Complex. Detrital PGM populations yield precise ^{190}Pt-^{186}Os isochron ages measured by laser ablation multi-collector ICPMS (LA-MC-ICPMS). We present an accurate Pt-Os isochron age of 2012 ± 47 Ma (2σ, n = 50, MSWD = 1.19, $^{186}Os/^{188}Os_i$ = 0.119818 ± 0.000006) measured by LA-MC-ICPMS for Bushveld PGM from three different horizons. This is consistent with published U-Pb, Re-Os, Ar-Ar and Rb-Sr ages for Bushveld samples. $^{187}Os/^{188}Os_i$ values cover a wide range (0.128149 – 0.180696) that is consistent with published data, thus no correlation is seen on a Re-Os isochron diagram.

In presenting an accurate Pt-Os age for PGM collected from *in situ* samples we demonstrate the utility of the LA-MC-ICPMS method as a potential tool for accurate Pt-Os dating of detrital PGM and their igneous parent bodies. We are able to place further constraints on Pt-Os fractionation that occurs during laser ablation MC-ICPMS analysis and we discuss the potential sources of scatter on Pt-Os isochrons and the implications of sampling within-grain heterogeneities.

3.1 Introduction

The Bushveld Complex is the largest known igneous intrusion on Earth (Harney and Vongruenewaldt, 1995). It hosts 75% of the world's platinum resources, as well as the majority of the other accessible PGE plus 16% of global nickel reserves (Naldrett, 2004). As a result it

has been widely and intensely studied, with a large body of research focussed on the age of the intrusion. Precise and accurate ages have been achieved using a variety of geochronometers, applied to a range of materials from various stratigraphic intervals throughout the complex (Table 3.1). These studies constrain the age of the Bushveld Complex to 1.921 – 2.165 Ga, though a figure of around 2.054 Ga is widely accepted (Scoates and Friedman, 2008). Although various techniques have been used to date a wide range of lithologies, few date ore-heavy horizons and none have directly dated the platinum minerals themselves.

Table 3. 1 Published ages for Bushveld rocks and minerals

Stratigraphic interval	Age (Ma)	System	Material dated	Event dated	Reference	#
Bushveld Granites	2099 ± 3	U-Pb	Cassiterite	Bushveld granites	Gulson & Jones, 1992	1
Rustenburg Layerd Suite	2058.9 ± 0.8	U-Pb	Titanite	Hydorthermal activity associated with final cooling of the RLS	Buick et al., 2001	2
Merensky Reef	2054.4 ± 1.3 2055.0 ± 3.9	U-Pb U-Pb	Zircon Rutile	Late Merensky pegmatitic feldspathic orthopyroxenite	Scoates & Friedman, 2008	3
UG-2 Chromitite	2042.4 ± 3.2	Ar-Ar	Biotite	UG-2 Chromitite	Nomade et al., 2004	4
Bastard Unit	2043 ± 11	Re-Os	Poikilitic pyroxenes	Bastard Unit	Schoenberg et al., 1999	5
Platreef	2011± 90	Re-Os	Pyroxenites	Platreef pyroxenites	Reisberg et al., 2006	6
Dullstroom & Damwal Fmt.s	2071+94/-65	Rb-Sr	Whole-rock	Earliest Bushveld magmatism	Buchanan et al., 2004	7

N.B. Reference # relates to Fig. 3.4

The ^{190}Pt-^{186}Os decay system, measured by laser ablation MC-ICPMS, has been demonstrated as a useful geochronometric tool for detrital PGM (platinum-group minerals), particularly PGE alloys (Lapland Greenstone Belt and Ural Mountains, Nowell et al., 2008b; southeast Borneo, Coggon et al., in review). In this paper we apply the Pt-Os chronometer to date PGM extracted from (i) *in situ* Bushveld chromitite of the layered series (the Merensky Reef at Rustenburg), a dunite pipe cross cutting the layered series (Onverwacht) and (iii) late Bushveld hydrothermal veins cross cutting the Banded Ironstone Formation directly beneath the layered series in the Northern Limb (Tweefontein Hill). The wide variation in mineralogy offers considerable potential for Pt/Os and Re/Os fractionation and hence is an attractive proposition for Pt-Os and Re-Os isochron studies. In terms of the Pt-Os chronometer this potential for a wide range in parent/daughter isotope ratios acts to counter-balance the very long half-life of the ^{190}Pt parent

isotope (Begemann et al., 2001). We evaluate the validity of multi-grain Pt-Os ages measured by LA-MC-ICPMS and show that the method has great potential for dating detrital PGM populations and the ultramafic rocks from which they are derived.

3.2 Samples

A selection of Bushveld PGM was obtained from collections at the Federal Institute for Geosciences and Natural Resources (BGR), Hannover and Muséum National d'Histoire Naturelle (MNHN), Paris.

BVD 8801 and BVD 8801-R2 are polished mounts of “metallic” heavy mineral concentrates from the Merensky reef, similar to the material used by Hart and Kinloch (1989). The material was collected in the 1970s at the Frank Shaft, Rustenburg Platinum Mine (AngloPlatinum) (Fig. 3.1). Concentrates were produced prior to fine milling and flotation of the ore using density separation methods. Only grains of laurite-erlichmanite, braggite, sperrylite and Pt-Fe alloy were selected for this study. 47 PGM grains with lengths ranging from approximately 150 to 500 µm were analysed.

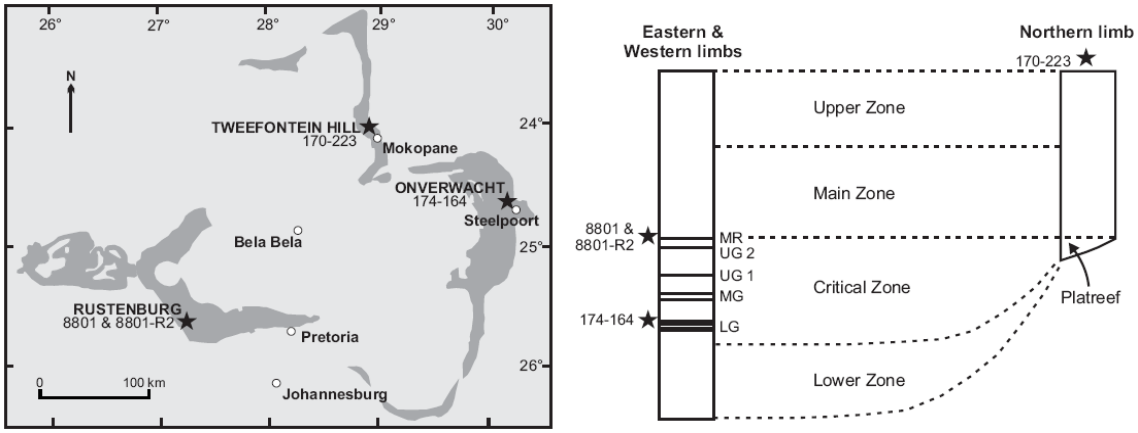

Figure 3. 1 Extent of exposure of the Rustenburg Layered Suite of the Bushveld Complex. After Naldrett et al. (2009). Black stars show sample locations and relative stratigraphic positions. Stratigraphic column after Cawthorn et al. (2002).

Sample BVD 174-164 is a polycrystalline nugget of Pt-Fe on chromite that measures approximately 4 x 3 x 2 mm. It was collected from the Onverwacht Mine, Eastern Bushveld (Fig. 3.1) most likely in the 1920s and was given to the MNHN, Paris, in 1955 by Colonel Jean Paul Louis Vésignié. The Onverwacht dunite pipe intrudes perpendicular to the typical igneous layering of the Bushveld complex and cuts through the LG6 chromitite layer. Fragments of chromitite occur at various depths in the pipe and are believed to be remnants of the disrupted

LG6 layer (Zaccarini et al., 2002). It is likely that PGM hosted in the pipe are derived from disrupted chromitites.

BVD 170-223 is an isolated, euhedral sperrylite crystal measuring ~ 1 mm across. The crystal was liberated from a hand specimen of vein material measuring approximately 4.5 x 3 x 2 cm. The host rock is composed predominantly of iron oxides, with limonite and malachite. It was most likely collected in the 1920s at Tweefontein Hill, on the northern limb of the Bushveld (Fig. 3.1). Large sperrylite crystals occur at this locality and are associated with hydrothermal veins in breccia zones within banded ironstone very close to the Platreef (Spencer, 1926; Nex, 2005).

Visual identification of samples BVD 170-223 and 174-164 was confirmed by EDS spectra using a Low-Vacuum, T Scan Scanning Electron Microscope at the MNHN. BVD 8801 and 8801-R2 were provided as polished blocks therefore no further preparation was needed for these samples. BVD 174-164 and 170-223 were mounted on adhesive carbon SEM tabs on a glass slide.

3.3 Method

3.3.1 Mass spectrometry

Isotopic analyses were performed at Durham University Northern Centre for Isotopic and Elemental Tracing (NCIET) using a New Wave UP 213 nm laser and Thermo Fisher Neptune multi-collector ICPMS (MC-ICPMS) via the method described in detail in Chapter 2 and by Nowell et al. (2008b). Bushveld PGM were analysed during six sessions between July 2009 and March 2010. All analyses consisted of one block of 40 cycles, with a cycle integration time of four seconds for standards and one second for samples. During ablation of samples laser power and spot size were tailored to the Os content of each grain in order to optimize signal size. The ranges of power and spot sizes used, along with fixed value laser parameters, are given in Table 3.2.

A 2 sigma rejection was applied to all analyses of standards and samples with the exception of BVD 8801_19. In this case the grain exhibits extreme internal heterogeneity and appears to define two distinct domains. For further details see section 3.4.2.

Table 3. 2 UP213 Operating conditions for LA Os isotopic analysis of Bushveld PGM grains

Parameter	Value
Wavelength	213 nm
Ablation cell	Std New Wave cell
Carrier gas	Ar
Carrier gas flow rate	1.5 l min^{-1}
Spot diameter	60 - 140 µm depending on Os content of sample
Crater depths	~40 - 80 µm
Repetition rate	20 Hz
Laser power	70-100 % depending on Os content of sample
Laser power density	~4.3 - 7 J cm^{-2}

3.3.2 DROsS standard solution

At the start of each analytical session the Neptune was tuned using a 1µg mL^{-1} Durham Romil Osmium Standard (DROsS) standard solution in order to achieve maximum sensitivity and peak shape quality. Baseline and gain calibrations were then carried out, followed by up to 15 analyses of a DROsS standard solution (Appendix 3). Mean $^{187}Os/^{188}Os$ and $^{186}Os/^{188}Os$ values of 0.160918 ± 0.000019 and 0.119918 ± 0.000010 respectively (2 SD, n = 72) are identical within uncertainty to the values of 0.160921 ± 0.000018 and 0.119917 ± 0.000020 (2 SD, n = 5) reported for this standard by Nowell et al. (2008b). Reproducibility over the six sessions for a total of 72 analyses of DROsS solutions was 120 ppm for $^{187}Os/^{188}Os$ and 82 ppm for $^{186}Os/^{188}Os$.

3.3.3 Mass bias, interfering element corrections (IECs) and error propagation

The $^{189}Os/^{188}Os$ ratio was used to correct for mass bias since it is not subject to any elemental interferences. We assumed a $^{189}Os/^{188}Os$ value of 1.21978 for this correction (Nowell et al., 2008b).

^{184}W, ^{186}W and ^{187}Re are elemental isobaric interferences on ^{184}Os, ^{186}Os and ^{187}Os during laser ablation. To correct for these interferences we monitored ^{182}W and ^{185}Re during analyses. Analyses of a 1µg mL^{-1} DROsS solution doped with varying concentrations of W and Re were used to derive values for the stable $^{182}W/^{184}W$, $^{182}W/^{186}W$ and $^{185}Re/^{187}Re$ ratios (see Table 2.6),

which were in turn used to calculate the interference for each 1 s integration. Interferences were subtracted to give the corrected Os isotope ratios.

Interferences on ^{190}Os and ^{192}Os by ^{190}Pt and ^{192}Pt cannot be corrected in the same way as Re and W interferences since the Faraday cup configuration used does not provide a Pt monitor isotope. Instead Os must be treated as the interfering element, with ^{188}Os taken as the monitor isotope. Mean ^{190}Os/^{188}Os was determined from measurements of the DROsS standard for each session. These values were then used to correct for Os overlap on mass 190.

If W corrections are systematically inaccurate then any correlation between W/Os and Pt/Os could cause rotation of a Pt-Os isochron, as discussed by Nowell et al. (2008b) and in Chapter 2, section 2.5.3.3 (Fig. 2.9). The Merensky data do show a general trend towards higher W/Os ratios in Pt-rich minerals, but no linear relationship is seen between W/Os and Pt/Os. Therefore any inaccuracies in the IECs will not cause systematic rotation of the isochrons constructed using these data. In any case, the W correction is very small for the majority of samples. Furthermore, the magnitude of the Os correction decreases as Pt/Os ratio increases, thus the correction is smaller for the samples that have the greatest influence on the Pt-Os isochron age.

Total errors on ^{186}Os /^{188}Os ratios were calculated to incorporate external reproducibility. A value of 176 ppm was used for grains with ^{188}Os beams of 1 V or more; grains with ^{188}Os beams < 1 V were assigned external reproducibility values of 352 ppm. These values were derived from repeat analyses over ~ 1 year of an in-house standard (Urals Os-rich PGE alloy 36720 G1, Nowell et al., 2008b). Similar data are not available for ^{190}Pt/^{188}Os since there is no Pt-rich homogeneous ablation standard. Total uncertainties on the ^{190}Pt/^{188}Os ratio include the within-run error plus a conservative estimate of 5 % uncertainty to account for elemental fractionation that is likely to occur at the ablation site (Nowell et al., 2008b) and external reproducibility on the measurement of this ratio. The method and corrections are discussed in greater detail in Chapter 2, section 2.5.2.

3.4 Results

3.4.1 Re-Os isotopes

Analysis of 47 Merensky PGM yielded ^{187}Os/^{188}Os ratios of 0.167254 – 0.180429 (BVD_8801) and < 0.000005 – 0.180697 (BVD_8801-R2), and ^{187}Re/^{188}Os ratios of < 0.000005 – 0.0539 (Appendix 4). Analyses of the heterogeneous Onverwacht Pt-Fe nugget generated ^{187}Os/^{188}Os

ratios ranging from 0.167449 to 0.178173 (mean = 0.174416) and $^{187}Re/^{188}Os$ values from 0.0612 to 0.1149 (mean = 0.0767) (Appendix 4). The Tweefontein Hill sperrylite contains extremely low concentrations of common osmium, with measured $^{187}Os/^{188}Os$ and $^{187}Re/^{188}Os$ ratios such that $^{187}Os/^{188}Os$ cannot be accurately corrected. No isochronous relationships exist within this Re-Os dataset, since $^{187}Os/^{188}Os$ values are generally elevated, while $^{187}Re/^{188}Os$ ratios are very low.

In comparison, Shoenberg et al. (1999) present a measured $^{187}Os/^{188}Os$ value of 0.1936 ± 0.0001 for a poikilitic pyroxenite from the Merensky Reef and a range of 0.1235 – 0.4696 for chromites and pyroxenites from the Rustenburg Layered Series. The much higher $^{187}Os/^{188}Os$ values of these whole rock samples relative to our PGM no doubt result from much higher Re concentrations; the PGM analysed in this study contain negligible Re.

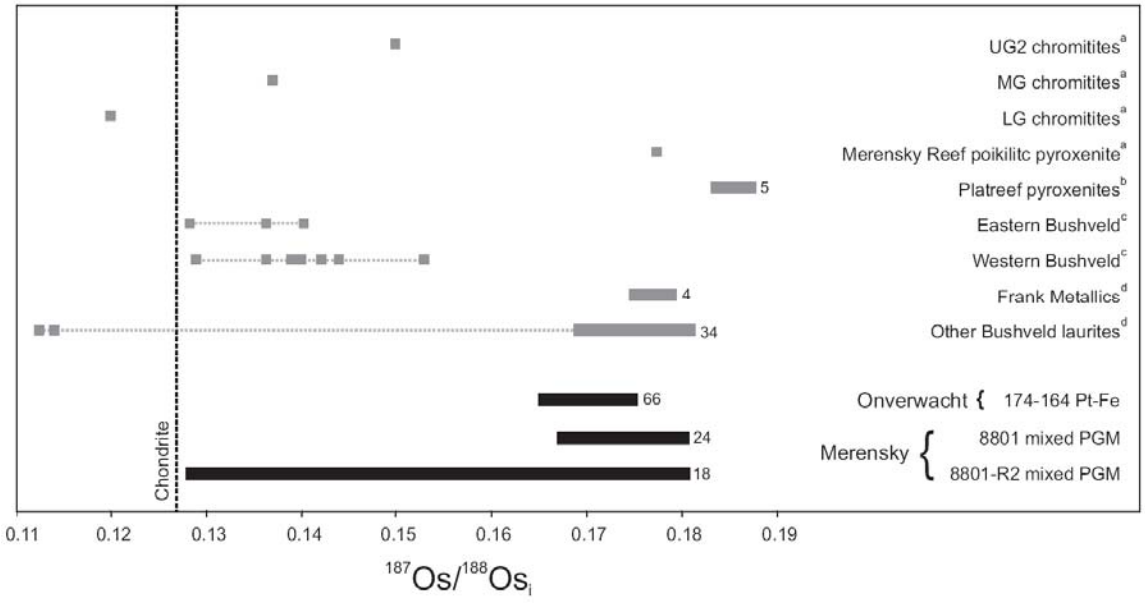

Figure 3. 2 Variation in $^{187}Os/^{188}Os_i$ values of Rustenburg (BVD 8801 and 8801-R2) and Onverwacht (BVD 174-164) PGM compared to published data for Bushveld rocks and minerals. a Schoenberg et al. (1999); b Reisberg et al. (2006); c McCandless et al. (1999); d Hart and Kinloch (1989).

Previous studies have found a huge range of initial $^{187}Os/^{188}Os_{(2054\ Ma)}$ values for Bushveld samples, from 0.1124 to 0.1878 (Fig. 3.2) (Hart and Kinloch, 1989; McCandless et al., 1999; Schoenberg et al., 1999; Reisberg et al., 2006). The range of initial ratios for all the PGM analysed in this study, calculated using the Pt-Os isochron age of 2012 Ma, is relatively restricted, with the exception of BVD 8801-R2 grains. All samples in this study fall within the very large range of γ_{Os} values calculated for a variety of silicate mineral, PGE sulphide and whole-rock studies (see Fig. 3.2), though the majority are markedly more elevated. The "Frank

metallics" analysed by Hart and Kinloch (1989) were taken from the same original sample of metallic concentrates as the BVD 8801 and 8801-R2 Merensky samples analysed in this study. The Hart and Kinloch data fall within the upper range of the initial $^{187}Os/^{188}Os$ values that we have measured for the samples from this location. In addition, the published $^{187}Os/^{188}Os_i$ value of 0.17773 exhibited by a Merensky poikilitic pyroxenite (Schoenberg et al., 1999) is consistent with our Merensky data (Fig. 3.2). Published $^{187}Os/^{188}Os_i$ ratios were not available for comparison with the Onverwacht data, although these are very similar to the Merensky BVD 8801 $^{187}Os/^{188}Os_i$ values.

No isochronous relationship is seen for the Re-Os system in any individual locality or in the dataset as a whole due to the significant heterogeneity in initial $^{187}Os/^{188}Os$ values.

3.4.2 Pt-Os isotopes and age

The 24 Merensky PGM grains of polished mount BVD 8801 display $^{186}Os/^{188}Os$ ratios ranging from 0.119789 to 0.139562 and $^{190}Pt/^{188}Os$ values from < 0.000005 to 6.05. Analyses of 23 grains from sample mount BVD 8801-R2 produced $^{186}Os/^{188}Os$ values of 0.119815 – 0.388721 and $^{190}Pt/^{188}Os$ ratios of 0.000008 – 90.9. The Onverwacht Pt-Fe nugget BVD 174-164 was analysed 66 times and yielded $^{186}Os/^{188}Os$ ratios of 0.132690 – 0.143752 (mean = 0.138426) and $^{190}Pt/^{188}Os$ ratios of 4.32 – 7.25 (mean = 5.95). The Tweefontein sperrylite yielded $^{186}Os/^{188}Os$ and $^{190}Pt/^{188}Os$ ratios of 0.675168 and 184 respectively (Appendix 4).

The entire dataset defines a Pt-Os isochron age of 2012 ± 47 Ma (2σ, n = 50) with an MSWD of 1.19, probability of fit of 0.18 and an $^{186}Os/^{188}Os_i$ value of 0.119818 ± 0.000006 (Fig. 3.3). The uncertainty on the age incorporates the 1 % uncertainty on the decay constant of ^{190}Pt as estimated by Begemann et al. (2001). This age is in excellent agreement with recent high precision U-Pb zircon dating (Scoates and Friedman, 2008) and other published ages for Bushveld samples (Fig. 3.4, Table 3.1). The initial $^{186}Os/^{188}Os$ ratio is very close to estimates for primitive upper mantle (PUM) at 2.05 Ga (0.1198326 ± 0.0000028, calculated using a present day PUM Os isotope composition of 0.1198382 ± 0.0000028, and Pt/Os ratio of 2.0 ± 0.2, Brandon et al., 2006; Fig. 3.5). Nowell et al. (2008a) and Luguet et al. (2008a) suggest that the Os isotope ratios determined by Brandon et al. (2006) are subject to an uncorrected interference on ^{186}Os resulting in systematically high $^{186}Os/^{188}Os$ values. Taking this into consideration, together with additional offset caused by the use of different mass bias ratios in this study and that of Brandon et al.,(2006) the mantle evolution line has been recalculated (Fig. 3.5) and the initial $^{186}Os/^{188}Os$ ratio yielded by the Pt-Os isochron is also within error of the modified evolution curve. The Pt-Os isochron was regressed using Merensky, Onverwacht (LG6?) and Tweefontein

Hill (late hydrothermal) data. We believe that the isochron shown in Figure 3.3 presents the data in the most consistent way, with each point on the isochron effectively representing a single grain. An isochron regression for the Merensky data as a single locality yields an age within uncertainty of that of the combined dataset but with lower precision; the same is true of Pt-Os model ages for the Onverwacht and Tweefontein Hill grains (see below).

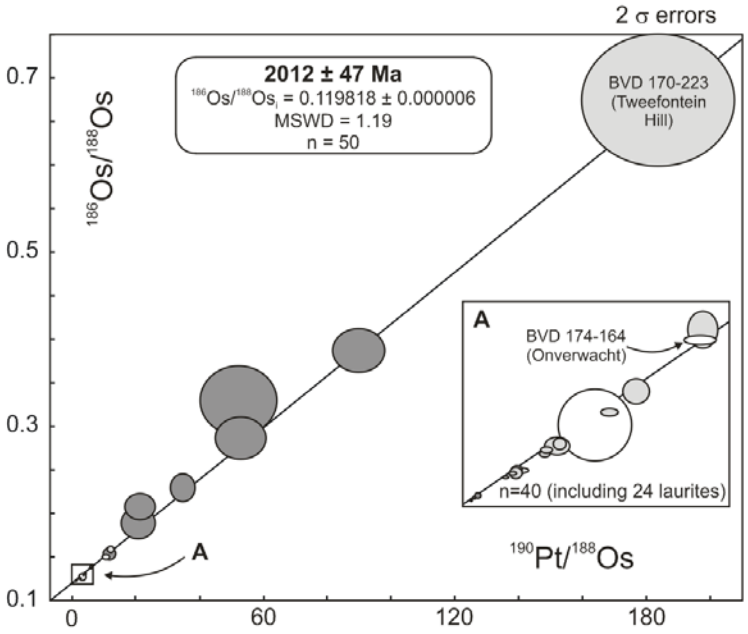

Figure 3. 3 Pt-Os isochron diagram plotted using data from Merensky, Onverwacht and Tweefontein Hill PGM. Fill colour of error ellipse indicates mineralogy: black, laurite-erlichmanite; dark grey, braggite; light grey, sperrylite; white, Pt-Fe alloy. The isochron age is calculated assuming that BVD 8801_19 consists of two separate components, BVD 8801_19a and _19b. Errors on $^{186}Os/^{188}Os$ incorporate within run uncertainties and long term external reproducibility on this ratio based on repeat analyses of an in-house standard grain (Urals Os-rich PGE alloy 36720 G1, Nowell et al., 2008b). $^{190}Pt/^{188}Os$ errors include 5% uncertainty to account for elemental (Pt/Os) fractionation that occurs at the ablation site and external reproducibility on the measurement of this ratio (Nowell et al., 2008b). The precision quoted for the isochron age incorporates an uncertainty of 1% on the decay constant of ^{190}Pt (Begemann et al., 2001). Plotted using Isoplot version 3.1 (Ludwig, 2003).

3.4.2.1 Merensky Reef

Each of the 24 PGM grains from polished mount BVD 8801 is shown on the isochron in Figure 3.3 as a single point representing a 40 second analysis, with three exceptions. An initial scan showed grain 8801_19 to be heterogeneous, with two isotopically distinct domains. It was analysed in two parts (8801_19a and _19b). These two analyses were combined (8801_19) to allow evaluation of the effect on the Pt-Os isochron of splitting the grain. The standard 2 sigma rejection was not applied to the un-split analysis due to the internal heterogeneity since in this

case applying a rejection would bias the data. Division of grain 8801_19 has a minor effect on the isochron age (2010 ± 47 Ma), the MSWD (1.16 compared to an original value of 1.19) and probability of fit (0.21 versus 0.18). The $^{186}Os/^{188}Os_i$ ratio is unchanged.

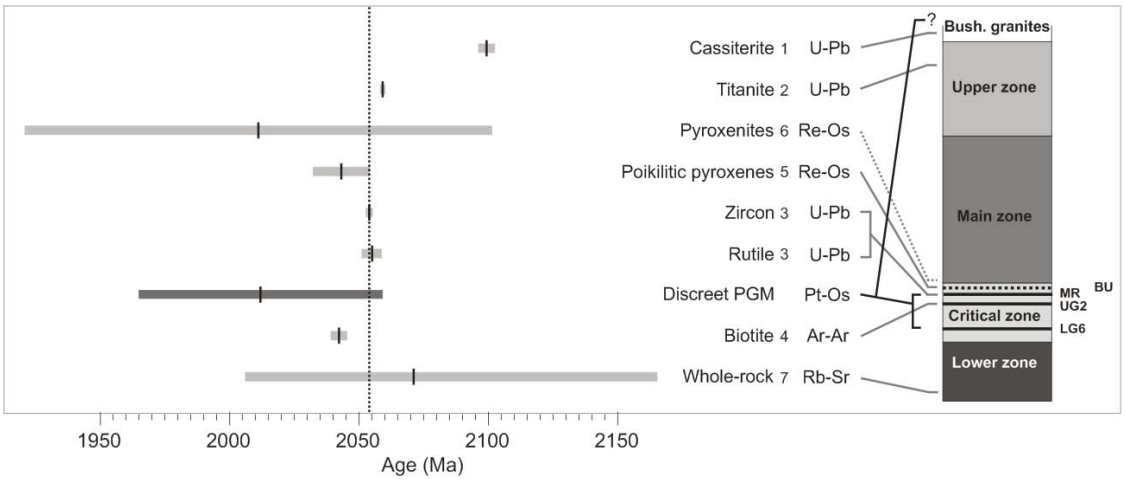

Figure 3. 4 Comparison of Pt-Os age and uncertainty (dark grey bar) with published data (light grey bars) for Bushveld rocks and minerals. Dashed line denotes accepted age for the Bushveld Complex (Scoates and Friedman, 2008). Numbers 1 – 7 refer to references in Table 1. Stratigraphic column after Mitchell (1990).

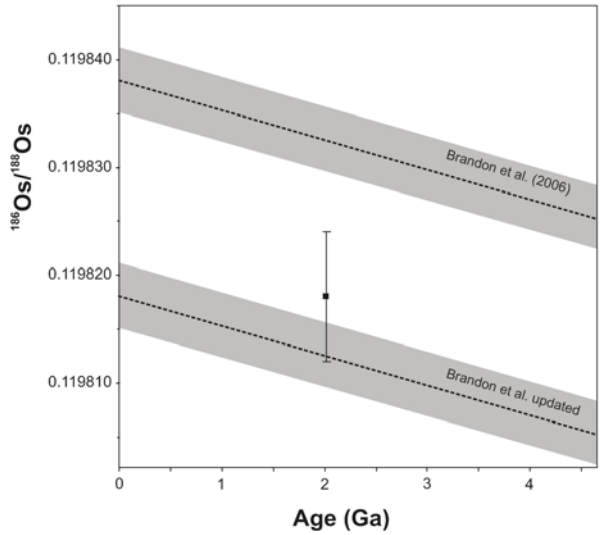

Figure 3. 5 Comparison of the initial $^{186}Os/^{188}Os$ ratio derived from the Bushveld isochron with the $^{186}Os/^{188}Os$ mantle evolution curve of Brandon et al. (2006). The Bushveld initial $^{186}Os/^{188}Os$ ratio is consistent with a corrected mantle evolution curve, which was calculated to account for the systematically high $^{186}Os/^{188}Os$ values and an additional offset caused by the use of different mass bias ratios in this study and that of Brandon et al. (2006). Uncertainties on both mantle curves are based on the quoted uncertainty of the present day PUM $^{186}Os/^{188}Os$ value determined by Brandon et al. (2006).

Grains 8801_22 and _24 were also found to be two-component grains. However, in both cases the more Pt-rich components contained negligible common Os. Consequently, accurate measurement of the $^{189}Os/^{188}Os$ ratio for the Pt-rich components was impossible, thus mass bias corrections are unreliable and these data must be rejected. The first nine and last 17 integrations were rejected from the analyses of grains 8801_22 and _24 respectively. The same procedure for removal of integrations was applied to five grains from BVD 8801-R2, though in these cases the reason for removal was that the grains were small thus there was insufficient material to sustain an entire 40 s ablation. The first seven, last nine and last 10 integrations were rejected from the analyses of grains 8801-R2_1, _5 and _8 respectively. The last 11 integrations were removed from both 8801-R2_17 and _25.

The most Pt-rich Merensky braggite grain (8801-R2_11) yields a Pt-Os model age of 2024 ± 101 (5 % uncertainty) and a Pt-Os isochron constructed using only Merensky data gives an age of 1995 ± 50 Ma (2σ; n = 48; MSWD = 1.16; probability of fit = 0.21). Both are within error of the Pt-Os isochron age for the entire Bushveld PGM dataset presented in Figure 3.3 and section 3.4.2 The Merensky isochron has an initial $^{186}Os/^{188}Os$ ratio (0.119819 ± 0.000006) that is identical within uncertainty to that of the combined Bushveld isochron.

3.4.2.2 Onverwacht Pipe

BVD 174-164 is a polycrystalline Pt-Fe nugget that exhibits internal heterogeneity. The 66 analyses of this sample do not provide a wide enough range of Pt/Os ratios to give a reliable isochron. However, the mean of these analyses was taken as a representation of the single nugget and was added to the combined Bushveld PGM Pt-Os isochron (Fig. 3.3).

A Pt-Os model age of 2113 ± 106 Ma (5 % uncertainty) was calculated for the mean of the Onverwacht nugget analyses, assuming an initial $^{186}Os/^{188}Os$ value of modern day primitive upper mantle (PUM). This is within error of the published ages (Fig. 3.4, Table 1) and the combined Bushveld dataset Pt-Os isochron age of 2012 ± 47 Ma (Fig. 3.3). An identical age was achieved when the initial $^{186}Os/^{188}Os$ value was assumed to be the same as PUM at 2054 Ma.

3.4.2.3 Tweefontein Hill

BVD 170-223 is a heterogeneous crystal of sperrylite. Four analyses were attempted on this sample, however only one of these ablations sampled a region of the crystal where the Os concentration was high enough to provide sufficient Os signal for reliable mass bias and interfering element corrections. A Pt-Os model age for the sperrylite crystal can be calculated using an initial $^{186}Os/^{188}Os$ value of PUM at 2054 Ma. This gives an estimated age for the Tweefontein Hill hydrothermal PGE mineralisation of 2042 ± 102 Ma (5 % uncertainty), which is

again within error of the Pt-Os isochron age for the entire Bushveld dataset. The 5 % uncertainty is dominated by the estimated uncertainty on the measurement of $^{190}Pt/^{188}Os$.

3.5 Discussion

3.5.1 Source variation versus crustal contamination – effects on the Re-Os and Pt-Os systems

Published data show that a variety of Bushveld rocks and minerals display a wide range of $^{187}Os/^{188}Os_i$ values (0.1124 to 0.1878, Fig. 3.2) (Hart and Kinloch, 1989; McCandless et al., 1999; Schoenberg et al., 1999; Reisberg et al., 2006), all of which are within error of, or greater than, estimates for PUM at 2054 Ma (γ_{Os} = - 0.78 up to + 65.8). Significant differences in initial $^{187}Os/^{188}Os$ are present between stratigraphic levels (see Fig. 3.2), but individual stratigraphic layers are relatively homogeneous, both isotopically (McCandless et al., 1999) and in terms PGE concentrations (Eales and Cawthorn, 1996; Cawthorn et al., 2002; Barnes et al., 2004). The majority of samples analysed in this study exhibit $^{187}Os/^{188}Os_i$ values that fall at the more radiogenic end of the published range, though BVD 8801-R2 samples cover almost the entire range (γ_{Os} = + 13.16 to + 59.55) (Fig. 3.2). The considerable range of $^{187}Os/^{188}Os_i$ values observed within and between individual PGM grains helps to explain the observed variation in bulk sample studies. It also clearly explains why Re-Os isochron correlations are not present for most bulk rock studies that have been attempted.

The various horizons of the Bushveld Complex are slightly less enriched in radiogenic ^{187}Os than the Muskox intrusion, but much less so than the Duluth, Sudbury and Voisey's Bay intrusions (Fig. 3.6). The radiogenic ^{187}Os signals of Bushveld samples have two potential causes. Numerous studies have suggested enrichment of Bushveld magmas in radiogenic ^{187}Os by assimilation of continental crust (both black shales and lower crustal granulite; e.g. McCandless et al., 1999; Schoenberg et al., 1999; Maier et al., 2000; Harris et al., 2005). In contrast, Richardson and Shirey (2008) have suggested that harzburgitic and eclogitic sulphide components in the lithospheric mantle underlying the Bushveld Complex are the source of radiogenic $^{187}Os/^{188}Os$ signals in Bushveld rocks and minerals.

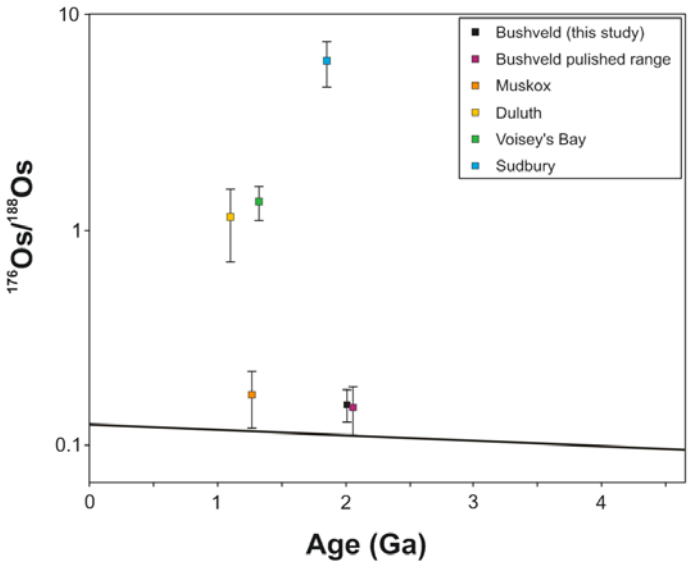

Figure 3. 6 Comparison of Bushveld initial $^{187}Os/^{188}Os$ values (this study and Hart and Kinloch, 1989; Schoenberg et al., 1999; McCandless et al., 1999; Reisberg et al., 2006) with the mantle evolution curve of Walker et al. (1989). While Bushveld rocks and minerals have significantly radiogenic $^{187}Os/^{188}Os_i$ ratios compared to PUM at 2.054 Ga, samples from the Muskox intrusion (Day et al., 2008), Duluth (Ripley et al., 1998), Sudbury (Walker et al., 1991) and Voisey's Bay (Lambert et al., 1999) exhibit far greater enrichment in radiogenic ^{187}Os.

3.5.1.1 Crustal variation

Numerous studies have modelled the effect on the Re-Os system of interaction of Bushveld primary melts with crustal lithologies (e.g. McCandless and Ruiz, 1991; McCandless et al., 1999; Schoenberg et al., 1999), though the effect on the Pt-Os system has not previously been investigated. We have chosen to model the effect of two different crustal end members on the Re-Os and Pt-Os isotope systems. We have modelled $^{187}Os/^{188}Os$ and $^{186}Os/^{188}Os$ isotopic mixing at 2054 Ma of a theoretical primary Bushveld magma with lower crust (Fig. 3.7), represented by 2.7 Ga mafic granulite based on the widespread occurrence of Ventersdorp basaltic magmatism (Marsh et al., 1992). This is intended to simulate interaction of a primary magma with the lower crust during residence of the melt in a magma chamber in the lower crust. We also show a model for contamination by black shale, to mimic interaction with shales of the 2.3 Ga Pretoria Group country rock during intrusion of Bushveld magmas (Fig. 3.7).

The primary Bushveld magma was assumed to be basaltic, with $^{187}Os/^{188}Os$ and $^{186}Os/^{188}Os$ ratios identical to convecting mantle at 2054 Ma (for values used in modelling see Table 3.3). Re and Os concentrations and Os isotope systematics of mafic lower crust at 2054 Ma were calculated using lower crust data from Saal et al. (1998). A Pt concentration was taken from a Granada basalt (Woodland et al., 2002) and PUM Os isotope systematics are assumed. PGE

concentrations and a value for initial $^{187}Os/^{188}Os$ at 2054 Ma for black shale were taken from Horan et al. (1994) and a chondritic $^{186}Os/^{188}Os$ ratio was assumed on the basis that shale sequesters seawater Os (McDaniel et al., 2004).

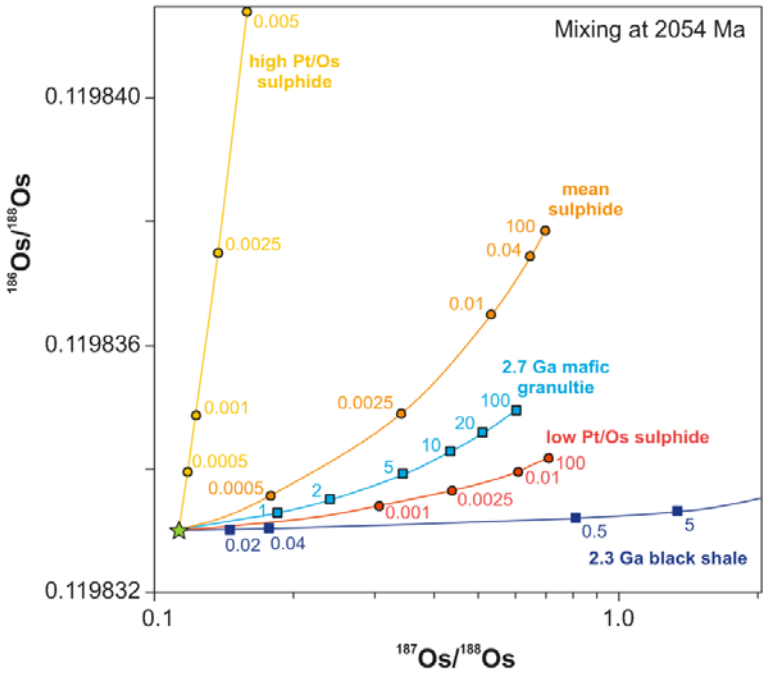

Figure 3. 7 Evolution of ^{187}Os-^{186}Os systematics of a theoretical primary Bushveld melt during simple binary mixing with potential crustal and mantle reservoirs at 2.054 Ga. Numbers adjacent to mixing curves give percentage of contaminant added to the melt. The Re-Os isotope system is very sensitive to crustal contamination and source heterogeneity while the Pt-Os system remains robust during mixing with all but the most Pt-rich components. Values used for modelling are given in Table 3.3.

Table 3. 3 Values used in modelling of crustal contamination vs. source variation of Bushveld magma

Component	Pt ppb	Re ppb	Os ppb	$^{187}Os/^{188}Os$	$^{186}Os/^{188}Os$
Bushveld primary melt	1.21[a]	0.84[b]	0.03[b]	0.113251	0.119833
2.7 Ga mafic granulite	1.84[c]	0.12[d]	0.54[d]	0.606227[d]	0.119835
2.3 Ga black shale	3.70[e]	140[e]	1.66[e]	4.938849[e]	0.119834
Low Pt/Os sulphides	444[f]	402[f]	1551[f]	0.712883	0.119834
High Pt/Os sulphides	1911[f]	261[f]	89[f]	0.481268	0.119901
Mean sulphides	1177[f]	331[f]	820[f]	0.699957	0.119838

[a]Rehkamper et al. (1999); [b]McCandless and Ruiz (1991); [c]Woodland et al. (2002); [d]Saal et al. (1998); [e]Horan et al. (1994); [f]Luguet et al. (2008).

Simple binary mixing shows that the Re-Os system is very sensitive to contamination by very small amounts of black shale, with only ~ 0.01 – 0.05 % assimilation necessary to produce the range of initial $^{187}Os/^{188}Os$ ratios seen in the PGM analysed in this study (0.128149 – 0.180696) (Fig. 3.7). In contrast, contamination of Bushveld magmas by black shale has little effect on the Pt-Os system due to the chondritic $^{186}Os/^{188}Os$ composition of this lithology.

Contamination of Bushveld melts by mafic granulitic lower crust yields different effects; assimilation of ~ 0.1 – 1 % mafic granulite during residence of Bushveld magma within a lower crustal magma chamber would generate the features observed in this dataset, i.e. a variety of initial $^{187}Os/^{188}Os$ ratios and a very small range of initial $^{186}Os/^{188}Os$ values (50 ppm).

Modelling of contamination of the Bushveld primary mafic magma by crustal lithologies shows that the Re-Os system is very sensitive to assimilation if the primary melt has normal basaltic Os concentrations, since crustal material is generally enriched in radiogenic ^{187}Os relative to the mantle. In contrast, the Pt-Os system is very robust to such contamination, as a result of the very small variation in $^{186}Os/^{188}Os$ values exhibited by crustal and mantle rocks. This means that variation produced in initial $^{186}Os/^{188}Os$ from crustal contamination processes is likely to have a minimal effect on any resulting Pt-Os isochrons.

3.5.1.2 Source variation

The Pt-Re-Os system in lithospheric mantle sulphides is heterogeneous (Luguet et al., 2008b), thus a wide range of time-integrated $^{186}Os/^{188}Os$ and $^{187}Os/^{188}Os$ ratios are observed in the mantle. Sulphides and PGE alloys in the mantle source of primitive Bushveld melt can produce wide variation in both Pt-Os and Re-Os systematics. Pt, Re and Os concentrations for two mantle sulphide end members (high Pt/Os sulphides and low Pt/Os sulphides; Table 3.3) were taken from Luguet et al. (2008b). Initial $^{186}Os/^{188}Os$ and $^{187}Os/^{188}Os$ ratios of PUM at 2.9 Ga were assumed (Pearson et al., 1998; Richardson et al., 2001) and were forward evolved to calculate the Os isotope compositions of both sulphide end members at 2.054 Ga. All values used in the modelling of simple binary mixing between mantle sulphides and a theoretical primitive Bushveld melt are given in Table 3.3.

Modelling (Fig. 3.7) shows that the Re-Os system is very sensitive to extremely small concentrations of high Os sulphides in the mantle source region. Addition of less than 0.0005 % low Pt/Os sulphides can account for the range of initial $^{187}Os/^{188}Os$ ratios observed in Bushveld PGM, but this reservoir has a negligible effect on the Pt-Os system. However, the presence of high Pt/Os sulphides in the source region has a strong influence on both the Pt-Os and Re-Os systems. The maximum initial $^{187}Os/^{188}Os$ ratio measured in this study can be achieved by adding < 0.01 % high Pt/Os sulphide to the mantle source, while addition of less than 0.0025 %

would elevate the initial $^{186}Os/^{188}Os$ value above the highest estimates of PUM at 2054 Ma (given quoted uncertainty, 0.119836, Brandon et al., 2006) (Fig. 3.7).

If the primary Bushveld magma sampled lithospheric mantle with significant sulphide heterogeneity without any mixing then we would expect to see more heterogeneity in measured $^{186}Os/^{188}Os$ values. If we assume homogenisation of such sulphides during assimilation by the Bushveld primary melt then the ^{186}Os and ^{187}Os isotope systematics observed in Bushveld PGM can be explained by inclusion of only ~ 0.0001 – 0.0005 % of such a reservoir (Fig. 3.7).

In summary, we cannot unequivocally differentiate between crustal or lithospheric interaction as a means of generating the variation in initial $^{187}Os/^{188}Os$ of Bushveld magma. The precise and chondritic nature of the initial $^{186}Os/^{188}Os$ ratio for Bushveld PGM reported here only allows the following constraints: whatever the origin of the significant initial $^{187}Os/^{188}Os$ variation of different components within the Bushveld Complex, the Pt-Os systematics of that component must be either homogenous and low in time-integrated Pt/Os, or if heterogeneous, must have efficiently mixed and be dominated by a component with a low time-integrated Pt/Os ratio.

3.5.2 Pt-Os geochronology

Our combined dataset of PGM from different horizons of the Bushveld Complex yields a Pt-Os isochron age of 2012 ± 47 Ma (2σ) (Fig. 3.3). This is identical, within uncertainty, to published ages for Bushveld samples (Fig. 3.4, Table 3.1) and in particular is consistent with the precise U-Pb zircon age of Scoates and Friedman (2008) (Fig. 3.4). The precision of the Pt-Os isochron is comparable with the Re-Os and Rb-Sr systems. The low MSWD (1.19) of the Pt-Os mineral isochron shows that the data fit the isochron well, despite minerals being derived from different horizons within the Bushveld Complex. Pt-poor phases (laurite-erlichmanite) constrain the initial $^{186}Os/^{188}Os$ ratio, while Pt-Fe alloys, sperrylite and braggite grains host a much wider range of $^{190}Pt/^{188}Os$ values. This result and its agreement with the published U-Pb zircon geochronology indicates that the Pt-Os system is less susceptible to initial ratio heterogeneity, resulting from either crustal contamination or source variability, than the Re-Os system. The well constrained initial $^{186}Os/^{188}Os$ ratio (0.119818 ± 0.000006) defined by the Pt-Os isochron for the combined Bushveld PGM dataset lies within error of the value estimated for PUM at 2045 Ma (Fig. 3.5).

Before interpreting these data further it is important to consider the possibility that the correlation observed on the Pt-Os isochron diagram (Fig. 3.3) might be a mixing line. Variation in $^{186}Os/^{188}Os$ in the convecting mantle is extremely limited (less than 100 ppm throughout the whole of the Phanerozoic; Brandon et al., 2006). On this basis, we may expect that any variability in $^{186}Os/^{188}Os_i$ due to the sampling of grains with varying initial ratios that are inherited

from their source would be small, even if their initial $^{187}Os/^{188}Os$ values are demonstrably variable (see Section 3.5.1.2; Fig. 3.7).

It is striking that the Pt-Os isochron age is within 2 % of the value obtained via precise U-Pb zircon geochronology (Scoates and Friedman, 2008) when one considers that these are two different decay systems, applied to two distinct mineralogical assemblages. However, despite the good correlation of Bushveld data on the Pt/Os isochron, it is apparent that there is a significant degree of scatter. If we assume that our Bushveld PGM Pt-Os age is dating the same event as the U-Pb zircon age (Scoates and Friedman 2008) for the Merensky Reef then there are several potential geological and analytical explanations for the scatter and disparity between these two ages.

The differences between the closure temperatures of the Pt-Os isotope system in sulphides and alloys and the U-Pb system in zircon and rutile could potentially cause a difference in the ages recorded by the two isotope systems, depending on the rate of cooling of the intrusion. The closure temperature of the U-Pb system in zircon is > 800°C (Heaman and Parrish, 1991). There are no published constraints for the closure temperatures of the Pt-Os system in alloys or sulphides although it can be postulated that these might be similar to Re-Os closure temperatures in sulphides (> 710°C in molybdenite, Bingen and Stein, 2003; > 300°C in pyrite, arsenopyrite, chalcopyrite, and bornite, Selby et al., 2009). However, Scoates and Friedman (2008) also present a U-Pb rutile age of 2055 ± 3.9 Ma for the Merensky Reef, an absolute age that is within 1 Ma of their U-Pb zircon age for the same horizon. The closure temperature for the U-Pb isotope system in rutile is relatively low (~ 400°C, Mezger et al., 1989), hence the very close agreement of the zircon and rutile ages provides strong evidence that the 42 Ma contrast between the Pt-Os and U-Pb ages is unlikely to result from variation in closure temperatures.

Other reasons for scatter of Pt-Os data may relate to crystal chemical and structural variations in the minerals analysed. Numerous studies have documented the decoupling of the Re-Os system within individual molybdenite grains due to polytypic transitions, low temperature hydrothermal alteration (McCandless et al., 1993) and micron-scale deformation (Stein et al., 2003). The difficulties in representative sampling of such grains via ID-NTIMS and laser ablation have been highlighted and discussed by several authors (e.g. Košler et al., 2003; Stein et al., 2003; Selby and Creaser, 2004, Nowell et al., 2008b). Immiscibility in Pt-S and Pt-Fe systems extends to < 400°C (Makovicky, 2002). This, combined with other miscibility gaps and crystallographic variations in the Os, Ir, Ru +/- S systems (Cabri, 2002; Makovicky, 2002; Hanley, 2006), indicates that chemical heterogeneity should be expected in slowly cooled assemblages of the minerals analysed here. This is confirmed by the high level of internal Pt/Os variation shown in some phases (e.g. samples 170-223 and 174-164, Appendix 4). The internal chemical

heterogeneity in Pt-Re-Os-heavy minerals documented here and in other studies (e.g. Richardson et al., 2001) mean that unless the entire grain is sampled during analysis (an unlikely occurrence in most laser ablation analyses) then inaccuracies will be generated in measured Re/Os, Pt/Os and Os isotope ratios. These inaccuracies are a function of the extent of internal heterogeneity, the extent of sampling, and the time elapsed since generation of the heterogeneity, e.g. via exsolution during cooling. The relatively slow cooling of the Bushveld Complex means that any such within-grain heterogeneity could have evolved into significantly different isotopic domains, as demonstrated in Figure 3.8. Such inaccuracies can never be fully removed during laser ablation analysis, thus they act as a fundamental limitation on the accuracy of measurement of the Pt-Os isotope system. It is possible that alloys are less sensitive to such disturbances than sulphides and arsenides; Nowell et al. (2008b) analysed Os-rich PGE alloys and saw no significant isotopic decoupling, despite evidence of domains with different $^{190}Pt/^{188}Os$ ratios.

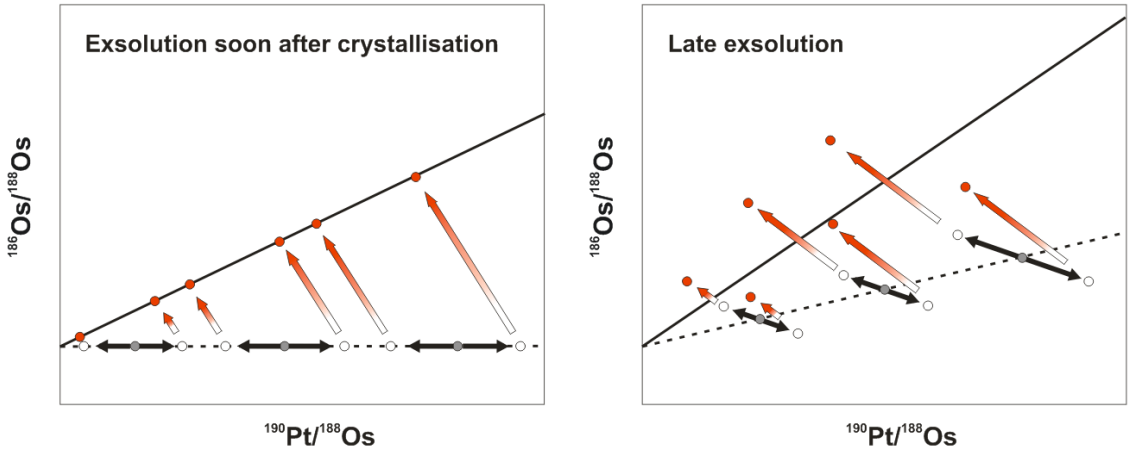

Figure 3. 8 Schematic Pt-Os isochrons showing the effect of timing of exsolution following PGM crystallisation. Early exsolution disturbs $^{190}Pt/^{188}Os$ within a PGM grain but $^{186}Os/^{188}Os$ remains constant, hence the isochron is unaffected. In contrast, exsolution that occurs later, when some radiogenic in-growth of ^{186}Os has occurred, can disturb both the $^{190}Pt/^{188}Os$ and $^{186}Os/^{188}Os$ ratios within a PGM grain. Incomplete sampling of a grain that has experienced late exsolution, and so is isotopically heterogeneous, will produce scatter on an isochron, thus reducing the precision and accuracy of the isochron age.

Alternatively, the contrast between the Pt-Os and U-Pb ages might be dominated by analytical inaccuracies. Inaccuracies in the Os and W interfering element corrections can cause translation of points on a Pt-Os isochron in the x- and y-orientation respectively (see Chapter 2, Fig. 2.10). If samples that comprise an isochron have variable Pt/W ratios which are correlated with Pt/Os ratios then inaccuracies in W and Os corrections can lead to more complex outcomes for the isochron including some degree of rotational translation (see Chapter 2, Fig. 2.10). No systematic correlation between W and Pt is seen in the Bushveld dataset and W concentrations

are generally low (see Appendix 4), hence the magnitude of W corrections is small and so any inaccuracy in this correction is minimised. The accuracy of the Os interfering element correction is more difficult to asses since the final $^{190}Pt/^{188}Os$ ratio is also subject to an uncertainty resulting from Pt/Os inter-element fractionation, which is very difficult to fully quantify (Nowell et al., 2008b).

The relative accuracy of the Pt-Os isochron age for Bushveld PGM implies that Pt/Os inter-element fractionation during laser ablation analysis must be relatively low; up to 2.2 % Pt/Os fractionation can be accommodated within the ± 47 Ma uncertainty on the Pt-Os isochron age, while only ~ 2 % fractionation is required to bring our Pt-Os age into agreement with the accepted U-Pb zircon age (Fig. 3.9). Unfortunately further and more accurate quantification of Pt/Os inter-element fractionation during laser ablation is not possible at present due to a lack of suitable solid PGM ablation reference materials with precisely known Pt/Os ratios and/or age. Furthermore, full quantification of the extent of Pt/Os inter-element fractionation that might occur in the range of mineral phases used in constructing the Bushveld isochron would require not one but several matrix-matched ablation reference materials. A dominant factor that has, thus far, prohibited the manufacture of such a suite of reference materials is the very high melting temperatures of the PGEs and their alloys.

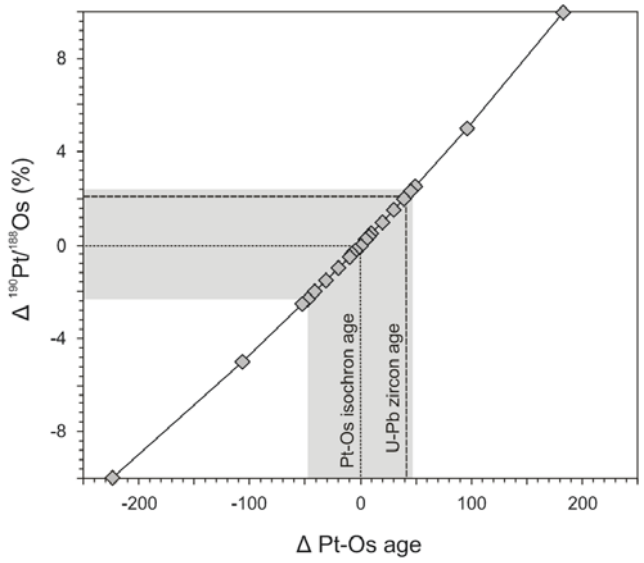

Figure 3. 9 Simple modeling of Pt/Os fractionation during laser ablation MC-ICPMS PGM analysis shows that ~2.2 % fractionation can be accommodated within the 47 Ma uncertainty on the Bushveld isochron age. 2.0 % fractionation could account for the disparity between the combined Bushveld PGM Pt-Os age presented in this study and the U-Pb zircon age of Scoates and Friedman (2008), however other factors may also contribute to this age contrast (see text for further discussion).

The agreement, within error, of the Bushveld Pt-Os isochron age with the U-Pb zircon age can be used to comment on other potential sources of scatter on the isochron diagram. In particular, very high-Pt low-Os samples are prone to larger uncertainties on Os isotopic ratios resulting from low Os signals. Low Os signals reduce the accuracy of mass bias and interfering element corrections. Since high Pt/Os samples have a strong influence on the isochron slope such inaccuracies have a significant effect on the overall accuracy and precision of the isochron age.

3.5.2.1 Stratigraphic/geographic variation in the Bushveld Complex

Emplacement of the Bushveld Complex is estimated to have occurred over a very short period of ~ 5 Ma or less (Scoates and Friedman, 2008), with dunite pipe emplacement, such as at Onverwacht, occurring during the final stages via processes involving late stage fluids (Schiffries, 1982). The samples provided for this study were collected from *in situ* deposits at three locations within the Bushveld Complex, allowing comparison of data from different stratigraphic layers on separate, geographically disparate limbs of the Bushveld Complex.

An isochron constructed using only data from the 8801 and 8801-R2 Merensky samples yields an age of 1995 ± 50 Ma ($^{186}Os/^{188}Os_i$ = 0.119819 ± 0.000006, MSWD = 1.16), which is identical within error to the combined Bushveld PGM isochron age. It is not possible to construct a reliable isochron using the Onverwacht data alone as the range of $^{190}Pt/^{188}Os$ is too limited and the $^{186}Os/^{188}Os_i$ value is poorly constrained. However, since mantle $^{186}Os/^{188}Os$ is essentially constant throughout Earth history we can take the initial $^{186}Os/^{188}Os$ ratio of PUM at either 0 Ga or 2.054 Ga and use this to calculate a Pt-Os model age for the Onverwacht Pt-Fe nugget. The difference between the two values used for initial $^{186}Os/^{188}Os$ is so small that both give the same age of 2113 ± 106 Ma (5 % uncertainty), which is within error of the Pt-Os model age of Merensky braggite 8801-R2_11 (2024 ± 101 Ma), the Merensky and combined Bushevld PGM Pt-Os isochron ages, and the U-Pb zircon age of Scoates and Friedman (2008).

Schiffries (1982) presents a strong case for genesis of the Dreikop, Onverwacht and Mooihoek dunite pipes via high-temperature metasomatism by a chloride brine, causing redistribution of mobilized components, including PGE. Despite evidence presented in later studies, showing that field relations are consistent with magmatic genesis (Viljoen and Scoon, 1985; Scoon and Mitchell, 1994), Eales and Cawthorn (1996) make the point that such a mechanism is inconsistent with various other features of the layered series of the Bushveld Complex. Hence, a metasomatic origin for these pipes is preferred. This process would cause mixing of the Pt-Os and Re-Os systematics of any PGE horizons that a pipe cross-cuts. The range of measured $^{187}Os/^{188}Os_i$ values in this and previous studies, both within and between different horizons of the Bushveld Complex, indicates that this process would sample and mix very disparate isotopic

signatures. The fact that the Onverwacht data lie on our well defined isochron for the combined Bushveld dataset, with a relatively well constrained initial $^{186}Os/^{188}Os$ ratio, indicates that the Pt-Os system experiences only minor disturbance from such mixing. In fact, the radiogenic nature of the Onverwacht nugget suggests that it inherited relatively little common Os from other horizons. Hence, even with a single Pt-rich grain it is possible to achieve a reconnaissance age estimate by calculating a Pt-Os model age, since such grains are very insensitive to wide variations in initial $^{186}Os/^{188}Os$, and $^{186}Os/^{188}Os_i$ can be estimated with a reasonable degree of certainty.

The same Pt-Os model age calculation, when applied to the Tweefontein Hill sperrylite data, gives an age of 2042 ± 102 Ma (5 % uncertainty), also within error of the Merensky isochron age. All three age estimates are within error of the combined Bushveld isochron and as such cannot be distinguished temporally using this technique.

3.5.2.2 Implications for detrital PGM

Each point plotted on the isochron shown in Figure 3.3 represents a single grain or distinct component. Without imposing any geological constraints on the samples, i.e. including all data from all locations within the Bushveld Complex, the result is an accurate isochron age. This has significant implications for the application of the Pt-Os system, measured by LA-MC-ICPMS, to detrital populations of PGM. *In situ* PGE alloys occur in stratiform chromitites in Alaskan-type layered intrusions and in podiform or stratiform chromitites in the ultramafic assemblages of ophiolites (Cabri, 2002) and are commonly accompanied by a range of other PGM. Detrital populations derived from a single body of significant volume may provide a reliable Pt-Os age despite genesis in a number of small chromitite pods or different stratigraphic layers, as demonstrated by a large population (n = 260) of detrital PGM derived from the Meratus ophiolite, southeast Borneo, which yield a Pt-Os isochron age with 4 % uncertainty (Coggon et al., in review). This feature is unique to the Pt-Os system and results from the very minor variation of $^{186}Os/^{188}Os$ in the convecting mantle throughout Earth history (Brandon et al., 2006).

3.5.3 Suggested requirements for Pt-Os laser ablation geochronology

When applying the Pt-Os isochron dating method it is clearly desirable to have a sample population with a wide range of Pt/Os ratios in order to produce a well constrained isochron and a precise age. For this to be achieved multi-PGM populations are preferable. However, some Pt-rich phases (e.g. sperrylites and Pt-Fe alloys) have such elevated Pt/Os ratios that insufficient common Os is present for the accurate and precise measurement of stable ratios and monitor isotopes used for mass bias and interfering element corrections. Laser parameters such as

power and spot size can be increased in such cases in order to achieve higher Os beam intensities. However, spot size is obviously limited by grain size while the total signal size is limited by the 50V limit of the Neptune MC-ICPMS amplifiers. Although 50V of even the most abundant ^{192}Os isotope is never likely to be achieved on Pt-rich phases such as sperrylites and Pt-Fe alloys, tailoring of the spot size and laser power for maximum Os signal is nevertheless restricted since beam intensities for masses 190 and 192, which are very significant in Pt-rich phases, must not exceed the 50V limit. It is possible to remove mass 192 from the cup configuration since the ^{189}Os/^{188}Os ratio can be used to correct for mass bias but mass 190 must remain in the cup configuration, since the ^{190}Pt/^{188}Os ratio is required for constructing an isochron, and ultimately is the limiting factor on the maximum achievable Os beam intensity in Pt-rich grains.

3.6 Conclusions

1) We have applied the LA-MC-ICPMS method of Nowell et al. (2008b) to produce an accurate Pt-Os age of 2012 ± 47 Ma (2σ; MSWD = 1.19) on Bushveld PGM extracted from *in situ* samples of very well constrained age. The close agreement of the Pt-Os age with published ages, particularly U-Pb zircon ages, demonstrates the validity of this technique, including the corrections for mass bias and isobaric interferences.

2) Precision on the Pt-Os age is comparable to the Re-Os and Rb-Sr systems for Bushveld samples. The technique generates a precise age overall for the Bushveld complex. It was also possible to use the method to produce a precise age for Merensky PGE mineralisation, however insufficient samples were analysed from Onverwacht and Tweefontein Hill to resolve any difference in age between these three episodes of mineralisation.

3) The close agreement between our LA age and precise U-Pb ages indicates that inter-element fractionation at the ablation site during analysis of PGE sulphides and alloys is minor and within the age resolution of this technique.

4) Modelling of isotopic mixing between primary mafic magmas and crustal rocks shows that the Re-Os system is very sensitive, even to low degrees of assimilation of crustal lithologies, while the Pt-Os isotope system is far more robust. Mixing with mantle sulphides has potential to produce variation in both the Re-Os and Pt-Os systems.

5) For application of the Pt-Os LA-MC-ICPMS technique to be successful, a given sample population must host a range of Pt/Os ratios, thus genetically linked multi-PGM populations are preferable. Although a wide range of Pt/Os ratios is desirable, grains with very low Os and high

Pt contents are difficult to analyse; if Os beams are too small then mass bias and interfering element corrections cannot be performed accurately, thus a balance must be found and mass 192 should be excluded from the cup configuration. Care must also be taken when considering data collected from laser ablation analysis of sulphides and arsenides. These minerals may be subject to significant heterogeneity resulting from within-grain decoupling of Pt-Os systematics due to exsolution and/or polytypic transitions.

6) Single grain ages can be estimated for Pt-rich samples by calculating a Pt-Os model age with $^{186}Os/^{188}Os_i$ derived from convecting mantle values, since variation of this ratio in the PUM through time is very restricted.

7) There is huge potential for application of the Pt-Os system as a dating tool for PGM in detrital deposits, despite potential derivation from various individual strata/podiform chromitites within ophiolites or layered intrusions.

3.7 Acknowledgements

This research was supported by a NERC research studentship to JAC (NE/F006497/1).

3.8 References

Barnes, S.-J., Maier, W.D., and Ashwal, L.D., 2004, Platinum-group element distribution in the Main Zone and Upper Zone of the Bushveld Complex, South Africa: Chemical Geology, 208, 293-317.

Begemann, F., Ludwig, K.R., Lugmair, G.W., Min, K., Nyquist, L.E., Patchett, P.J., Renne, P.R., Shih, C.Y., Villa, I.M., and Walker, R.J., 2001, Call for an improved set of decay constants for geochronological use: Geochimica et Cosmochimica Acta, 65, 111-121.

Bingen, B., and Stein, H., 2003, Molybdenite Re-Os dating of biotite dehydration melting in the Rogaland high-temperature granulites, S Norway: Earth and Planetary Science Letters, 208, 181-195.

Brandon, A.D., Walker, R.J., and Puchtel, I.S., 2006, Platinum-osmium isotope evolution of the Earth's mantle: Constraints from chondrites and Os-rich alloys: Geochimica et Cosmochimica Acta, 70, 2093-2103.

Buchanan, P.C., Reimold, W.U., Koeberl, C., and Kruger, F.J., 2004, Rb-Sr and Sm-Nd isotopic compositions of the Rooiberg Group, South Africa: early Bushveld-related volcanism: Lithos, 75, 373-388.

Buick, I.S., Maas, R., and Gibson, R., 2001, Precise U-Pb titanite age constraints on the emplacement of the Bushveld Complex, South Africa: Journal of the Geological Society, 158, 3-6.

Cabri, L.J., 2002, The Platinum-Group Minerals, *in* Cabri, L.J., ed., The Geology, Geochemistry, Mineralogy and Mineral Beneficiation of Platinum-Group Elements, Special Volume 54, Canadian Institute of Mining, Metallurgy and Petroleum, 13-130.

Cawthorn, R.G., Lee, C.A., Schouwstra, R.P., and Mellowship, P., 2002, Relationship between PGE and PGM in the Bushveld Complex: Canadian Mineralogist, 40, 311-328.

Coggon, J.A., Nowell, G.M., Pearson, D.G., and Parman, S.W., *In Review,* Application of the ^{190}Pt-^{186}Os isotope system to dating platinum mineralization and ophiolite formation – An example from the Meratus Mountains, Borneo: Economic Geology.

Day, J.M.D., Pearson, D.G., and Hulbert, L.J., 2008, Rhenium-Osmium Isotope and Platinum-Group Element Constraints on the Origin and Evolution of the 127 Ga Muskox Layered Intrusion: Journal of Petrology, 49, 1255-1295.

Eales, H.V., and Cawthorn, R.G., 1996, The Bushveld Complex, *in* Richard Grant, C., ed., Developments in Petrology, Volume Volume 15, Elsevier, 181-229.

Gulson, B.L., and Jones, M.T., 1992, Cassiterite - Potential for Direct Dating of Mineral-Deposits and a Precise Age for the Bushveld Complex Granites: Geology, 20, 355-358.

Hanley, J.J., 2006, The Aqueous Geochemistry of the Platinum Group Elements (PGE) in Surficial, Low-T Hydrothermal and High-T Magmatic-Hydrothermal Environments, *in* Mungall, J.E., ed., Exploration for Platinum-Group Element Deposits: Toronto, Mineralogical Association of Canada, 498.

Harney, D.M.W., and Vongruenewaldt, G., 1995, Ore-Forming Processes in the Upper Part of the Bushveld Complex, South-Africa: Journal of African Earth Sciences, 20, 77-89.

Harris, C., Pronost, J.J.M., Ashwal, L.D., and Cawthorn, R.G., 2005, Oxygen and hydrogen isotope stratigraphy of the Rustenburg Layered Suite, Bushveld Complex: Constraints on crustal contamination: Journal of Petrology 46, 579-601.

Hart, S.R., and Kinloch, E.D., 1989, Osmium Isotope Systematics in Witwatersrand and Bushveld Ore-Deposits: Economic Geology, 84, 1651-1655.

Heaman, L., and Parrish, R., 1991, U-Pb Geochronology of Accessory Minerals, *in* Heaman, L., and Ludden, J.N., eds., Applications of Radiogenic Isotope Systems to Problems in Geology: Toronto, Mineralogical Association of Canada, 498.

Horan, M.F., Morgan, J.W., Grauch, R.I., Coveney Jr, R.M., Murowchick, J.B., and Hulbert, L.J., 1994, Rhenium and osmium isotopes in black shales and Ni-Mo-PGE-rich sulfide layers, Yukon Territory, Canada, and Hunan and Guizhou provinces, China: Geochimica et Cosmochimica Acta, 58, 257-265.

Kosler, J., Simonetti, A., Sylvester, P.J., Cox, R.A., Tubrett, M.N., and Wilton, D.H.C., 2003, Laser-ablation ICPMS measurements of Re/Os in molybdenite and implications for Re-Os geochronology: Canadian Mineralogist, 41, 307-320.

Lambert, D.D., Foster, J.G., Frick, L.R., Li, C., and Naldrett, A.J., 1999, Re-Os isotopic systematics of the Voisey's Bay Ni-Cu-Co magmatic ore system, Labrador, Canada: Lithos, 47, 69-88.

Ludwig, K., 2003, Isoplot/Ex, version 3: a geochronological toolkit for Microsoft Excel, Geochronology Centre Berkeley.

Luguet, A., Nowell, G.M., and Pearson, D.G., 2008a, $^{184}Os/^{188}Os$ and $^{186}Os/^{188}Os$ measurements by Negative Thermal Ionisation Mass Spectrometry (N-TIMS): Effects of interfering element and mass fractionation corrections on data accuracy and precision: Chemical Geology, 248, 342-362.

Luguet, A., Pearson, D.G., Nowell, G.M., Dreher, S.T., Coggon, J.A., Spetsius, Z.V., and Parman, S.W., 2008b, Enriched Pt-Re-Os isotope systematics in plume lavas explained by metasomatic sulfides: Science, 319, 453-456.

Maier, W.D., Arndt, N.T., and Curl, E.A., 2000, Progressive crustal contamination of the Bushveld Complex: evidence from Nd isotopic analyses of the cumulate rocks: Contributions to Mineralogy and Petrology, 140, 316-327.

Makovicky, E., 2002, Ternary and Quaternary Phase Systems with PGE, *in* Cabri, L.J., ed., The Geology, Geochemistry, Mineralogy and Mineral Beneficiation of Platinum-Group Elements, Volume Special Volume 54, Canadian Institute of Mining, Metallurgy and Petroleum, 131-175.

Marsh, J.S., Bowen, M.P., Rogers, N.W., and Bowen, T.B., 1992, Petrogenesis of Late Archean flood-type basic lavas from the Klipriviersberg group, Ventersdorp Supergroup, South Africa: Journal of Petrology, 33, 817-847.

McCandless, T.E., and Ruiz, J., 1991, Osmium isotopes and crustal sources for platinum-group mineralization in the Bushveld Complex, South Africa: Geology, 19, 1225-1228.

McCandless, T.E., Ruiz, J., Adair, B.I., and Freydier, C., 1999, Re-Os isotope and Pd/Ru variations in chromitites from the Critical Zone, Bushveld Complex, South Africa: Geochimica et Cosmochimica Acta, 63, 911-923.

McCandless, T.E., Ruiz, J., and Campbell, A.R., 1993, Rhenium behavior in molybdenite in hypogene and near-surface environments: Implications for Re-Os geochronometry: Geochimica et Cosmochimica Acta, 57, 889-905.

McDaniel, D.K., Walker, R.J., Hemming, S.R., Horan, M.F., Becker, H., and Grauch, R.I., 2004, Sources of osmium to the modern oceans: new evidence from the ^{190}Pt-^{186}Os system: Geochimica et Cosmochimica Acta, 68, 1243-1252.

Mezger, K., Hanson, G.N., and Bohlen, S.R., 1989, High-precision UPb ages of metamorphic rutile: application to the cooling history of high-grade terranes: Earth and Planetary Science Letters, 96, 106-118.

Mitchell, A.A., 1990, The stratigraphy, petrography and mineralogy of the Main Zone of the northwestern Bushveld Complex: South African Journal of Geology, 93, 818-831.

Naldrett, A.J., 2004, Magmatic Sulfide Deposits: Geology, Geochemistry and Exploration: Berlin, Springer, 728.

Naldrett, A.J., Wilson, A., Kinnaird, J., and Chunnett, G., 2009, PGE Tenor and Metal Ratios within and below the Merensky Reef, Bushveld Complex: Implications for its Genesis: Journal of Petrology, 50, 625-659.

Nex, P.A.M., 2005, The structural setting of mineralisation on Tweefontein Hill, northern limb of the Bushveld Complex, South Africa: Applied Earth Science, 114, 243-251.

Nomade, S., Renne, P.R., and Merkle, R.K.W., 2004, ^{40}Ar/^{39}Ar age constraints on ore deposition and cooling of the Bushveld Complex, South Africa: Journal of the Geological Society, 161, 411-420.

Nowell, G.M., Luguet, A., Pearson, D.G., and Horstwood, M.S.A., 2008a, Precise and accurate ^{186}Os/^{188}Os and ^{187}Os/^{188}Os measurements by multi-collector plasma ionisation mass spectrometry (MC-ICPMS) part I: Solution analyses: Chemical Geology, 248, 363-393.

Nowell, G.M., Pearson, D.G., Parman, S.W., Luguet, A., and Hanski, E., 2008b, Precise and accurate ^{186}Os/^{188}Os and ^{187}Os/^{188}Os measurements by Multi-collector Plasma Ionisation Mass Spectrometry, part II: Laser ablation and its application to single-grain Pt-Os and Re-Os geochronology: Chemical Geology, 248, 394-426.

Pearson, D.G., Shirey, S.B., Harris, J.W., and Carlson, R.W., 1998, Sulphide inclusions in diamonds from the Koffiefontein kimberlite, S Africa: constraints on diamond ages and mantle Re-Os systematics: Earth and Planetary Science Letters, 160, 311-326.

Rehkämper, M., Halliday, A.N., Fitton, J.G., Lee, D.C., Wieneke, M., and Arndt, N.T., 1999, Ir, Ru, Pt, and Pd in basalts and komatiites: new constraints for the geochemical behavior of the platinum-group elements in the mantle: Geochimica et Cosmochimica Acta, 63, 3915-3934.

Reisberg, L.C., Tredoux, M., and Harris, C., 2006, Re-Os systematics of the Platreef (Sandsloot mine) of the northern limb of the Bushveld Complex: Geochimica et Cosmochimica Acta, 70, A526-A526.

Richardson, S.H., and Shirey, S.B., 2008, Continental mantle signature of Bushveld magmas and coeval diamonds: Nature, 453, 910-913.

Richardson, S.H., Shirey, S.B., Harris, J.W., and Carlson, R.W., 2001, Archean subduction recorded by Re-Os isotopes in eclogitic sulfide inclusions in Kimberley diamonds: Earth and Planetary Science Letters, 191, 257-266.

Ripley, E.M., Lambert, D.D., and Frick, L.R., 1998, Re-Os, Sm-Nd, and Pb isotopic constraints on mantle and crustal contributions to magmatic sulfide mineralization in the Duluth Complex: Geochimica et Cosmochimica Acta, 62, 3349-3365.

Saal, A.E., Rudnick, R.L., Ravizza, G.E., and Hart, S.R., 1998, Re–Os isotope evidence for the composition, formation and age of the lower continental crust: Nature, 393, 58-61.

Schiffries, C.M., 1982, The petrogenesis of a platiniferous dunite pipe in the Bushveld Complex; infiltration metasomatism by a chloride solution: Economic Geology, 77, 1439-1453.

Schoenberg, R., Kruger, F.J., Nagler, T.F., Meisel, T., and Kramers, J.D., 1999, PGE enrichment in chromitite layers and the Merensky Reef of the western Bushveld Complex; a Re-Os and Rb-Sr isotope study: Earth and Planetary Science Letters, 172, 49-64.

Scoates, J.S., and Friedman, R.M., 2008, Precise age of the platiniferous Merensky reef, Bushveld Complex, South Africa, by the U-Pb zircon chemical abrasion ID-TIMS technique: Economic Geology, 103, 465-471.

Scoon, R.N., and Mitchell, A.A., 1994, Discordant Iron-Rich Ultramafic Pegmatites in the Bushveld Complex and their Relationship to Iron-Rich Intercumulus and Residual Liquids: Journal of Petrology, 35, 881-917.

Selby, D., and Creaser, R.A., 2004, Macroscale NTIMS and microscale LA-MC-ICP-MS Re-Os isotopic analysis of molybdenite: Testing spatial restrictions for reliable Re-Os age determinations, and implications for the decoupling of Re and Os within molybdenite: Geochimica et Cosmochimica Acta, 68, 3897-3908.

Selby, D., Creaser, R.A., Hart, C.J.R., Rombach, C.S., Thompson, J.F.H., Smith, M.T., Bakke, A.A., and Goldfarb, R.J., 2002, Absolute timing of sulfide and gold mineralization: A comparison of Re-Os molybdenite and Ar-Ar mica methods from the Tintina Gold Belt, Alaska: Geology, 30, 791-794.

Spencer, L.J., 1926, Sperrylite crystals from the Transvaal: Mineralogical Magazine, 21, 94-97.

Stein, H., Scherstén, A., Hannah, J., and Markey, R., 2003, Subgrain-scale decoupling of Re and ^{187}Os and assessment of laser ablation ICP-MS spot dating in molybdenite: Geochimica et Cosmochimica Acta, 67, 3673-3686.

Viljoen, M.J., and Scoon, R.N., 1985, The distribution and main geologic features of discordant bodies of iron-rich ultramafic pegmatite in the Bushveld Complex: Economic Geology, 80, 1109-1128.

Walker, R.J., Carlson, R.W., Shirey, S.B., and Boyd, F.R., 1989, Os, Sr, Nd, and Pb isotope systematics of Southern African peridotite xenoliths; implications for the chemical evolution of subcontinental mantle: Geochimica et Cosmochimica Acta, 53, 1583-1595.

Walker, R.J., Hanski, E., Vuollo, J., and Liipo, J., 1996, The Os isotopic composition of Proterozoic upper mantle: Evidence for chondritic upper mantle from the Outokumpu ophiolite, Finland: Earth and Planetary Science Letters, 141, 161-173.

Walker, R.J., Morgan, J.W., Naldrett, A.J., Li, C., and Fassett, J.D., 1991, Re-Os Isotope Systematics of Ni-Cu Sulfide Ores, Sudbury Igneous Complex, Ontario - Evidence for a Major Crustal Component: Earth and Planetary Science Letters, 105, 416-429.

Woodland, S.J., Pearson, D.G., and Thirlwall, M.F., 2002, A Platinum Group Element and Re-Os Isotope Investigation of Siderophile Element Recycling in Subduction Zones: Comparison of Grenada, Lesser Antilles Arc, and the Izu-Bonin Arc: Journal of Petrology, 43, 171-198.

Zaccarini, F., Garuti, G., and Cawthorn, R.G., 2002, Platinum-group minerals in chromitite xenoliths from the Onverwacht and Tweefontein ultramafic pipes, Eastern Bushveld Complex, South Africa: Canadian Mineralogist, 40, 481-497.

4 Application of the ^{190}Pt-^{186}Os isotope system to dating platinum mineralization and ophiolite formation – An example from the Meratus Mountains, Borneo

Abstract

The formation age of platinum-group minerals (PGM) in placer deposits has traditionally been difficult to constrain. We have applied the Pt-Os and Re-Os isotope systems to this problem by analyzing a suite of PGM from a placer deposit in southeastern Borneo that are derived, by mechanical processes, from chromitites of the Meratus ophiolite. Published subduction and emplacement ages and biostratigraphy of pelagic sediments of the ophiolite sequence define a minimum age for genesis at a spreading ridge. However, igneous components of the ophiolite have previously been undateable. 260 PGM grains from the Pontyn River, which drains the Meratus Mountains, were analysed by laser ablation multi-collector inductively coupled mass spectrometry (LA-MC-ICPMS). Re-Os data do not show any isochronous relationship. Despite a significant range in $^{187}Os/^{188}Os$ (0.122 – 0.141), $^{187}Re/^{188}Os$ values show a very narrow range (0.000005 – 0.002980). In contrast, the PGM have a wide range in $^{186}Os/^{188}Os$ (0.119801 - 0.120315) and $^{190}Pt/^{188}Os$ (<0.00001 - 1.529227) that yields a precise Pt-Os isochron age of 197.8 ± 8.1 Ma (2σ). This age fits well with published age constraints for this ophiolite and we argue that it dates the crystallization of the PGM. Previous studies have shown that the Pontyn PGM are derived from ophiolitic chromitite, therefore the PGM Pt-Os isochron age also provides the first absolute age constraint for the genesis of igneous rocks of the Meratus ophiolite. These results highlight the potential of the Pt-Os geochronometer as a tool for dating the crystallization age of PGM found in placer deposits, for dating primary platinum mineralization in general and for use in ophiolite geochronology.

4.1 Introduction

Since it was first applied by Walker et al. (1991), there has been a surge in interest in the application of the ^{190}Pt-^{186}Os decay system as a tracer of deep Earth processes (e.g. Walker, et al., 1997a; Brandon, et al., 1998; Brandon, et al., 2007; Luguet, et al., 2008). However, the application of this decay system to geochronology has been limited (Walker, et al., 1997b) with very few applications to ore genesis, despite the economic relevance of the parent and daughter isotopes. The reasons for this stem from the very low decay constant of ^{190}Pt ($\lambda = 1.477 \times 10^{-12}$ yr^{-1} ± 1 %, Begemann et al., 2001) and the very small resultant variations in the $^{186}Os/^{188}Os$ ratio.

These practical difficulties make PGE alloys and certain other PGM clear targets for study because of the wide range of potential Pt/Os ratios that these mineral groups may display (Harris and Cabri, 1991). Nowell et al., (2008b) recently showed that it is possible to produce accurate and precise $^{186}Os/^{188}Os$ measurements of PGM grains via laser ablation multi-collector ICPMS (LA-MC-ICPMS) and the additional Re-Os isotope data produced from such analyses can be used to examine mantle Os isotope variations on a global scale (Pearson et al., 2007). The former study also demonstrated that the substantial variation in Pt/Os within and between PGM can be used to obtain geochronological information for samples from ultramafic rocks that are often difficult to date. This offers obvious opportunities in terms of the dating of ophiolite massifs, which is notoriously problematic when using traditional geochronology methods.

In this study we apply the Pt-Os chronometer to a suite of detrital PGM grains derived from the Meratus ophiolite, Borneo. The source of the PGM grains is well constrained and comparison with existing geochronology and geochemistry allows us to evaluate the accuracy of the Pt-Os age. The result illustrates the potential for the Pt-Os isotope system in constraining the age and origin of alluvial PGM deposits.

4.2 Samples and Provenance

PGM grains from Borneo were provided for this study by the Smithsonian Institution National Museum of Natural History from sample NMNH96511. The grains were collected by A. Lacroix from the Pontyn River, Tanah Laut, in the province of South Kalimantan, Indonesian Borneo and were labelled as “Laurite”.

4.2.1 Regional Geology and Provenance

The Pontyn River drains the southern Meratus Mountains and flows into the Java Sea near the town of Asemasen on the southeast coast of Borneo (Fig. 4.1). The catchment of the river and its tributaries is geologically varied. It includes various clastic sedimentary rocks, limestones, intermediate to felsic volcanics, metamorphic rocks and the ultramafic, gabbroic and leucocratic rocks that make up the Meratus Ophiolite (Sikumbang, 1990; Guntoro, 1999). Trace element abundances (particularly negative Nb-Ta anomalies and $(La/Nb)_N$ ratios of 1.7 – 3.5) of Meratus lavas have been interpreted as evidence that a back-arc-basin setting may have produced the oceanic lithosphere that forms the Meratus ophiolite (Monnier et al., 1999). However, the same authors conclude that Cr# of spinel, orthopyroxene and clinopyroxene in peridotites, along with low Na_2O and TiO_2 contents and depletion in incompatible elements, demonstrates that Meratus

peridotites represent subcontinental lithospheric mantle that experienced low degrees of localised partial melting during the final stages of an episode of continental rifting.

Burgath and Mohr (1986) and Burgath (1988) reported the occurrence of PGE-rich chromitite seams in the serpentinised dunite of the Meratus ultramafic rocks. Hattori et al. (1992) analysed the osmium isotope composition of laurite grains from these chromitites by SIMS. These authors also analysed PGM from associated alluvial placers and concluded that the isotopic data support a detrital origin for the placer grains, which were mechanically eroded from their host chromitites.

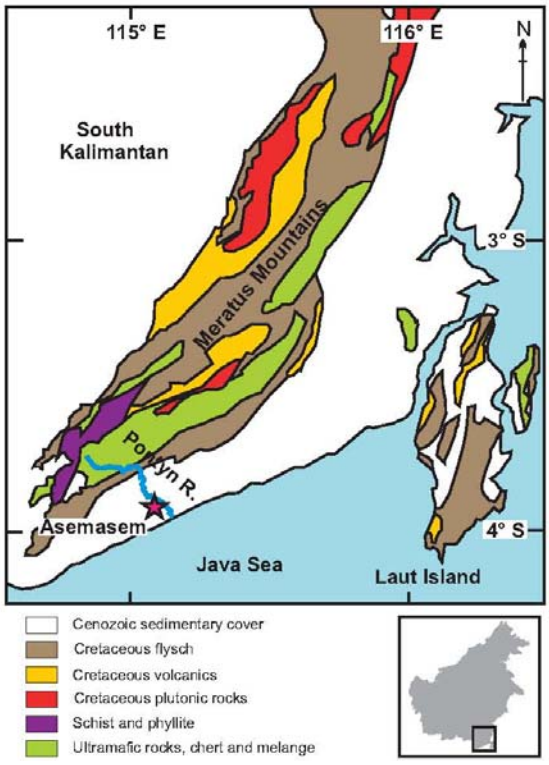

Figure 4. 1 Map showing the geology of the Meratus Mountains, including ophiolitic rocks (green), schists formed by subduction zone metamorphism (purple) and location of the Pontyn River (after Wakita et al., 1998).

4.2.2 PGM Mineralogy and Morphology

260 placer PGM grains were analysed in this study. Electron microprobe analyses confirmed two main compositional groups: 82 grains of Os-bearing laurite (14.3 to 31.1 wt % Os) and 174 grains of Pt-Fe alloy (73.8 – 91.5 wt % Pt, 0.4 – 4.0 wt % Os) (Fig. 4.2, Appendices 10 and 11). Two grains of Ir-Os-Pt alloy (iridium), with 53.0 wt % Ir (BRN-2-076 and BRN-3-024), one of $PtAs_2$ (sperrylite) (BRN-2-045) and one of PGE-bearing Au-Ag alloy were also identified.

Long-axis dimensions range from circa 250 µm to 2000 µm. The three largest grains are alloys; sulfide grains are generally smaller with a maximum diameter of 800 µm. Sulfides are predominantly equidimensional and sub-rounded to rounded, although rare examples of more elongate and sub-angular grains are present in this population. Subhedral grains show cubic systems (e.g. Fig. 4.3A). PGE alloys have more varied morphologies; rounded, sub-spherical to ellipsoid alloys (e.g. Fig. 4.3C) are uncommon, with the majority displaying irregular, angular and "nodular" forms (e.g. Fig. 4.3D-F). Two grains in this group are subhedral; they have cubic crystal systems (e.g. Fig. 4.3B), which are typical of isoferroplatinum (Pt_3Fe) (Harris and Cabri 1991). Surface features are varied and include pits (rounded and irregular, cubic, linear) ranging from approximately 1 µm to 40 µm in diameter, scratches and fractures (Fig. 4.3G-L). These surface features, with the exception of euhedral pits, are typical of alluvially transported PGM grains (Cabri, et al., 1996; Oberthür, et al., 2004). Euhedral pits are likely to represent negative crystals or melt inclusions, removed by weathering, that inherited the morphology of the host PGM grain, as described by Brenker et al., (2003).

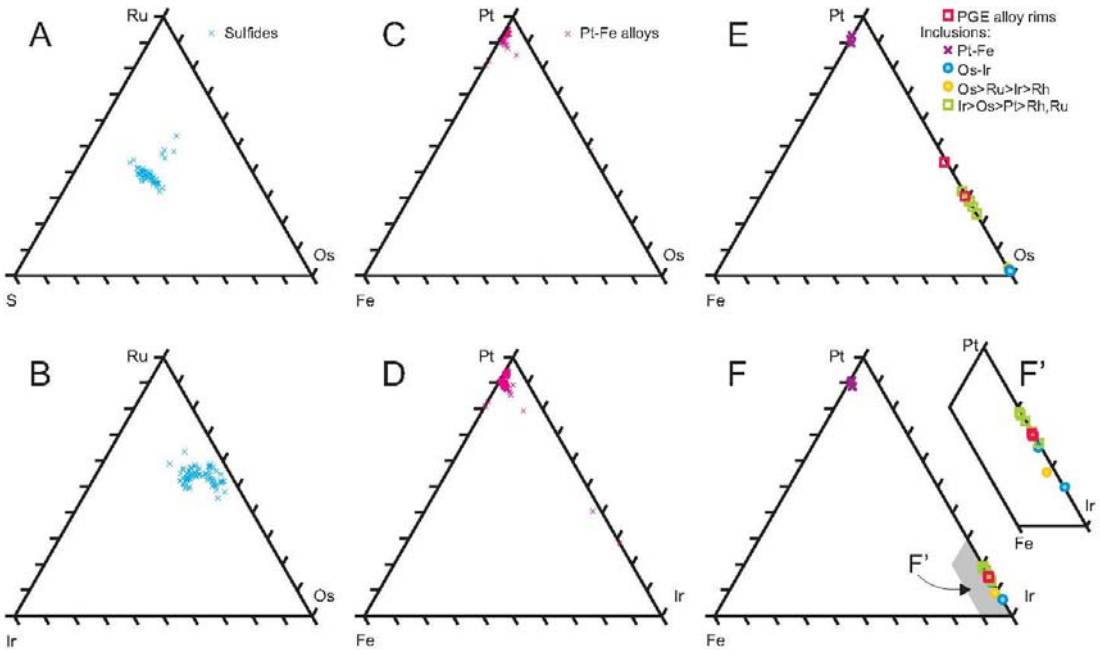

Figure 4. 2 Ternary plots showing relative (wt %) compositions of dominant elements in Borneo placer PGM and their inclusions, measured by Electron Microprobe. A, B, sulfides. C, D, alloys. E, F, PGE alloy rims on Pt-Fe alloy grains and inclusions in alloy grains. Full compositional data are displayed in Appendices 10, 11 and 12.

4.3 Methods

4.3.1 Laser Ablation Multi-Collector ICPMS (LA MC-ICPMS)

Grains were mounted in 10 x 10 grids on adhesive carbon SEM tabs fixed to glass microscope slides. Samples were imaged prior to isotopic analysis at Durham University using a Hitachi TM-1000 Tabletop Scanning Electron Microscope.

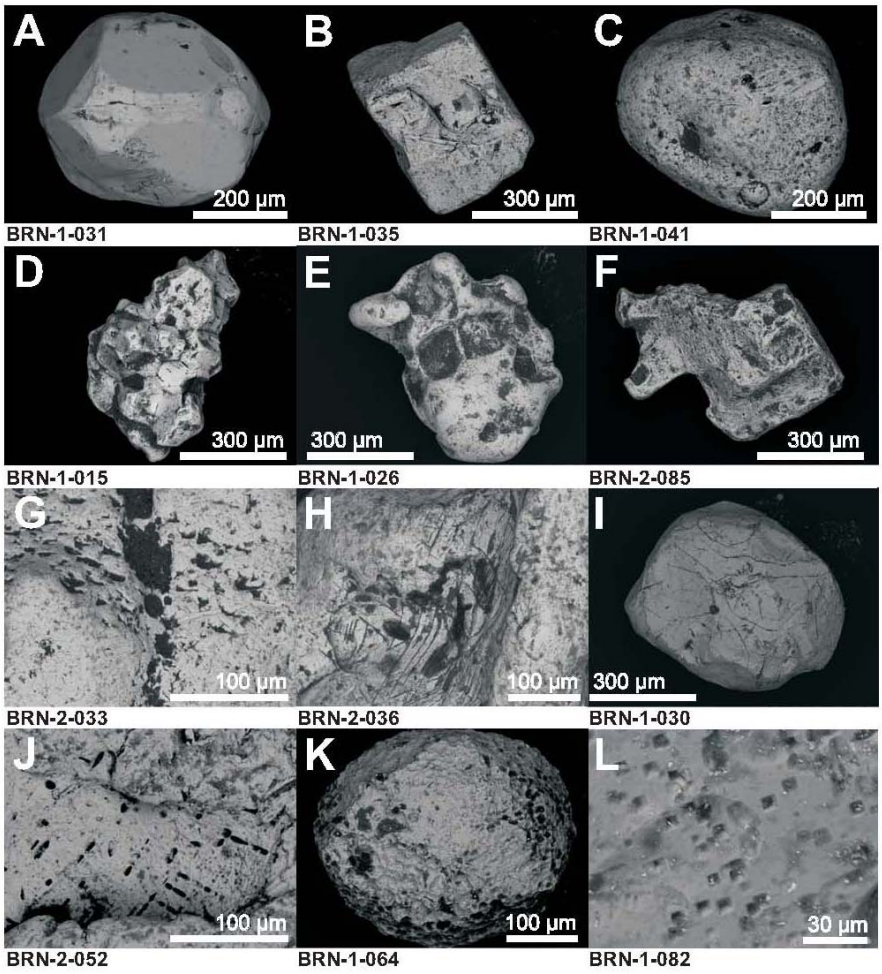

Figure 4. 3 BSE images showing examples of grain morphologies and surface textures seen in Borneo placer sulfides (A, I, K, L) and Pt-Fe alloys (B – H, J). A, subhedral laurite showing cubic crystal habit. B, subhedral, cubic Pt-Fe alloy. C, Sub-spherical Pt-Fe alloy. D – F, irregular, angular and "nodular" forms, typical of Pt-Fe alloys in this population. G, K, irregular pits on grain surfaces, often infilled with granular (dark) material, possibly chromite. H, I, scratches and fractures consistent with transport in an alluvial system. J, rounded pits following linear trends. L, cubic, parallel pits in the surface of a Pt-Fe alloy.

Pt-Os isotopic analyses were carried out at Durham University Northern Centre for Isotopic and Elemental Tracing (NCIET) using a New Wave UP 213 nm laser and Thermo Fisher Neptune multi-collector ICPMS (MC-ICPMS) via the method presented in (Nowell, et al., 2008b). Borneo samples were analysed over six sessions between 17-12-2007 and 18-02-2008. Laser spot sizes of 120 µm to 125 µm were used for Os-rich grains, while 250 µm spots were used for Pt-rich/Os-poor samples. Laser repetition rate was varied between 9 and 20 Hz, and laser power density from 40 to 100 percent. Fixed value laser parameters used are given in Nowell et al. (2008b).

At the start of each analytical session a 1µg ml^{-1} DROsS standard solution was analysed ten times in order to assess instrument accuracy and reproducibility. Over the six analytical sessions the reproducibility was 122 ppm for $^{187}Os/^{188}Os$ and 125 ppm for $^{186}Os/^{188}Os$. Mean $^{187}Os/^{188}Os$ and $^{186}Os/^{188}Os$ ratios of 0.160918 ± 0.000020 and 0.119917 ± 0.000015 respectively (2 SD, n = 60) (Appendix 7) are identical to the values of 0.160921 ± 0.000018 and 0.119917 ± 0.000020 (2 SD, n = 5) reported for this standard by Nowell et al. (2008b).

The $^{189}Os/^{188}Os$ ratio is free of elemental interferences so it was used to correct for mass bias. A value of 1.21978 (Nowell, et al., 2008b) was assumed for this correction.

^{184}W, ^{186}W and ^{187}Re occur as elemental isobaric interferences on ^{184}Os, ^{186}Os and ^{187}Os during laser ablation. To correct for these interferences ^{182}W and ^{185}Re were monitored during analyses and, assuming $^{182}W/^{184}W$ = 0.863376 ± 15, $^{182}W/^{186}W$ = 0.929231 ± 13 and $^{185}Re/^{187}Re$ = 0.598050 ± 13 (derived from analyses of a 1µg ml-1 DROsS solution doped with varying concentrations of W and Re; see Nowell, et al., 2008a), the appropriate level of interference was subtracted for each 1 s integrationto yield the corrected Os isotope ratios.

Interferences on ^{190}Os and ^{192}Os by ^{190}Pt and ^{192}Pt cannot be corrected in the same way since the faraday cup configuration used does not provide a Pt monitor isotope. Instead Os must be treated as the interfering element, with ^{188}Os taken as the monitor isotope. The mean $^{190}Os/^{188}Os$ ratio determined from measurements of the DROsS standard at the start of each session was used to subtract the Os interference on mass 190 and thereby derive the ^{190}Pt intensity and the $^{190}Pt/^{188}Os$ ratio.

Each analysis is made up of 40 one second integrations. After mass bias and interfering element corrections were applied to each measurement the analyses were subject to a 2 sigma rejection. The method and corrections are discussed in greater detail by Nowell et al. (2008b).

For plotting Pt-Os isochrons total errors on $^{186}Os/^{188}Os$ ratios were calculated to incorporate external reproducibility. A value of 176 ppm was used for grains with 188 beams of 1 V or more;

grains with 188 beams < 1 V were assigned external reproducibility values of 352 ppm. These values were derived from repeat analyses over one year of an in-house standard (Urals Os-rich PGE alloy 36720 G1, Nowell, et al., 2008b). No such data is available for $^{190}Pt/^{188}Os$ since there is no Pt-rich homogeneous ablation standard. However, small scale isotopic heterogeneity of individual samples leads to relatively large within run precision contributing a major component of the overall uncertainty on this ratio. In addition, a significant portion of the uncertainty on $^{190}Pt/^{188}Os$ measurements may result from Pt-Os fractionation at the ablation site. Such interelement fractionation is poorly understood, but is estimated to be 5 % or less by Nowell et al. (2008b). Total uncertainty on the $^{190}Pt/^{188}Os$ ratio therefore includes the within run error and 5 % uncertainty to account for external reproducibility and potential elemental fractionation that may occur at the ablation site.

4.3.2 Electron Microprobe and SEM

The PGM were transferred to polished sections for compositional analysis using a CAMECA SX-100 electron microprobe at Brown University, Rhode Island. WDS analyses were carried out with an accelerating voltage of 20 keV, beam current of 25 nA and beam diameter of ~1 µm. Measurement times of 10 seconds were used on peaks, with five second measurements on the backgrounds above and below each peak. Pure metal standards were used for all elements analysed with the exception of S and As, where FeS and GaAs were used respectively. Detection limits are 3 sigma and range from 0.088 to 0.589 wt % for analyses of sulfides. During analyses of alloys (high Pt samples) Pt interference occurs on the Fe L alpha peak, therefore Fe was analyzed on the K alpha peak for these samples with a detection limit of 1.37 wt %. Full details of detection limits are given in Appendix 9. Silicate and base metal sulfide inclusions were analysed qualitatively using EDS analyses.

4.4 Results

4.4.1 Inclusions and other internal features of Borneo PGM grains

BSE images of polished grains reveal distinct groups of internal features. Sulfides are poorly polished since there is a considerable contrast in hardness between these grains and PGE alloys, with which they are mounted. Despite this it is possible to identify inclusions hosted within many of the Borneo laurites. These appear as dark patches, approximately 5 to 30 µm in diameter, that range from rounded to euhedral (hexagonal) and are crystallographically orientated (Appendix 5). The shape of euhedral inclusions and their orientation relative to each

other suggests that they may have been included as liquids and their morphological features are inherited from the host grains. EDS analyses of the inclusions show a range of phases; silicates (amphibole, epidote, clinopyroxene, serpentine, olivine, anorthite, melt,), base metal sulfides (pyrite, pyrrhotite, pentlandite, chalcopyrite,) and two composite inclusions of silicate+sulfide+alloy were identified.

Silicate inclusions in alloy grains have diameters as great as 75 µm and may be sub- or euhedral and crystallographically orientated, or anhedral – in the form of linear 'blebs' (Appendix 6A, B). Additional internal features of alloys can be grouped together: inclusions or intergrowths of Os- and Ir-dominated PGE alloys (Appendix 6C-E, Appendix 12) ranging from ~20 – 100 µm in length; micro-PGE alloy inclusions, up to 15 µm in diameter (Appendix 6F, H); and PGE alloy rims (Appendix 6K, L) up to ~200 µm on composite grains. BSE images also highlight sets of bright (or, rarely, dark), sub-micron thickness linear features (Appendix 6G, I, J) which may be cogenetic or a product of exsolution (Cabri and Genkin, 1991).

4.4.2 Pt-Os isotopes and age

260 PGM grains were analysed by LA-MC-ICPMS. $^{190}Pt/^{188}Os$ values measured range from <0.00001 to 1.529227 and $^{186}Os/^{188}Os$ values range from 0.119801 to 0.120315 (Appendix 8). This range in $^{186}Os/^{188}Os$ is more than 25 times greater than that observed in typical convecting mantle (Brandon, et al., 1999). Measured $^{186}Os/^{188}Os$ correlates positively with $^{190}Pt/^{188}Os$. The initial $^{186}Os/^{188}Os$ ratio calculated from the data is 0.119830 ± 0.000003 and the resulting isochron has an MSWD of 0.90, a probability of fit of 0.88 and an age of 197.8 ± 8.1 Ma (2σ; Fig. 4.4). The uncertainty on the age incorporates the 1 % uncertainty on the decay constant of ^{190}Pt as estimated by Begemann et al. (2001).

Variation in $^{190}Pt/^{188}Os$ is dominated by mineralogy (Pt-Fe alloys versus Os-rich laurites), while $^{186}Os/^{188}Os$ ratio variation is minor and is most likely dominated by radiogenic in-growth. This is addressed further in the Discussion section. Pt-Fe alloys and sperrylite have ~ 76 – 91 wt % Pt, 0.4 – 4.0 wt % Os, $^{190}Pt/^{188}Os$ ratios that range from 0.00098 to 1.494 and $^{186}Os/^{188}Os$ values of 0.119801 – 0.120315; these phases are predominant in defining the slope of the isochron. Laurite grains in this population have <0.2 wt % Pt, 14.3 – 31.1 wt % Os and $^{190}Pt/^{188}Os$ values up to only 0.0743 and therefore contribute to defining the initial $^{186}Os/^{188}Os$ ratio.

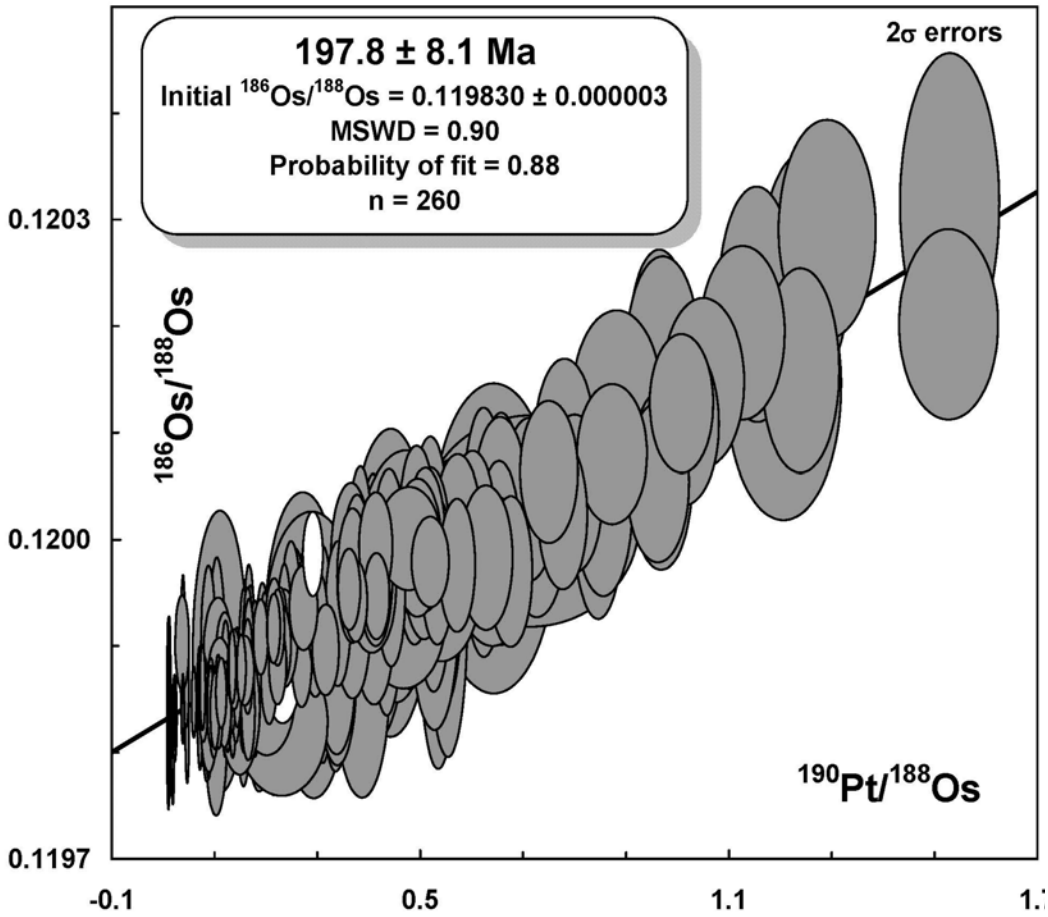

Figure 4. 4 Pt-Os isochron diagram for 260 Borneo placer PGM. Fill color of error ellipse indicates mineralogy: grey, Pt-Fe alloy; black, laurites and one Au-Ag alloy; white, grains not exposed by/lost during polishing. Errors on $^{186}Os/^{188}Os$ incorporate within run uncertainties and long term external reproducibility on this ratio based on repeat analyses of an in-house standard grain. $^{190}Pt/^{188}Os$ errors include 5% uncertainty to account for potential elemental (Pt/Os) fractionation that may occur at the ablation site (Nowell, et al., 2008b). The uncertainty quoted on the isochron age incorporates an uncertainty of 1% on the decay constant of ^{190}Pt (Begemann, et al., 2001). Plotted using Isoplot version 3.1 (Ludwig, 2003).

4.4.3 Re-Os isotopes

Despite a very restricted range in $^{187}Re/^{188}Os$ values (0.000005 – 0.002980), there is considerable variation in $^{187}Os/^{188}Os$ (0.122117 – 0.140674). The extremely low Re/Os ratios result in calculated initial $^{187}Os/^{188}Os$ values that are almost identical to measured $^{187}Os/^{188}Os$, illustrating that these samples do not share a common initial $^{187}Os/^{188}Os$ value. Hence Re-Os isotope systematics are scattered and do not exhibit an isochronous relationship. Studies of other ophiolite related PGM have shown considerable variation in $^{187}Os/^{188}Os$ that is not related to Re/Os variation (Meibom, et al., 2002; Walker, et al., 2002; Pearson, et al., 2007).

Variations in $^{187}Re/^{188}Os$ and $^{187}Os/^{188}Os$ ratios may be related to R-Factor fractionation (Campbell and Naldrett, 1979) during PGM growth. Alternatively these variations may result from the PGM population being derived from several different chromitite pods, essentially formed from isolated melts with differing initial $^{187}Os/^{188}Os$.

4.5 Discussion

4.5.1 PGM genesis

There has been much debate over the formation of alluvial or detrital PGA grains. Bowles (1988) has proposed a secondary origin for PGM associated with the Freetown layered intrusion in Sierra Leone by lateritic-type crystallisation within placers in a tropical environment. Perhaps more widely applicable on a global scale is the proposal of a magmatic origin for these minerals. Several scenarios have been suggested for crystallisation of PGM in the deep mantle or core (Bird and Bassett, 1980; Bird, et al., 1999), however many workers now conclude that ophiolitic PGM grains are formed during chromitite genesis (Ahmed, 2007; Pearson, et al., 2007; Tsoupas and Economou-Eliopoulos, 2008) in the lithospheric upper mantle (podiform chromitites) or base of the crust (stratiform chromitites; Paktunc, 1990).

In the case of Borneo and the Meratus grains, the tropical climate provides the potential for secondary crystallisation of PGM by the weathering mechanism described by Bowles (1988). If the PGM grains analysed in this study were formed by a secondary process involving re-crystallization within laterites, then the Pt-Os isochron must represent a mixing line and not a true or meaningful age because lateritization is well below any likely diffusional re-equilibration temperature for the Pt-Os (or Re-Os) isotope system. In such a scenario PGM formation would be late in the geological history of the Meratus ophiolite, occurring after high level exhumation of the mantle section. This greatly reduces the time available for radiogenic Os in-growth and means that any proposed precursors to the PGM grains, such as ultramafic rocks or chromitite veins, would need to have evolved to high $^{186}Os/^{188}Os$ ratios rapidly and with unusually high Pt/Os ratios. Since the initial $^{186}Os/^{188}Os$ ratio of typical mantle materials varies so little both spatially and throughout geological time, such a scenario seems very unlikely on this basis alone.

Further evidence against a secondary origin for the Meratus PGM grains comes from Re-Os isotope systematics and S isotope data. The similarity of $^{187}Os/^{188}Os$ ratios in placer and in-situ chromite-hosted PGM in the Meratus area led Hattori et al. (1992) to conclude that mechanical processes are responsible for transporting the PGE (in the form of alloys and sulfides) to the

placer deposits and that the placer grains are direct samples of the mantle-hosted PGM grains. Sulfur isotopes along with arsenic and selenium contents of placer laurite (RuS_2) from the Pontyn and Tambanio Rivers, southeast Borneo, confirm that these grains are derived from their host chromites by purely mechanical processes. The sulfur isotopic ratio of the PGM grains, originating from S-bearing inclusions such as laurite, has a clear mantle signature as opposed to the fractionated and variable S isotope signatures expected if these grains had formed in near-surface environments (Hattori et al., 2004). Hence there is powerful evidence against a low-T secondary origin for the Meratus alluvial PGM.

Silicate, sulfide, and multiphase or composite inclusions are observed in the Borneo PGM grains. Composite inclusions may represent inclusions of trapped melt that later experienced fractional crystallisation. Peck et al., (1992) and Brenker et al., (2003) have used the presence of mineral and melt inclusions, respectively, within PGM from alluvial deposits to argue strongly for a magmatic origin for such grains. A magmatic origin is further supported by the presence of PGM (both sulfides and PGE alloys) as inclusions in chromite grains (Hattori, et al., 2004; Ahmed, 2007; Tsoupas and Economou-Eliopoulos, 2008; Petrou and Economou-Eliopoulos, 2009). Ophiolitic chromitite formation may occur by crystallization from a partial mantle melt after melt-rock interaction (Paktunc, 1990; Zhou, et al., 1998) or by magma mixing (Ballhaus, 1998). In either case, significant volumes of partial melting must occur to produce the parent magmas; thus chromitite mineralization is interpreted as a near-ridge process (Paktunc, 1990) that takes place relatively soon after generation of oceanic lithosphere.

4.5.2 Age of the Meratus Ophiolite

The varied Pt-Os fractionation within the Meratus PGM grains clearly offers possible geochronological constraints on the timing of formation of the Meratus ophiolite. The first issue to consider in evaluating this potential is the likelihood of a single source for the PGM grains and the possibility that the correlation observed on the Pt-Os isochron diagram (Fig. 4.4) may be a mixing line. Addressing the first of these issues, we specifically selected the Meratus samples because their provenance is well constrained. There is good consensus that the PGM grains were derived directly from the single ophiolite body based on close proximity and lack of any other plausible host lithologies in the area (Hattori, et al., 1992; Monnier, et al., 1999). These factors mean that it is unlikely that our PGM grain population is derived from a mixture of ultramafic bodies with differing ages. Nonetheless, it is possible that several different chromitite bodies within the single massif may have contributed to the population of grains that we have analysed. Analyses of different chromitite bodies within a single ophiolite confirm that such bodies can have variable $^{187}Os/^{188}Os$ ratios (e.g. Walker et al., 1996). This variability in initial

$^{187}Os/^{188}Os$ ratios, combined with subsequent post-formation in-growth, may be a major reason why the Re-Os data for Meratus PGM are scattered, with no correlation on the isochron diagram. In contrast to the Re-Os decay system, any variability in initial isotopic ratios due to the derivation of grains from multiple chromitite bodies would be masked in the Pt-Os system because the variation in $^{186}Os/^{188}Os$ of the convecting mantle throughout the whole of the Phanerozoic is less than 100 ppm (Brandon et al., 2006). Hence, the Pt-Os isochron correlation, in this instance, is unlikely to reflect mixing phenomena between bodies with significantly different initial $^{186}Os/^{188}Os$ and seems best explained as reflecting radiogenic in-growth from variable Pt-Os since the time of PGM formation.

Taking the Pt-Os isochron age for Meratus PGM grains as a genesis age allows us to examine its potential accuracy in the context of other geochronlogic data. Published plate reconstructions for the tectonically complex Java Sea allow imprecise but independent age estimates for the Meratus ophiolite that range from Jurassic (Monnier, et al., 1999) to Cretaceous (Parkinson et al., 1998). The application of traditional geochronological techniques to constrain the emplacement of the Meratus ophiolite body has proven problematic. K-Ar dating of terrigenous sediments within the infra-ophiolitic sole gives an estimated age of ophiolite accretion to the continental margin of ~145 Ma, and obduction at ~90 Ma (Monnier, et al., 1999). Uncertainty estimates are not provided and we note the inherent problems of dating the deposition of sediments using the K-Ar system (Dickin, 2005; Selby, 2009). Perhaps the most extensive work on dating the Meratus ophiolite is that of Wakita et al., (1998) who used the K-Ar system to analyze micas from the Hauren schist. This work yielded K-Ar ages of 102 – 190 Ma, suggesting that subduction of oceanic lithosphere was occurring as early as 190 Ma ago, thus, both oceanic plates at this convergent margin must be at least 190 Ma old. Chromitite ore forms relatively early in the history of the host lithosphere, and certainly before the slab is subducted, thus a subduction age for this lithosphere provides a minimum age for the chromitite and hence the PGM grains. Wakita et al. (1998) provide support for an Early Jurassic or latest Triassic age for the ophiolite in the form of radiolarian biostratigraphy of the chert that was originally deposited as a siliceous ooze overlying the igneous succession of the ophiolite. They observed an assemblage that is assigned as early Middle Jurassic to late Early Cretaceous (equivalent to ~180 – 100 Ma). Assuming that sedimentation began immediately after formation of the crust at a spreading centre, and complete preservation of the pelagic assemblage, this gives an estimated formation age for the oceanic lithosphere at around 180 Ma.

Our Pt-Os isochron age of 197.8 ± 8.1 Ma is conformable with the available age constraints. The initial $^{186}Os/^{188}Os$ ratio of the isochron is well within error of that expected for derivation from a convecting mantle source (Brandon et al., 2006). These factors, together with the low MSWD and high probability of fit, indicate a viable age for the Pt-Os isochron; hence we propose that

the precise Pt-Os isochron age determined on the Meratus PGM grains is an accurate representation of the genesis of the PGE mineralization.

Further interpretation of the Pt-Os age is possible when we consider the event that it most likely represents. The likely formation of PGM grains during chromitite genesis is a clearly definable event in the early evolution of the oceanic lithosphere. The crystallisation of the PGM grains from magmas, with each grain acquiring a distinct Pt-Os ratio depending on its mineralogy, most likely occurred at this time. If each grain is isolated from others via chromite or olivine it is likely that the radiometric clock is set at this instant, despite the relatively high temperatures of this part of the oceanic lithosphere. This early formation of PGM grains means that any Pt-Os isochron derived from them will give an age that is equivalent to the genesis age of the lithosphere itself and dates one of the earliest events recorded in the evolution of the rocks of the ophiolite complex.

4.6 Conclusions and prospects for dating detrital PGM deposits

We have analysed a suite of PGM grains collected from alluvial deposits derived from the Meratus ophiolite massif for their Pt-Os and Re-Os isotope systematics. These grains display a wide variety of Pt/Os fractionations while Re/Os values are restricted to a narrow range. In the case of the Re-Os system no correlation exists on a Re-Os isochron diagram and no chronological information can be derived. We attribute this largely to inherent Os isotope heterogeneity in the original magmas from which the PGM grains formed. The mean value of the initial $^{187}Os/^{188}Os_{(197.8\ Ma)}$ ratios of the grains analysed is similar to the average value found in other PGM suites of Mesozoic age (Hattori and Hart, 1991; Büchl, et al., 2002; Meibom, et al., 2004). This composition most likely represents that of the depleted upper convecting mantle at the time of lithosphere formation.

In contrast to the non-systematic Re-Os isotope characteristics, a well defined correlation exists on a Pt-Os isochron diagram, defining an age of 197.8 ± 8.1 Ma that we interpret as the age of formation of the PGM grains in the lower oceanic lithosphere. This age is consistent with radiometric and biostratigraphic age constraints available for the Meratus ophiolite (Wakita, et al., 1998). This result, along with other examples recently documented by Nowell et al. (2008b) illustrates the potential of the laser ablation Pt-Os isotope method in dating PGM mineralization associated with ultramafic rocks. This type of LA-MC-ICPMS analysis can be applied to detrital or *in situ* populations but a given sample type needs to yield a large population of PGM grains, preferably >100, with a variety of Pt/Os ratios. Not all PGM suites possess this range of Pt-Os ratios. Alternatively, Nowell et al., (2008b) have shown that there may be sufficient Pt/Os

variation in exsolved or polycrystalline PGM to enable geochronological data to be obtained. This approach thus provides a new way of dating PGE mineralization both within ophiolites and within placer or detrital deposits derived from these sources.

4.7 Acknowledgements

This research was supported by a NERC research studentship to JAC and a NERC research grant (NE/F006497/1). We thank Paul Pohwat of the Smithsonian Institution National Museum of Natural History for the provision of the Meratus samples. Joe Devine and Kassandra Costa are thanked for their assistance with electron microprobe analyses. KH and BE are thanked for providing valuable critical reviews of the manuscript.

4.8 References

Ahmed, A.H., 2007, Diversity of platinum-group minerals in podiform chromitites of the late Proterozoic ophiolite, Eastern Desert, Egypt: Genetic implications: Ore Geology Reviews, 32, 1-19.

Ballhaus, C., 1998, Origin of podiform chromite deposits by magma mingling: Earth and Planetary Science Letters, 156, 185-193.

Begemann, F., Ludwig, K.R., Lugmair, G.W., Min, K., Nyquist, L.E., Patchett, P.J., Renne, P.R., Shih, C.Y., Villa, I.M. and Walker, R.J., 2001, Call for an improved set of decay constants for geochronological use: Geochimica et Cosmochimica Acta, 65, 111-121.

Bird, J.M. and Bassett, W.A., 1980, Evidence of a Deep Mantle History in Terrestrial Osmium-Iridium-Ruthenium Alloys: Journal of Geophysical Research, 85, 5461-5470.

Bird, J.M., Meibom, A., Frei, R. and Nägler, T.F., 1999, Osmium and lead isotopes of rare OsIrRu minerals: derivation from the core-mantle boundary region?: Earth and Planetary Science Letters, 170, 83-92.

Bowles, J.F.W., 1988, Further Studies of the Development of Platinum-Group Minerals in the Laterites of the Freetown Layered Complex, Sierra Leone, *in* Prichard, H.M., Potts, P.J., Bowles, J.F.W. and Cribb, S.J., ed., Geo-Platinum 87, New York, Elsevier Applied Science, 422.

Brandon, A.D., Walker, R.J. and Puchtel, I.S., 2006, Platinum-osmium isotope evolution of the Earth's mantle: Constraints from chondrites and Os-rich alloys: Geochimica et Cosmochimica Acta, 70, 2093-2103.

Brandon, A.D., Norman, M.D., Walker, R.J. and Morgan, J.W., 1999, ^{186}Os-^{187}Os systematics of Hawaiian Picrites: Earth and Planetary Science Letters, 174, 25-42.

Brandon, A.D., Graham, D.W., Waight, T. and Gautason, B., 2007, ^{186}Os and ^{187}Os enrichments and high-^{3}He/^{4}He sources in the Earth's mantle: Evidence from Icelandic picrites: Geochimica et Cosmochimica Acta, 71, 4570-4591.

Brandon, A.D., Walker, R.J., Morgan, J.W., Norman, M.D. and Prichard, H.M., 1998, Coupled ^{186}Os and ^{187}Os evidence for core-mantle interaction: Science, 280, 1570-1573.

Brenker, F.E., Meibom, A. and Frei, R., 2003, On the formation of peridotite-derived Os-rich PGE alloys.: American Mineralogist, 88, 1731-1740.

Büchl, A., Brügmann, G., Batanova, V.G., Münker, C. and Hofmann, A.W., 2002, Melt percolation monitored by Os isotopes and HSE abundances: a case study from the mantle section of the Troodos Ophiolite: Earth and Planetary Science Letters, 204, 385-402.

Burgath, K.P., 1988, Platinum-Group Minerals in Ophiolitic Chromitites and Alluvial Placer Deposits, Meratus-Bobaris Area, Southeast Kalimantan, *in* Prichard, H.M., Potts, P.J., Bowles, J.F.W. and Cribb, S.J., ed., Geo-Platinum '87, New York, Elsevier Applied Science, 422.

Burgath, K.P. and Mohr, M., 1986, Chromitites and platinum-group minerals in the Meratus-Bobaris ophiolite zone, south-east Borneo, *in* Gallagher, M.J., Ixer, R.A., Neary, C.R. and Prichard, H.M., ed., Metallogeny of Basic and Ultrabasic Rocks, London, The Institution of Mining and Metallurgy, 522.

Cabri, L.J. and Genkin, A.D., 1991, Reexamination of Pt-Alloys from Lode and Placer Deposits, Urals: Canadian Mineralogist, 29, 419-425.

Cabri, L.J., Harris, D.C. and Weiser, T.W., 1996, Mineralogy and distribution of platinum-group mineral (PGM) placer deposits of the world: Exploration and Mining Geology, 5, 73-167.

Campbell, I.H. and Naldrett, A.J., 1979, The influence of silicate:sulfide ratios on the geochemistry of magmatic sulfides: Economic Geology, 74, 1503-1506.

Dickin, A.P., 2005, Radiogenic isotope geology: Cambridge, Cambridge University Press, 492.

Guntoro, A., 1999, The formation of the Makassar Strait and the separation between SE Kalimantan and SW Sulawesi: Journal of Asian Earth Sciences, 17, 79-98.

Harris, D.C. and Cabri, L.J., 1991, Nomenclature of Platinum-Group-Element Alloys - Review and Revision: Canadian Mineralogist, 29, 231-237.

Hattori, K. and Hart, S.R., 1991, Osmium-isotope ratios of platinum-group minerals associated with ultramafic intrusions: Os-isotopic evolution of the oceanic mantle: Earth and Planetary Science Letters, 107, 499-514.

Hattori, K., Burgath, K.P. and Hart, S.R., 1992, Os-Isotope Study of Platinum-Group Minerals in Chromitites in Alpine-Type Ultramafic Intrusions and the Associated Placers in Borneo: Mineralogical Magazine, 56, 157-164.

Hattori, K.H., Cabri, L.J., Johanson, B. and Zientek, M.L., 2004, Origin of placer laurite from Borneo: Se and As contents, and S isotopic compositions: Mineralogical Magazine, 68, 353-368.

Ludwig, K., 2003, Isoplot/Ex, version 3: a geochronological toolkit for Microsoft Excel, Geochronology Centre Berkeley.

Luguet, A., Pearson, D.G., Nowell, G.M., Dreher, S.T., Coggon, J.A., Spetsius, Z.V. and Parman, S.W., 2008, Enriched Pt-Re-Os isotope systematics in plume lavas explained by metasomatic sulfides: Science, 319, 453-456.

Meibom, A., Frei, R. and Sleep, N.H., 2004, Osmium isotopic compositions of Os-rich platinum group element alloys from the Klamath and Siskiyou Mountains.: Journal of Geophysical Research, 109, B02203.

Meibom, A., Sleep, N.H., Chamberlain, C.P., Coleman, R.G., Frei, R., Hren, M.T. and Wooden, J.L., 2002, Re-Os isotopic evidence for long-lived heterogeneity and equilibration processes in the Earth's upper mantle.: Nature, 419, 705-708.

Monnier, C., Polve, M., Girardeau, J., Pubellier, M., Maury, R.C., Bellon, H. and Permana, H., 1999, Extensional to compressive Mesozoic magmatism at the SE Eurasia margin as recorded from the Meratus ophiolite (SE Borneo, Indonesia): Geodinamica Acta, 12, 43-55.

Nowell, G.M., Luguet, A., Pearson, D.G. and Horstwood, M.S.A., 2008a, Precise and accurate $^{186}Os/^{188}Os$ and $^{187}Os/^{188}Os$ measurements by multi-collector plasma ionisation mass spectrometry (MC-ICPMS) part I: Solution analyses: Chemical Geology, 248, 363-393.

Nowell, G.M., Pearson, D.G., Parman, S.W., Luguet, A. and Hanski, E., 2008b, Precise and accurate $^{186}Os/^{188}Os$ and $^{187}Os/^{188}Os$ measurements by Multi-collector Plasma Ionisation Mass Spectrometry, part II: Laser ablation and its application to single-grain Pt-Os and Re-Os geochronology: Chemical Geology, 248, 394-426.

Oberthur, T., Melcher, F., Gast, L., Wohrl, C. and Lodziak, J., 2004, Detrital platinum-group minerals in rivers draining the eastern Bushveld complex, South Africa: Canadian Mineralogist, 42, 563-582.

Paktunc, A.D., 1990, Origin of podiform chromite deposits by multistage melting, melt segregation and magma mixing in the upper mantle: Ore Geology Reviews, 5, 211-222.

Parkinson, C.D., Miyazaki, K., Wakita, K., Barber, A.J. and Carswell, D.A., 1998, An overview and tectonic synthesis of the pre-Tertiary very-high-pressure metamorphic and associated rocks of Java, Sulawesi and Kalimantan, Indonesia: The Island Arc, 7, 184-200.

Pearson, D.G., Parman, S.W. and Nowell, G.M., 2007, A link between large mantle melting events and continent growth seen in osmium isotopes: Nature, 449, 202-205.

Peck, D.C., Keays, R., R. and Ford, R.J., 1992, Direct crystallization of refractory platinum-group element alloys from boninitic magmas: Evidence from western Tasmania: Australian Journal of Earth Sciences, 39, 373-387.

Petrou, A.L. and Economou-Eliopoulos, M., 2009, The activation energy values estimated by the Arrhenius equation as a controlling factor of platinum-group mineral formation: Geochimica et Cosmochimica Acta, 73, 1625-1636.

Selby, D., 2009, U-Pb zircon geochronology of the Aptian/Albian boundary implies that the GL-O international glauconite standard is anomalously young: Cretaceous Research, 30, 1263-1267.

Sikumbang, N., 1990, The geology and tectonics of the Meratus mountains, South Kalimantan, Indonesia: Geologi Indonesia, 13, 1-31.

Tsoupas, G. and Economou-Eliopoulos, M., 2008, High PGE contents and extremely abundant PGE-minerals hosted in chromitites from the Veria ophiolite complex, northern Greece: Ore Geology Reviews, 33, 3-19.

Wakita, K., Miyazaki, K., Zulkarnain, I., Sopaheluwakan, J. and Sanyoto, P., 1998, Tectonic implications of new age data for the Meratus complex of south Kalimantan, Indonesia: Island Arc, 7, 202-222.

Walker, R.J., Hanski, E., Vuollo, J. and Liipo, J., 1996, The Os isotopic composition of Proterozoic upper mantle: Evidence for chondritic upper mantle from the Outokumpu ophiolite, Finland: Earth and Planetary Science Letters, 141, 161-173.

Walker, R.J., Morgan, J.W., Hanski, E.J. and Smolkin, V.F., 1997a, Re-Os systematics of Early Proterozoic ferropicrites, Pechenga Complex, northwestern Russia: Evidence for ancient ^{187}Os-enriched plumes: Geochimica et Cosmochimica Acta, 61, 3145-3160.

Walker, R.J., Prichard, H.M., Ishiwatari, A. and Pimentel, M., 2002, The osmium isotopic composition of convecting upper mantle deduced from ophiolite chromites: Geochimica et Cosmochimica Acta, 66, 329-345.

Walker, R.J., Morgan, J.W., Naldrett, A.J., Li, C. and Fassett, J.D., 1991, Re-Os Isotope Systematics of Ni-Cu Sulfide Ores, Sudbury Igneous Complex, Ontario - Evidence for a Major Crustal Component: Earth and Planetary Science Letters, 105, 416-429.

Walker, R.J., Morgan, J.W., Beary, E.S., Smoliar, M.I., Gzamanske, G.K. and Horan, M.F., 1997b, Applications of the ^{190}Pt-^{186}Os isotope sytem to geochemistry and cosmochemistry: Geochimica et Cosmochimica Acta, 61, 4799-807.

Zhou, M.-F., Sun, M., Keays, R.R. and Kerrich, R.W., 1998, Controls on Platinum-Group Elemental Distributions of Podiform Chromitites: A Case Study of High-Cr and High-Al Chromitites from Chinese Orogenic Belts: Geochimica et Cosmochimica Acta, 62, 677-688.

5 Conclusions

5.1 Introduction

In this chapter the conclusions of this research are brought together to allow comprehensive evaluation of the laser ablation MC-ICPMS Pt-Os geochronometry technique, it's advantages, disadvantages and analytical limitations. The data collected in each chapter are applied in order to address the questions and thesis aims outlined in Chapter 1. Finally, suggestions are made for further work and improvements to be made to the method.

The aims for this thesis were outlined in the introduction as follows:

1) The principal aim of this project is to further develop the laser ablation MC-ICPMS Pt-Os geochronometry technique and demonstrate its application to a broad range of PGM in addition to the Os-rich minerals that have previously been analysed. By applying the technique to a primary PGM deposit of well constrained age, to generate the first multi-grain laser ablation Pt-Os isochrons, it will be possible to evaluate the validity of the method, including the corrections and processing applied to the raw data. This should also reveal, and allow quantification of, any Pt/Os inter-element fractionation that may occur during ablation and facilitate the refinement of the method to generate a more robust chronometer.

2) A further objective is to apply the Pt-Os geochronometer, measured by LA-MC-ICPMS, to a large population of detrital PGM that can be confidently assumed to be derived from a single ophiolite. The purpose of this is to demonstrate that the method can provide precise and accurate ages for detrital PGM, despite the likelihood that PGM genesis most likely occurred in distinct melt lenses that were isolated during formation within the ophiolite crust.

3) Accurate dating of a population of detrital PGM, including alloys, will provide an opportunity for the evaluation of the assertion of Bowles (1988), that alluvial PGE alloys are secondary minerals precipitated at low temperatures within placers and will allow further constraints of genetic models for PGE alloys.

5.2 Validity of the laser ablation Pt-Os method for dating platinum mineralisation

For the first time laser ablation Pt-Os geochronometry has been applied directly to platinum-group mineralisation of known age, thus presenting a unique opportunity to assess the validity of the technique. By applying the LA-MC-ICPMS Pt-Os method to in-situ Bushveld PGM to produce

the first multi-grain laser ablation Pt-Os isochron, with an age of 2012 ± 47 Ma (2σ; n = 50, MSWD = 1.19), which is within 42 Ma (~2 %) of the published U-Pb zircon age (Scoates and Friedman, 2008), the potential accuracy of ages yielded by this method can be evaluated.

The Borneo PGM suite offered an opportunity to evaluate the effectiveness of the Pt-Os LA-MC-ICPMS technique when applied to a large population of detrital PGM grains derived from a single, geologically well constrained source, but with the likelihood of PGM genesis in a number of isolated chromitite pods. The well defined Pt-Os isochron, yields a precise age of 197.8 Ma ± 8.1 Ma, which appears entirely consistent with available indirect age constraints. The age is interpreted as recording the formation of the PGM in the lower oceanic lithosphere, and thus provides the first direct measurement of the age of the Meratus ophiolite. Hence the Pt-Os chronometer is shown to provide a novel and reliable approach to dating ophiolites and other primary deposits, as well as detrital PGM derived from such bodies.

5.2.1 Sources of scatter on Pt-Os isochrons

Scatter observed on the Pt-Os Bushveld isochron may be geological or analytical in origin. The extremely close agreement of the Merensky Reef U-Pb zircon and rutile ages of Scoates and Friedman (2008) provides strong evidence that the 42Ma difference between our Pt-Os PGM age and the U-Pb zircon age of Scoates and Friedman (2008) is unlikely to be due to differences in closure temperature for the two chronometers. A more probable geological explanation for the disparity between the Pt-Os and U-Pb ages and the scatter on the Pt-Os isochron is the non-representative sampling of internally heterogeneous PGM. Isotopic heterogeneities may result from complex exsolution, which has been documented in various PGM species (e.g. Makovicky, 2002).

Inter-element fractionation is likely to occur during laser ablation analysis and may produce further non-systematic scatter on Pt-Os isochrons. Quantification of this phenomenon is problematic, though it has been possible to constrain the maximum potential amount of fractionation that occurred during analysis of Bushveld samples (see section 5.4). A further potential analytical source of scatter is an inaccuracy in the W and Os interfering element corrections. In the majority of the Bushveld samples, however, W concentrations are at trace levels so for these samples the magnitude of the W corrections is very small. No correlation is seen between Pt and W in these samples and Pt/Os inter-element fractionation is likely to be the largest source of uncertainty on $^{190}Pt/^{188}Os$ ratios.

The Borneo Pt-Os isochron is subject to very little scatter. This may be due to the much smaller range in $^{190}Pt/^{188}Os$ ratios relative to the Bushveld samples, hence leading to far smaller

inaccuracies in the measurement of this ratio. Alternatively, the less scattered isochron might result from mineralogical differences between the two sample populations. While the Borneo PGM suite comprises almost exclusively (Pt-poor) laurites and Pt-Fe alloys, the Bushveld PGM population also includes sperrylites and braggites. It is possible that Pt-rich sulphides and arsenides are more sensitive to disturbance of the Pt-Os isotope system than alloys and Pt-poor sulphides during exsolution and weathering. This hypothesis is potentially supported by the single grain Pt-Os isochron presented by Nowell et al. (2008) for PGE alloy grains; in this case, despite internal heterogeneity, the Pt-Os system appears undisturbed.

5.2.2 Pt-Os vs. Re-Os

The high precision of Pt-Os isochron ages measured by LA-MC-ICPMS (~2.3 %, Bushveld; 4 %, Borneo) illustrates that the Pt-Os ages are not only accurate, but also geologically useful. Precision of these Pt-Os ages is comparable to that of Re-Os isochron ages for ultramafic rocks. However, simple mixing models show that in mafic magmas the Re-Os system is extremely sensitive to disturbance by crustal contamination and to heterogeneity in the melt source region, whereas the Pt-Os system is far more robust as a result of the very small variation in $^{186}Os/^{188}Os$ in the convecting mantle throughout Earth history.

The well constrained initial ratio produced by the Borneo isochron is a further indicator of the resilience of the Pt-Os system to initial $^{186}Os/^{188}Os$ variation, despite probable genesis of PGM in multiple isolated melt lenses. In contrast, the Re-Os system yields no isochron or chronological information as a result of wide variation in initial $^{187}Os/^{188}Os$. It is probable that this heterogeneity is inherited from the parent magmas from which the PGM crystallised.

5.2.3 Single grain Pt-Os model ages

A further advantage of the limited evolution of $^{186}Os/^{188}Os$ in the mantle during the lifetime of the Earth is that this ratio can be estimated with reasonable certainty in order to calculate Pt-Os model ages for individual Pt-rich phases. In fact, the difference in the $^{186}Os/^{188}Os$ ratio of primitive upper mantle (PUM) over 2 Ga is so small that Pt-Os model ages calculated using a present day $^{186}Os/^{188}Os$ value are identical to those calculated for the same data with an initial $^{186}Os/^{188}Os$ ratio of PUM at 2 Ga. As shown in Chapter 3, sperrylite, braggite and Pt-Fe alloy can be used in this way as single mineral chronometers, given sufficiently elevated Pt/Os ratios, though model ages are still sensitive to uncertainties in the $^{190}Pt/^{188}Os$ ratio that arise from inter-element fractionation and/or inaccuracies in the Os IEC. As the mantle evolution curve for $^{186}Os/^{188}Os$ is very shallow and the evolution curve of a given high Pt/Os phase is relatively

steep the angle of intercept between the two is high, hence higher precision is achieved on model ages for PGM with higher Pt/Os ratios, highlighting the potential for single grain Pt-Os dating of PGM deposits.

5.3 Genesis of alluvial PGM

The age of the Pt-Os isochron yielded by detrital PGM from the Pontyn River, southeast Borneo (197.8 Ma) supports previous Os isotope, S isotope and As and Se studies that suggest that these are primary PGM, derived by mechanical processes from the mantle section of the Meratus ophiolite. Given published constraints on the age of the Meratus ophiolite, the antiquity of the Pt-Os age, along with distinctive morphological features of many of these PGM, is not consistent with lateritic genesis. Magmatic genesis is also confirmed by the presence of silicate and melt inclusions within PGE alloys (Peck et al., 1992; Brenker et al., 2003) and the intimate intergrowth of chromite with millimetre-scale PGE alloys (Nixon et al., 1990).

5.4 Quantification of Pt-Os inter-element fractionation

Nowell et al. (2008) were able to crudely estimate that inter-element fractionation between Pt and Os during LA-MC-ICPMS must be approximately 5 % or less. The lack of a suitable suite of laser ablation PGM reference materials has prohibited the thorough investigation and quantification of inter-element fractionation. However, the precision of our Pt-Os Bushveld age allows the more confident quantification of this fractionation value. Assuming accurate definition of the decay constant of ^{190}Pt by Begemann et al. (2001), Pt/Os fractionation is estimated as less than or equal to 2.2 %. Only ~ 2 % fractionation is required to bring our Pt-Os age into absolute agreement with the U-Pb zircon age of Scoates and Friedman (2008).

5.5 Desirable characteristics of potential sample populations

For successful application of the LA-MC-ICPMS Pt-Os geochronometer a sample population must fulfil a minimum set of requirements. First and foremost it must host a range of $^{190}Pt/^{188}Os$ ratios, hence poly-mineralic assemblages are desirable. It is difficult to quantify an absolute minimum range of $^{190}Pt/^{188}Os$ ratios necessary since the quality of the isochron correlation (and so the precision and accuracy of the age) is also dependent on the number of samples and the amount of common Os present in each grain (since this affects the accuracy of mass bias and interfering element corrections). However, with a sample population of ~ 200 or more grains a $^{190}Pt/^{188}Os$ range of two units appears to be sufficient to produce an accurate and precise

isochron age, provided that some of these grains have $^{190}Pt/^{188}Os$ ratios of around zero. Clearly larger populations and wider ranges of $^{190}Pt/^{188}Os$ ratios contribute greater precision to Pt-Os isochron ages, but a balance must be found between high $^{190}Pt/^{188}Os$ values and low Os contents. Isotopic heterogeneities within individual PGM grains must also be considered when carrying out laser ablation analyses, as outlined in section 5.2.1. Homogeneous grains are preferred, or those in which the total within-grain mineral variation has been characterised.

5.5 Outstanding questions and future work

5.5.1 Analytical developments

If a suite of suitable PGM laser ablation reference materials could be acquired then further investigation of Pt/Os inter-element fractionation could be carried out. Quantification of such fractionation could be achieved relatively easily by analysing PGM of known $^{190}Pt/^{186}Os$ ratios. Defining the nature of Pt/Os fractionation during laser ablation of various species of PGM would in turn allow development of a better understanding of geological scatter on Pt-Os isochrons. In addition, by analysing reference materials of known isotopic composition it would be possible to place stronger constraints on the accuracy of interfering element corrections during ablation analyses and the extents at which these corrections break down. Analysis of a homogeneous, high-Pt/Os PGM over several analytical sessions during an extended period of time would also allow better estimation of external reproducibility for measurement of the $^{190}Pt/^{186}Os$ ratio.

Disturbance of the Re-Os isotope system in molybdenites has been widely studied and characterised, providing a detailed understanding of the sampling requirements necessary for robust isotopic measurements. Detailed SEM EDS analysis of exsolution textures and compositional heterogeneity within PGE sulphides and alloys would provide a more thorough understanding of the requirements for accurate analysis of the Pt-Os chronometer in such grains.

5.5.2 Further application of the Pt-Os geochronometer

There is great potential for further application of the Pt-Os chronometer in PGM. This research has demonstrated that it can be applied to both primary and detrital PGM to produce robust ages; it therefore presents a new tool for dating the mantle rocks of ophiolites, which has previously been notoriously difficult. The laser ablation Pt-Os dating method provides a possible way of dating komatiites and the ore deposits that are hosted within such rocks, which has also

proven difficult using conventional methods. Direct isotopic dating of komatiites would greatly improve our understanding of these enigmatic, ancient igneous events and their associated mineral wealth.

The Pt-Os chronometer could become a useful exploration tool, in prospecting for primary PGM deposits and constructing ore genesis models. In addition there is potential for using the Pt-Os PGM chronometer for terrain reconstruction, in a similar manner to detrital zircons, as a way of distinguishing and dating multiple PGM sources within a single detrital PGM suite. Areas such as California, western South America, Europe and the Ural Mountains are examples of areas where Pt-Os PGM terrain reconstructions may be applicable, though age contrasts would need to be significant in order to be distinguishable.

5.6 References

Begemann, F., Ludwig, K.R., Lugmair, G.W., Min, K., Nyquist, L.E., Patchett, P.J., Renne, P.R., Shih, C.Y., Villa, I.M., and Walker, R.J., 2001, Call for an improved set of decay constants for geochronological use: Geochimica et Cosmochimica Acta, 65, 111-121.

Bowles, J.F.W., 1988, Further Studies of the Development of Platinum-Group Minerals in the Laterites of the Freetown Layered Complex, Sierra Leone, *in* Prichard, H.M., Potts, P.J., Bowles, J.F.W., and Cribb, S.J., eds., Geo-Platinum 87: New York, Elsevier Applied Science, 422.

Brenker, F.E., Meibom, A., and Frei, R., 2003, On the formation of peridotite-derived Os-rich PGE alloys.: American Mineralogist, 88, 1731-1740.

Makovicky, E., 2002, Ternary and Quaternary Phase Systems with PGE, *in* Cabri, L.J., ed., The Geology, Geochemistry, Mineralogy and Mineral Beneficiation of Platinum-Group Elements, Special Volume 54, Canadian Institute of Mining, Metallurgy and Petroleum, 131-175.

Nixon, G.T., Cabri, L.J., and Laflamme, J.H.G., 1990, Platinum-group-element mineralization in lode and placer deposits associated with the Tulameen alaskan-type complex, British Columbia: Canadian Mineralogist, 28, 503-535.

Nowell, G.M., Pearson, D.G., Parman, S.W., Luguet, A., and Hanski, E., 2008, Precise and accurate $^{186}Os/^{188}Os$ and $^{187}Os/^{188}Os$ measurements by Multi-collector Plasma Ionisation Mass Spectrometry, part II: Laser ablation and its application to single-grain Pt-Os and Re-Os geochronology: Chemical Geology, 248, 394-426.

Peck, D.C., Keays, R., R., and Ford, R.J., 1992, Direct crystallization of refractory platinum-group element alloys from boninitic magmas: Evidence from western Tasmania: Australian Journal of Earth Sciences, 39, 373-387.

Scoates, J.S., and Friedman, R.M., 2008, Precise age of the platiniferous Merensky reef, Bushveld Complex, South Africa, by the U-Pb zircon chemical abrasion ID-TIMS technique: Economic Geology, 103, 465-471.

Appendix 4

Os isotope compositions of Bushveld PGM grains analyzed by Laser Ablation-Multi-Collector-ICPMS at Durham University

Grain	Mineralogy	^{188}Os (V)	± 2SE	^{187}Os/^{188}Os	± 2SE	^{186}Os/^{188}Os	± 2SE	Total abs. error	^{184}Os/^{188}Os	± 2SE	^{187}Re/^{188}Os	± 2SE	^{185}Re/^{188}Os	± 2SE	^{182}W/^{188}Os	± 2SE	^{190}Pt/^{188}Os	± 2SE	Total abs. error
8801_1	laurite-erlichmanite	7.0256	0.5606	0.176705	0.000043	0.119822	0.000028	0.000035	0.001296	0.000003	0.000025	0.000005	0.000016	0.000003	0.000000	0.000002	0.000234	0.000890	0.000890
8801_2	laurite-erlichmanite	6.5426	0.3807	0.179793	0.000061	0.119826	0.000039	0.000044	0.001299	0.000003	0.000060	0.000007	0.000036	0.000004	0.000000	0.000002	0.000006	0.001262	0.001262
8801_3	laurite-erlichmanite	4.5118	0.4000	0.171443	0.000082	0.119842	0.000063	0.000067	0.001298	0.000006	0.000113	0.000020	0.000061	0.000009	-0.000002	0.000003	-0.000175	0.001951	0.001951
8801_4	laurite-erlichmanite	5.6286	0.9054	0.179412	0.000113	0.119877	0.000072	0.000075	0.001298	0.000006	0.000018	0.000016	0.000012	0.000006	0.000001	0.000004	-0.000082	0.003430	0.003430
8801_5	laurite-erlichmanite	8.2448	0.3194	0.179010	0.000062	0.119809	0.000045	0.000050	0.001301	0.000003	0.000017	0.000005	0.000012	0.000003	-0.000002	0.000002	0.000338	0.001328	0.001328
8801_6	laurite-erlichmanite	8.8856	0.2836	0.178496	0.000065	0.119829	0.000044	0.000049	0.001300	0.000002	0.000030	0.000007	0.000017	0.000004	0.000000	0.000002	-0.000531	0.001316	0.001317
8801_7	laurite-erlichmanite	5.0664	0.4817	0.178285	0.000103	0.119789	0.000069	0.000072	0.001297	0.000005	0.000038	0.000012	0.000021	0.000005	-0.000001	0.000003	0.001857	0.002363	0.002364
8801_8	laurite-erlichmanite	9.2150	0.2474	0.177737	0.000045	0.119810	0.000033	0.000039	0.001299	0.000003	0.000024	0.000004	0.000015	0.000002	0.000000	0.000001	0.000825	0.001056	0.001056
8801_9	laurite-erlichmanite	7.4451	0.5602	0.170581	0.000057	0.119840	0.000036	0.000042	0.001299	0.000003	0.000018	0.000007	0.000011	0.000004	0.000000	0.000002	-0.000064	0.001172	0.001172
8801_11	laurite-erlichmanite	12.9751	0.2907	0.180429	0.000043	0.119802	0.000027	0.000034	0.001300	0.000002	-0.000001	0.000004	0.000000	0.000002	-0.000002	0.000001	0.000162	0.000872	0.000872
8801_12	laurite-erlichmanite	7.2133	0.5459	0.171337	0.000070	0.119841	0.000045	0.000049	0.001300	0.000004	0.000030	0.000007	0.000018	0.000003	-0.000001	0.000002	-0.000951	0.001491	0.001492
8801_13	laurite-erlichmanite	6.5457	0.4579	0.178487	0.000050	0.119805	0.000035	0.000041	0.001297	0.000004	0.000071	0.000014	0.000039	0.000008	0.000002	0.000002	0.000437	0.001130	0.001131
8801_14	laurite-erlichmanite	8.1222	0.6421	0.169392	0.000055	0.119859	0.000038	0.000043	0.001300	0.000003	0.000051	0.000020	0.000021	0.000006	-0.000001	0.000002	-0.001321	0.001247	0.001248
8801_15	laurite-erlichmanite	11.4356	0.4248	0.171945	0.000047	0.119813	0.000033	0.000039	0.001299	0.000002	0.000016	0.000004	0.000010	0.000002	-0.000001	0.000001	-0.000429	0.001085	0.001085
8801_16	sperrylite	0.1090	0.0020	0.175366	0.000204	0.125240	0.000286	0.000289	0.000972	0.000134	0.000036	0.000238	-0.000008	0.000132	0.000251	0.000124	1.943730	0.042325	0.106003
8801_17	braggite	1.2514	0.3229	0.169631	0.000184	0.120398	0.000272	0.000273	0.001297	0.000020	0.000209	0.000065	0.000115	0.000028	0.000155	0.000071	0.187334	0.057001	0.057766
8801_18	sperrylite	0.1012	0.0057	0.172053	0.000254	0.125725	0.000244	0.000248	0.001244	0.000167	0.000648	0.000272	0.000338	0.000133	0.002589	0.000781	1.981967	0.061639	0.116704
8801_19	sperrylite	0.0283	0.0037	0.178558	0.000558	0.136512	0.000843	0.000845	0.000538	0.000418	-0.000909	0.000542	-0.000543	0.000324	0.000728	0.000294	5.398618	0.286514	0.393641
8801_19a*	sperrylite	0.0204	0.0037	0.179118	0.001520	0.139562	0.001728	0.001729	0.000426	0.000997	-0.001544	0.001619	-0.001140	0.000903	0.000123	0.000607	6.049224	0.121694	0.326025
8801_19b*	sperrylite	0.0415	0.0037	0.178324	0.001059	0.132461	0.001182	0.001183	0.000297	0.000751	0.000150	0.000860	-0.000063	0.000445	0.001194	0.000584	4.314273	0.173183	0.276631
8801_20	sperrylite	0.2290	0.0062	0.176690	0.000115	0.122483	0.000113	0.000121	0.001141	0.000082	-0.000081	0.000124	-0.000080	0.000063	0.000093	0.000063	0.898336	0.015406	0.047485
8801_22*	braggite	8.5113	1.5815	0.176438	0.000347	0.119941	0.000204	0.000205	0.001298	0.000006	-0.000002	0.000022	0.000002	0.000012	0.000003	0.000003	0.019362	0.008837	0.008890
8801_24*	sperrylite	0.0594	0.0097	0.168781	0.000592	0.123112	0.000607	0.000608	0.001194	0.000598	0.001408	0.000722	0.000739	0.000398	0.030685	0.020080	1.189567	0.120944	0.134778
8801_25	sperrylite	0.0606	0.0013	0.167254	0.000354	0.130027	0.000324	0.000327	0.000833	0.000344	-0.000401	0.000376	-0.000187	0.000204	0.000465	0.000193	3.596375	0.049504	0.186509
8801_26	sperrylite	0.0736	0.0136	0.176190	0.000636	0.126134	0.000821	0.000822	0.001471	0.000357	0.000131	0.000442	0.000028	0.000251	0.000439	0.000297	2.263548	0.239719	0.265093
8801_27	sperrylite	0.2202	0.0113	0.174881	0.000143	0.122950	0.000144	0.000151	0.001217	0.000077	0.000047	0.000090	0.000049	0.000047	0.000081	0.000054	1.084274	0.047051	0.071784
8801-R2_1*	laurite-erlichmanite	9.4679	1.4727	0.177204	0.000128	0.119819	0.000012	0.000024	0.001309	0.000023	0.000038	0.000104	0.000050	0.000031	0.000000	0.000019	0.003125	0.003348	0.003351
8801-R2_2	Pt-Fe alloy	0.0872	0.0825	0.154182	0.004889	0.128605	0.003386	0.003386	0.002485	0.001971	0.053836	0.016805	0.027208	0.007532	0.011377	0.003013	3.252784	0.761555	0.778728
8801-R2_3	laurite-erlichmanite	4.4840	0.5758	0.178868	0.000126	0.119830	0.000018	0.000027	0.001291	0.000025	0.000134	0.000079	0.000082	0.000039	0.000011	0.000019	0.000683	0.001418	0.001418
8801-R2_4	braggite	0.0105	0.0031	0.128341	0.006081	0.154929	0.005974	0.005974	0.001249	0.002747	0.005537	0.005096	0.002544	0.002402	0.008773	0.003809	11.823540	1.472275	1.586532
8801-R2_5*	braggite	0.0032	0.0030	0.077871	0.014087	0.208950	0.013352	0.013353	0.004661	0.006227	0.008938	0.009025	0.005346	0.005398	0.006320	0.005022	21.557674	3.682386	3.836899
8801-R2_6	braggite	0.0031	0.0005	0.073260	0.011532	0.231221	0.012734	0.012734	0.001246	0.005943	0.009139	0.006280	0.005330	0.003348	0.001620	0.004896	34.791776	2.588982	3.119134
8801-R2_7	laurite-erlichmanite	20.7089	0.3674	0.178543	0.000042	0.119821	0.000006	0.000022	0.001303	0.000007	0.000011	0.000023	0.000004	0.000013	0.000001	0.000006	0.000008	0.000389	0.000389
8801-R2_8*	laurite-erlichmanite	6.8555	0.9460	0.176349	0.000064	0.119823	0.000011	0.000024	0.001288	0.000014	0.000141	0.000037	0.000094	0.000019	0.000018	0.000013	0.003333	0.001621	0.001629
8801-R2_9	sperrylite	0.0784	0.0051	0.171200	0.000377	0.123280	0.000283	0.000286	0.001247	0.000232	0.002147	0.000907	0.000962	0.000318	0.000269	0.000172	1.272331	0.020220	0.066753
8801-R2_10	sperrylite	0.0096	0.0008	0.149091	0.003054	0.151475	0.002311	0.002312	0.000551	0.002208	0.002329	0.002667	0.001342	0.001442	0.000243	0.001447	10.713399	0.660799	0.850645
8801-R2_11	braggite	0.0015	0.0001	-0.011863	0.016212	0.388721	0.020463	0.020463	0.000974	0.014137	0.026086	0.016627	0.011716	0.008774	0.019647	0.013350	89.811889	4.980030	6.705679
8801-R2_12	braggite	0.0020	0.0002	0.051612	0.016908	0.287777	0.019864	0.019864	0.002838	0.010671	0.052865	0.023449	0.029810	0.011152	0.019367	0.009835	52.861477	5.910361	6.474427
8801-R2_13	sperrylite	0.0507	0.0043	0.165937	0.000617	0.126410	0.000512	0.000514	0.001749	0.000387	0.000117	0.000572	0.000016	0.000301	0.000094	0.000249	2.345932	0.065060	0.134132
8801-R2_14	braggite	1.2343	0.2390	0.175433	0.000882	0.120100	0.000094	0.000097	0.001321	0.000038	0.000324	0.000175	0.000147	0.000050	0.000033	0.000025	0.090269	0.030296	0.030630
8801-R2_15	laurite-erlichmanite	16.4674	0.3720	0.180697	0.000030	0.119822	0.000006	0.000022	0.001302	0.000004	0.000027	0.000017	0.000014	0.000009	0.000002	0.000004	0.000033	0.000252	0.000252
8801-R2_16	laurite-erlichmanite	3.4391	0.5343	0.172012	0.000114	0.119849	0.000017	0.000027	0.001279	0.000026	0.000136	0.000093	0.000101	0.000041	0.000026	0.000021	0.007194	0.003078	0.003099
8801-R2_17*	braggite	0.0015	0.0009	0.026597	0.020468	0.330340	0.032054	0.032054	-0.018310	0.017385	0.021823	0.019551	0.012660	0.010231	0.030912	0.013653	52.142428	9.510729	9.861594
8801-R2_19	sperrylite	0.0052	0.0006	0.152386	0.006192	0.160012	0.003450	0.003450	0.003491	0.003126	0.009871	0.006087	0.004205	0.002838	0.008247	0.002503	12.163315	0.485488	0.778180
8801-R2_20	laurite-erlichmanite	11.1280	1.3639	0.177874	0.000106	0.119817	0.000013	0.000025	0.001299	0.000019	0.000028	0.000065	0.000035	0.000030	0.000009	0.000016	0.000775	0.001164	0.001164
8801-R2_21	braggite	0.0057	0.0021	0.130748	0.013505	0.189920	0.015014	0.015014	0.004114	0.006411	0.035405	0.019267	0.014523	0.006668	0.016329	0.004598	20.915157	4.072498	4.204623
8801-R2_23	laurite-erlichmanite	13.6532	0.3218	0.177649	0.000034	0.119821	0.000004	0.000021	0.001302	0.000006	0.000049	0.000023	0.000032	0.000013	0.000003	0.000005	0.000039	0.000311	0.000311
8801-R2_24	laurite-erlichmanite	14.3463	0.7415	0.179346	0.000058	0.119815	0.000007	0.000022	0.001292	0.000009	0.000026	0.000040	0.000027	0.000019	0.000015	0.000007	0.001063	0.000488	0.000491
8801-R2_25*	laurite-erlichmanite	9.1137	1.3959	0.162951	0.000096	0.119843	0.000012	0.000024	0.001288	0.000018	0.000094	0.000063	0.000056	0.000030	0.000018	0.000015	0.020058	0.010453	0.010501
170-223	sperrylite	0.0018	0.0002	-0.317126	0.038209	0.675168	0.062576	0.062577	-0.029805	0.019607	0.056909	0.041917	0.022215	0.008544	0.428260	0.129764	183.89	17.362463	19.646830
174-164_mean	Pt-Fe alloy	0.0273	0.0016	0.174416	0.000545	0.138426	0.000426	0.000429	0.001258	0.000126	0.076729	0.002294	0.045162	0.001318	0.000279	0.000230	5.9489	0.129660	0.324476

Appendix 4 continued

Grain/spot	Mineralogy	^{188}Os (V)	± 2SE	^{187}Os/^{188}Os	± 2SE	^{186}Os/^{188}Os	± 2SE	Total abs. error	^{184}Os/^{188}Os	± 2SE	^{187}Re/^{188}Os	± 2SE	^{185}Re/^{188}Os	± 2SE	^{182}W/^{188}Os	± 2SE	^{190}Pt/^{188}Os	± 2SE	Total abs. error
174-164_01	Pt-Fe alloy	0.0272	0.0019	0.171763	0.001042	0.137492	0.000696	0.000698	0.000994	0.000611	0.068299	0.001965	0.040099	0.000877	0.001529	0.000647	5.5174	0.051825	0.280697
174-164_02	Pt-Fe alloy	0.0228	0.0007	0.170845	0.001027	0.140812	0.001122	0.001123	0.001864	0.000775	0.071690	0.001986	0.042379	0.001008	0.001357	0.000551	6.2343	0.151583	0.346618
174-164_03	Pt-Fe alloy	0.0249	0.0006	0.172856	0.000893	0.137842	0.000886	0.000887	0.001389	0.001012	0.079062	0.004777	0.046203	0.002547	0.002694	0.000846	5.4756	0.069577	0.282483
174-164_04	Pt-Fe alloy	0.0237	0.0010	0.172482	0.001132	0.137774	0.000795	0.000796	0.001729	0.000698	0.066612	0.001795	0.039287	0.000766	0.001201	0.000585	5.5504	0.051265	0.282215
174-164_05	Pt-Fe alloy	0.0241	0.0003	0.171815	0.000861	0.139968	0.000873	0.000874	0.001589	0.000591	0.080860	0.004312	0.046844	0.002077	0.000374	0.000591	5.9624	0.078180	0.308199
174-164_06	Pt-Fe alloy	0.0215	0.0013	0.172778	0.001015	0.138719	0.001099	0.001100	0.001364	0.000708	0.080962	0.006852	0.044920	0.002553	0.001238	0.000512	5.9575	0.156479	0.336472
174-164_07	Pt-Fe alloy	0.0173	0.0004	0.170917	0.001459	0.139609	0.001287	0.001288	0.000857	0.000839	0.074767	0.004319	0.043206	0.001310	0.000925	0.000571	5.9932	0.118466	0.322227
174-164_08	Pt-Fe alloy	0.0167	0.0004	0.170891	0.001324	0.137654	0.001666	0.001667	0.001291	0.001055	0.079960	0.006480	0.044787	0.001923	0.001501	0.000793	5.5999	0.040378	0.282894
174-164_09	Pt-Fe alloy	0.0205	0.0007	0.171516	0.001245	0.138835	0.000799	0.000801	0.001762	0.000858	0.071552	0.001829	0.042604	0.001048	0.001275	0.000529	5.6596	0.030334	0.284603
174-164_10	Pt-Fe alloy	0.0219	0.0005	0.172080	0.001118	0.139364	0.000895	0.000897	0.001209	0.000766	0.075322	0.002606	0.044402	0.001330	0.001622	0.000628	5.7311	0.104244	0.304930
174-164_11	Pt-Fe alloy	0.0341	0.0009	0.172672	0.000805	0.138958	0.000638	0.000640	0.001328	0.000460	0.091129	0.006027	0.052954	0.003029	0.000627	0.000337	5.4371	0.135076	0.303563
174-164_12	Pt-Fe alloy	0.0356	0.0009	0.173529	0.000631	0.139515	0.000602	0.000604	0.001139	0.000521	0.078583	0.004518	0.046440	0.002518	0.000964	0.000456	5.7807	0.066905	0.296676
174-164_13	Pt-Fe alloy	0.0283	0.0014	0.171730	0.001093	0.143752	0.001603	0.001604	0.001658	0.000598	0.092394	0.006114	0.055266	0.003657	0.001234	0.000658	6.9970	0.320387	0.474388
174-164_14	Pt-Fe alloy	0.0291	0.0007	0.173465	0.000907	0.138913	0.000662	0.000664	0.001893	0.000595	0.071808	0.002499	0.042040	0.000797	0.000677	0.000529	5.3137	0.061993	0.272824
174-164_15	Pt-Fe alloy	0.0272	0.0024	0.173189	0.000992	0.136972	0.000941	0.000943	0.001213	0.000850	0.094301	0.005915	0.054228	0.002741	0.001332	0.000722	5.1834	0.139990	0.294562
174-164_16	Pt-Fe alloy	0.0277	0.0022	0.173206	0.000875	0.138798	0.000747	0.000748	0.001280	0.000702	0.083283	0.004710	0.049817	0.002817	0.000653	0.000490	5.4381	0.114271	0.294942
174-164_17	Pt-Fe alloy	0.0347	0.0011	0.173076	0.000651	0.139316	0.000624	0.000626	0.001408	0.000628	0.086189	0.008322	0.047830	0.002847	0.001120	0.000403	5.6966	0.060203	0.291123
174-164_18	Pt-Fe alloy	0.0277	0.0016	0.173068	0.000922	0.138315	0.000678	0.000680	0.000821	0.000729	0.070238	0.001750	0.041447	0.000712	0.000743	0.000398	5.5986	0.018428	0.280536
174-164_19	Pt-Fe alloy	0.0330	0.0017	0.173899	0.000890	0.137778	0.000727	0.000729	0.001300	0.000599	0.087669	0.004356	0.050898	0.002099	0.001097	0.000385	5.5318	0.151605	0.315412
174-164_20	Pt-Fe alloy	0.0271	0.0028	0.173892	0.000818	0.137905	0.000957	0.000958	0.000558	0.000671	0.072342	0.002817	0.042287	0.000979	0.001535	0.000574	5.4840	0.038879	0.276943
174-164_21	Pt-Fe alloy	0.0319	0.0009	0.175780	0.000635	0.140114	0.000705	0.000707	0.001608	0.000524	0.068849	0.001923	0.040629	0.000892	-0.000889	0.000418	5.9077	0.086378	0.307754
174-164_22	Pt-Fe alloy	0.0345	0.0013	0.175767	0.000853	0.139339	0.000799	0.000801	0.001614	0.000576	0.069967	0.002306	0.041167	0.001030	0.000517	0.000685	6.2036	0.088281	0.322498
174-164_23	Pt-Fe alloy	0.0444	0.0017	0.176293	0.000617	0.137493	0.000457	0.000460	0.001383	0.000369	0.070269	0.001523	0.041559	0.000657	-0.000238	0.000359	5.5078	0.019438	0.276076
174-164_24	Pt-Fe alloy	0.0414	0.0016	0.175956	0.000658	0.136509	0.000497	0.000499	0.001221	0.000395	0.071243	0.001048	0.042355	0.000537	-0.000392	0.000307	5.5459	0.052322	0.282188
174-164_25	Pt-Fe alloy	0.0320	0.0013	0.176208	0.000739	0.137065	0.000584	0.000586	0.001309	0.000678	0.070737	0.001423	0.041985	0.000756	-0.000303	0.000579	5.7615	0.041548	0.291056
174-164_26	Pt-Fe alloy	0.0396	0.0031	0.176779	0.000546	0.132690	0.000765	0.000767	0.001084	0.000502	0.079243	0.006156	0.046642	0.003443	0.001117	0.000555	4.3160	0.281939	0.355049
174-164_27	Pt-Fe alloy	0.0272	0.0006	0.176937	0.000966	0.140542	0.000762	0.000763	0.002145	0.000648	0.077961	0.003835	0.045473	0.001688	-0.000980	0.000375	5.9180	0.083115	0.307351
174-164_28	Pt-Fe alloy	0.0278	0.0010	0.176600	0.000916	0.137922	0.000861	0.000862	0.001078	0.000754	0.069807	0.001696	0.041289	0.000805	-0.000683	0.000465	5.5576	0.086514	0.291038
174-164_29	Pt-Fe alloy	0.0284	0.0005	0.176547	0.001047	0.139552	0.000933	0.000934	0.000852	0.000719	0.065021	0.001223	0.038771	0.000707	-0.000450	0.000512	6.2325	0.077276	0.321065
174-164_30	Pt-Fe alloy	0.0289	0.0017	0.175818	0.000874	0.140546	0.000829	0.000830	0.001937	0.000720	0.068675	0.001309	0.041235	0.000736	0.000496	0.000569	6.1595	0.055937	0.313014
174-164_31	Pt-Fe alloy	0.0154	0.0011	0.176575	0.001532	0.143129	0.001630	0.001631	0.000538	0.001245	0.114856	0.005760	0.066417	0.002478	-0.000044	0.000932	7.1033	0.405593	0.539116
174-164_32	Pt-Fe alloy	0.0214	0.0013	0.176663	0.001184	0.138832	0.001032	0.001033	0.001416	0.000857	0.071721	0.001972	0.042448	0.001050	-0.001409	0.000575	5.7612	0.034326	0.290099
174-164_33	Pt-Fe alloy	0.0244	0.0008	0.176531	0.000941	0.137718	0.000841	0.000842	-0.000259	0.000612	0.063400	0.001089	0.037532	0.000519	-0.000194	0.000578	5.8059	0.048953	0.294393
174-164_34	Pt-Fe alloy	0.0269	0.0015	0.176012	0.000977	0.137776	0.000909	0.000911	0.001499	0.000648	0.069119	0.002316	0.041084	0.001317	-0.000637	0.000488	5.9359	0.095131	0.311668
174-164_35	Pt-Fe alloy	0.0230	0.0010	0.175940	0.001018	0.137069	0.000810	0.000811	0.001549	0.000638	0.072719	0.002315	0.043261	0.001335	-0.000326	0.000585	5.9211	0.083565	0.307621
174-164_36	Pt-Fe alloy	0.0271	0.0007	0.176705	0.000926	0.139414	0.000634	0.000636	0.001524	0.000729	0.062307	0.000933	0.037165	0.000531	0.001138	0.000641	6.1099	0.048323	0.309292
174-164_37	Pt-Fe alloy	0.0177	0.0004	0.175620	0.001317	0.139359	0.001217	0.001218	0.002176	0.001150	0.061161	0.001457	0.036417	0.000826	-0.002171	0.000795	6.0562	0.099226	0.318655
174-164_38	Pt-Fe alloy	0.0173	0.0002	0.177058	0.001322	0.137726	0.001165	0.001166	0.002241	0.001203	0.070638	0.002074	0.042218	0.001116	-0.001549	0.000764	5.7203	0.033501	0.287968
174-164_39	Pt-Fe alloy	0.0308	0.0012	0.176555	0.000844	0.137758	0.000952	0.000954	0.001386	0.000664	0.069579	0.002678	0.040518	0.001092	-0.000789	0.000455	5.5149	0.221244	0.353529
174-164_40	Pt-Fe alloy	0.0254	0.0009	0.176400	0.001070	0.139220	0.000855	0.000856	0.001140	0.000774	0.064684	0.001025	0.038691	0.000613	-0.000813	0.000419	5.7433	0.057627	0.292890
174-164_41	Pt-Fe alloy	0.0328	0.0019	0.175790	0.000673	0.138673	0.000663	0.000665	0.001729	0.000519	0.071427	0.004289	0.040884	0.001635	-0.000732	0.000402	5.8165	0.048681	0.294873
174-164_42	Pt-Fe alloy	0.0129	0.0006	0.178173	0.001269	0.139780	0.001399	0.001399	0.002374	0.001410	0.083891	0.001609	0.049997	0.000913	-0.001642	0.001198	5.9559	0.056244	0.303060
174-164_43	Pt-Fe alloy	0.0275	0.0022	0.175270	0.000935	0.139755	0.001001	0.001003	0.001979	0.000661	0.066485	0.004945	0.037227	0.001805	-0.000299	0.000405	6.2897	0.099425	0.329829
174-164_44	Pt-Fe alloy	0.0255	0.0028	0.176691	0.001372	0.138802	0.000697	0.000699	0.000869	0.000857	0.087111	0.003921	0.051705	0.002261	-0.000146	0.000544	5.3657	0.056753	0.274221
174-164_45	Pt-Fe alloy	0.0304	0.0013	0.177339	0.000696	0.139471	0.000814	0.000815	0.001474	0.000655	0.088229	0.002112	0.052534	0.001198	-0.000601	0.000391	5.4173	0.090347	0.285536
174-164_46	Pt-Fe alloy	0.0285	0.0032	0.177682	0.001158	0.134940	0.001270	0.001271	0.002059	0.000859	0.077402	0.004017	0.047882	0.001723	-0.001063	0.000435	4.7417	0.258014	0.350399
174-164_47	Pt-Fe alloy	0.0109	0.0002	0.167449	0.002094	0.135996	0.002332	0.002333	0.001307	0.001915	0.073897	0.002330	0.043900	0.001297	-0.001113	0.001180	6.1540	0.026358	0.308826
174-164_48	Pt-Fe alloy	0.0277	0.0027	0.169675	0.000697	0.136630	0.000826	0.000827	0.000991	0.000811	0.084272	0.004432	0.049688	0.002296	0.000869	0.000646	6.3015	0.046857	0.318540
174-164_49	Pt-Fe alloy	0.0247	0.0011	0.171351	0.001046	0.138660	0.000797	0.000798	0.000429	0.000848	0.092858	0.004687	0.055532	0.002803	0.000729	0.000688	6.4958	0.090361	0.337126
174-164_50	Pt-Fe alloy	0.0287	0.0010	0.171961	0.000990	0.139627	0.000732	0.000734	0.000686	0.000748	0.085381	0.003822	0.050131	0.001978	0.000934	0.000502	6.4446	0.081685	0.332424
174-164_51	Pt-Fe alloy	0.0309	0.0015	0.172578	0.000825	0.138714	0.000770	0.000771	0.000401	0.000549	0.072483	0.002045	0.043065	0.001113	0.001209	0.000573	6.5220	0.063686	0.332261
174-164_52	Pt-Fe alloy	0.0284	0.0010	0.173225	0.000941	0.139376	0.000719	0.000720	0.001017	0.000757	0.078189	0.002545	0.046194	0.001370	0.000449	0.000462	6.4182	0.085859	0.332195
174-164_53	Pt-Fe alloy	0.0231	0.0009	0.174108	0.001115	0.137805	0.000775	0.000776	0.001312	0.000840	0.076204	0.002768	0.045224	0.001541	0.000190	0.000664	6.2693	0.072999	0.321852
174-164_54	Pt-Fe alloy	0.0355	0.0105	0.172156	0.001474	0.136720	0.001987	0.001987	0.001243	0.000720	0.092206	0.006239	0.053755	0.003358	0.000391	0.000468	6.2420	0.575778	0.654926
174-164_55	Pt-Fe alloy	0.0307	0.0016	0.174488	0.000902	0.139144	0.001077	0.001078	0.000907	0.000587	0.081745	0.005489	0.047625	0.002918	0.000418	0.000474	6.7318	0.172863	0.378384
174-164_56	Pt-Fe alloy	0.0253	0.0014	0.174154	0.000909	0.140539	0.001203	0.001204	0.001517	0.000549	0.072985	0.002118	0.043816	0.001059	-0.000083	0.000472	7.2530	0.287985	0.463088
174-164_57	Pt-Fe alloy	0.0255	0.0009	0.174696	0.001145	0.138203	0.000871	0.000872	0.001151	0.000925	0.073352	0.002103	0.043371	0.001102	0.000111	0.000495	6.8256	0.098023	0.355076
174-164_58	Pt-Fe alloy	0.0287	0.0008	0.175207	0.001027	0.137643	0.000571	0.000573	0.000457	0.000641	0.072874	0.001245	0.043438	0.000705	0.000486	0.000384	6.2196	0.058970	0.316523
174-164_59	Pt-Fe alloy	0.0255	0.0009	0.175073	0.000907	0.137260	0.000783	0.000785	0.000907	0.000760	0.075804	0.002493	0.044323	0.001036	0.000385	0.000455	6.3369	0.052733	0.321201
174-164_60	Pt-Fe alloy	0.0471	0.0116	0.175194	0.000953	0.135446	0.002010	0.002011	0.001097	0.000417	0.082562	0.004400	0.049375	0.002631	0.000758	0.000408	5.6466	0.547929	0.616390
174-164_61	Pt-Fe alloy	0.0250	0.0009	0.174338	0.000909	0.136860	0.000634	0.000635	0.000550	0.000756	0.082428	0.002867	0.049600	0.001644	0.000256	0.000463	6.1054	0.095925	0.319988
174-164_62	Pt-Fe alloy	0.0283	0.0013	0.175976	0.000910	0.136234	0.000782	0.000783	0.001068	0.000713	0.086916	0.002445	0.051156	0.001223	0.000489	0.000500	6.1217	0.121538	0.329332
174-164_63	Pt-Fe alloy	0.0215	0.0004	0.175197	0.001187	0.138731	0.000813	0.000815	0.000321	0.000779	0.074975	0.002062	0.043986	0.000833	0.000713	0.000513	6.8607	0.122464	0.364239
174-164_64	Pt-Fe alloy	0.0310	0.0005	0.175309	0.000645	0.137530	0.000657	0.000659	0.001434	0.000509	0.069908	0.000881	0.041462	0.000382	-0.000015	0.000377	6.4055	0.027430	0.321449
174-164_65	Pt-Fe alloy	0.0250	0.0012	0.176391	0.001099	0.135606	0.000763	0.000764	0.000410	0.000791	0.076287	0.001258	0.045890	0.000688	0.000438	0.000547	6.0125	0.048324	0.304483
174-164_66	Pt-Fe alloy	0.0310	0.0011	0.175574	0.000666	0.139936	0.000594	0.000596	0.001233	0.000645	0.075294	0.002364	0.044136	0.001071	0.000214	0.000418	6.7478	0.073809	0.345370

Within run uncertainties are quoted as 2SE. Total absolute error for ^{186}Os/^{188}Os ratios incorporates an estimate of external reproducibility based on repeat analyses, over a period of ~ one year, of an in house LA standard (Urals Os-rich PGE alloy 36720 G

Appendix 5

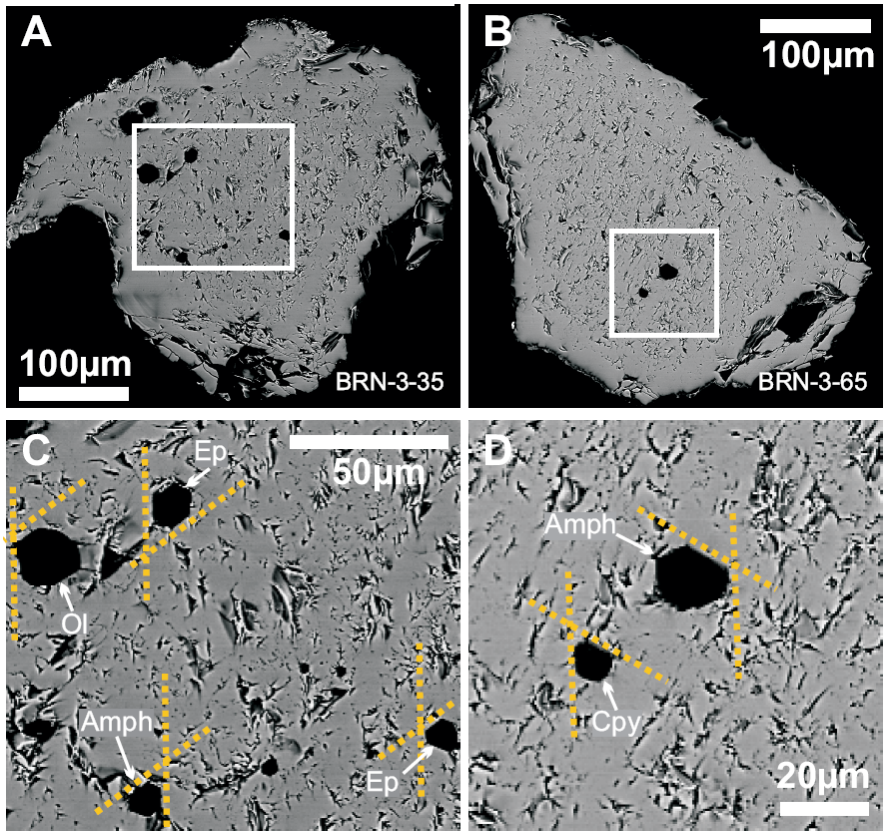

BSE images of inclusions in laurite grains. Dashed lines highlight the parallel orientation of different inclusions within the same grain, indicating that the habit of inclusions is likely dominated by the host PGM grain. Boxes in A and B show areas enlarged in C and D respectively. Irregular pits and fractures are an artifact of poor polishing, due to polishing both sulfides and PGE alloys in the same mount.

Appendix 6

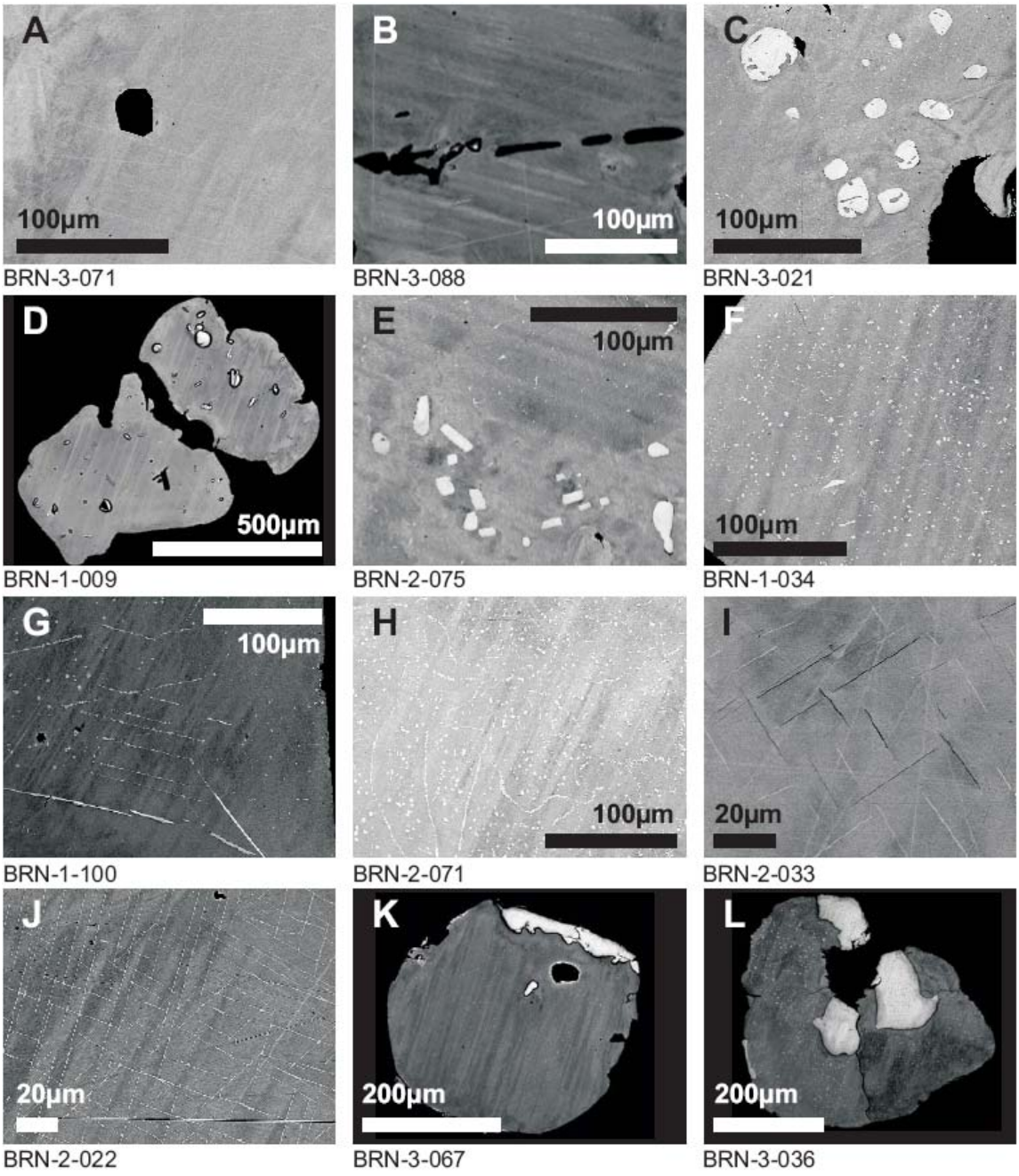

BSE images of internal features in Pt-Fe alloy grains show that internal heterogeneity in this population spans a range of scales and compositions. A and B, silicate inclusions. C-E, PGE alloy inclusions or intergrowths dominated by Os and Ir. F and H, micro PGE alloy inclusions. G, I and J, linear features that may be cogenetic or products of exsolution. K and L, irregular PGE alloy rims.

Appendix 9

Detection limits for EMP analyses of Borneo PGM

Element	Peak	Detection limit (%)
Ru	La	0.120
Rh	La	0.088
Pd	Lb	0.220
Re	La	0.308
Ir	La	0.352
Pt	La	0.473
Os	Ma	0.163
Fe (low Pt)	La	1.37
Fe (high Pt)	Ka	0.120
Co	Ka	0.135
Ni	Ka	0.097
Cu	La	0.297
W	La	0.589
S	Ka	0.090
As	Lb	0.482
Mo	La	0.109

Detection limits are 3 sigma standard deviation. For high Pt samples Fe was analyzed on the K alpha peak since Pt interference occurs on the Fe L alpha peak.